Aspects of turbulent-shear-layer dynamics and mixing

Thesis by

Michael David Slessor

In partial fulfillment of the requirements
for the degree of
Doctor of Philosophy

Graduate Aeronautical Laboratories
California Institute of Technology
Pasadena, California 91125

1998

(Submitted March 6, 1998)

Abstract

Experiments have been conducted in the GALCIT Supersonic Shear Layer Facility to investigate some aspects of high-Reynolds-number, turbulent, shear-layer flows in both incompressible- and compressible-flow regimes. Experiments designed to address several issues were performed; effects of inflow boundary conditions, freestream conditions (supersonic/subsonic flow), and compressibility, on both large-scale dynamics and small-scale mixing, are described.

Chemically-reacting and non-reacting flows were investigated, the former relying on the $(H_2 + NO)/F_2$ chemical system, in the fast-kinetic regime, to infer the structure and amount of molecular-scale mixing through use of "flip" experiments. A variety of experimental techniques, including a color-schlieren visualization system developed as part of this work, were used to study the flows.

Both inflow conditions and compressibility are found to have significant effects on the flow. In particular, inflow conditions are "remembered" for long distances downstream, a sensitivity similar to that observed in low-dimensionality, non-linear (chaotic) systems. The global flowfields (freestreams coupled by the shear layer) of transonic flows exhibit a sensitivity to imposed boundary conditions, *i.e.*, local area ratios. A previously-proposed mode-selection rule for turbulent-structure convection speeds, based on the presence of a lab-frame subsonic freestream, was experimentally demonstrated to be incorrect. Compressibility, when decoupled from all other parameters, *e.g.*, Reynolds number, velocity and density ratios, *etc.*, reduces large-scale entrainment and turbulent growth, but slightly enhances small-scale mixing, with an associated change in the structure of the molecularly-mixed fluid. This reduction in shear-layer growth rate is examined and a new parameter that interprets compressibility as an energy-exchange mechanism is proposed. The parameter reconciles and collapses experimentally-observed growth rates.

Acknowledgements

First and foremost, I am indebted to my advisor, Paul Dimotakis, for providing an environment in which graduate education spanned many arenas, both scientific and non. In addition, the technical mentorship and guidance he brought to this work were critical in its planning, execution, and completion.

I also wish to thank Earl Dahl, whose expert technical assistance and good humor were equally critical in completing the experimental phase of the work.

I would be remiss if I did not thank Chris Bond and Dominique Fourguette, both of whom were key collaborators in much of this work, as well as Dan Lang, for his help with the electronics and computer systems. In addition, considerable design and planning assistance for various lab upgrades was provided by Bertin Brothers Construction, as well as Paul Winter and John Rousseau of the Caltech Physical Plant.

Finally, I wish to thank my parents, who provided the various forms of "activation energy" that led me to Caltech, and to Erin, for her constant encouragement, support, and strength.

This work was funded by the Air Force Office of Scientific Research, Grant Nos. F49620–93–1–0338 and F49620–94–1–0353.

Contents

CHAPTER 1

Introduction and background

During the past three decades, turbulent shear-layer flows have been the subject of rather intense experimental and numerical scrutiny. This interest is due, in large part, to their inherent geometric simplicity; the nearly-parallel, isobaric freestreams provide a spatially-uniform boundary condition for the flow (Fig. 1.1). Despite this simplicity, the response of the flow to various parameters remains a matter of ongoing study and controversy. On a practical note, as a relatively efficient mixer of initially-separated constituents, this flow, and others like it, play a critical role in the performance of many industrial devices, ranging from chemical lasers to envisaged hypersonic-propulsion engines.

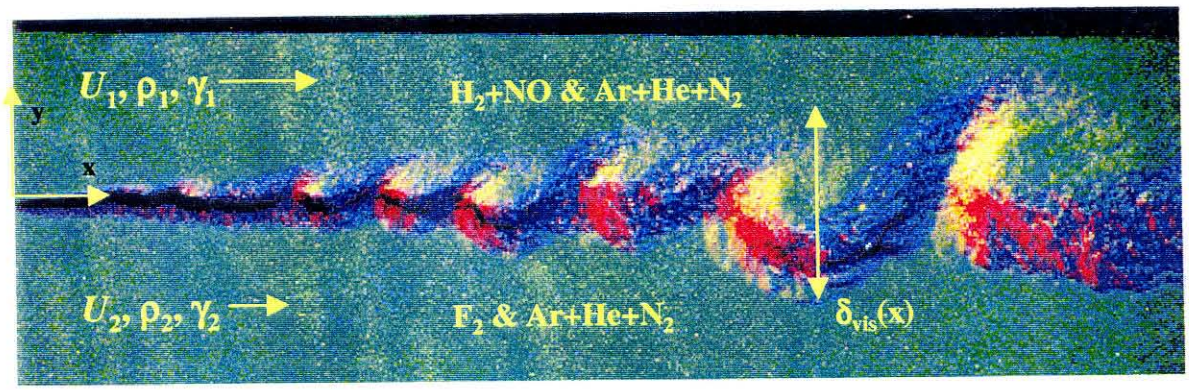

FIG. 1.1 Color-schlieren photograph of a subsonic, turbulent, shear-layer flow. The flow in this, and all subsequent, flow visualizations is from left to right. The subscript $()_1$ refers to the properties of the high-speed freestream flow, and the subscript $()_2$ refers to those of the low-speed freestream flow.

This thesis explores several aspects of high-Reynolds-number, turbulent, shear-layer flows, extending previous work in both the incompressible- and compressible-flow regimes. In particular, experiments to investigate effects of inflow conditions, freestream boundary conditions, and compressibility will be presented, along with flow-modeling considerations describing these, and previous, results. Comprehensive review articles discussing turbulent shear-layer mixing and combustion (Dimotakis 1991a), incompressible-flow combustion (Coats 1996), and compressibility effects on turbulence (Lele 1994) are relevant. A brief overview of the particular subjects of interest is offered below.

An important catalyst for this recent activity was the discovery of large-scale, spanwise-coherent structures in fully-turbulent, incompressible, shear-layer flows (Brown & Roshko 1974). Examples of these structures are evident in Fig. 1.1. In addition to casting high-Reynolds-number free-shear flows in a new light, this finding spawned a series of models that recognize the importance of the large-scale-structure (Galilean) rest frame, *e.g.*, Brown (1974) and Dimotakis (1986). These models, extending previous work for uniform-density flow, *e.g.*, Abramovich (1963) and Sabin (1965), exhibit a dependence of the incompressible-flow ($M = 0$)* growth rate, $\delta_0(x)/x$, on freestream-velocity and -density ratios, *i.e.*,

$$\frac{\delta_0}{x} \simeq \frac{\delta_0}{x}\left(r \equiv \frac{U_2}{U_1},\, s \equiv \frac{\rho_2}{\rho_1}\right). \tag{1.1}$$

In particular, the geometric and similarity considerations employed by Dimotakis (1986) yield an estimate for a spatially-growing layer given by,

$$\frac{\delta_0}{x}(r,s) \simeq C_\delta \frac{(1-r)(1+s^{1/2})}{2(1+s^{1/2}r)}\left\{1 - \frac{(1-s^{1/2})/(1+s^{1/2})}{1+2.9(1+r)/(1-r)}\right\}, \tag{1.2}$$

where C_δ is independent of r and s. The temporal-growth model of Brown (1974) provides an expression equivalent to Eq. 1.2 above, with the exception of the term in braces that accounts for the upstream/downstream asymmetries arising from spatial growth. Although experimental data are in accord with the overall dependence suggested by Eq. 1.2, there is substantial variance in inferred values for C_δ, *i.e.*,

$$0.25 \lesssim C_\delta \lesssim 0.45, \tag{1.3}$$

---

* The subscript $()_0$ denotes incompressible flow, *e.g.*, δ_0/x is the shear-layer growth rate at incompressible-flow conditions.

especially between experiments performed in different facilities (Dimotakis 1991a). Significantly, initial, or inflow, conditions are known to affect far-field properties of the turbulence, including growth rates. As a consequence, it is widely speculated that such an influence is at least partially responsible for the range exhibited in Eq. 1.3. Inflow conditions and their influence on shear-layer growth and mixing are discussed in Ch. 3.

The experiments of Brown & Roshko (1974) also addressed compressibility effects, albeit in an indirect manner. At the time of those experiments, it was well appreciated that Mach number had a significant effect on shear-layer growth. In particular, increasing Mach number was associated with decreasing growth rate. A proposed explanation was that an appropriate transformation, *e.g.*, Howarth-Doridnitsyn type, would account for this decreased growth. Such an explanation implicitly assumes that compressibility acts by modifying the density field in a passive manner. Similar explanations have been relatively successful in describing wall-bounded flows, up to Mach numbers of 5 or so (*e.g.*, Bradshaw 1977). The variable-density experiments of Brown & Roshko, however, showed that the incompressible shear-layer growth-rate decreases by about 30% for $s = 1/7$ (relative to $s = 1$), much less than the 300% decrease observed for an equivalent ($M \simeq 5.7$) compressible flow. This result demonstrates that compressibility, beyond its effects on the density field, fundamentally alters large-scale dynamics in free-shear turbulence.

The success of convective-frame views in describing incompressible flows inspired an extension of those ideas to the compressible-flow regime. To scale compressibility effects, Papamoschou & Roshko (1988) suggested the convective Mach numbers,

$$M_{c1} = \frac{U_1 - U_c}{a_1} , \qquad M_{c2} = \frac{U_c - U_2}{a_2} , \tag{1.4}$$

where U_i are the freestream speeds, a_i the corresponding freestream speeds of sound, and U_c the large-scale structure convection speed, extending ideas employed by Mack (1969, 1975, and 1984) in supersonic, boundary-layer transition. A single parameter was subsequently suggested by Papamoschou (1989), termed here the (total) convective Mach number,

$$M_c = \frac{\Delta U}{a_1 + a_2} , \tag{1.5}$$

where $\Delta U = U_1 - U_2$ is the freestream-speed difference. For equal freestream specific-heat ratios ($\gamma_1 = \gamma_2$), extension of the Dimotakis (1986) stagnation-point recovery model to isentropic, compressible flow (Papamoschou & Roshko 1988) predicts symmetric convection, *i.e.*, $M_{c1} = M_{c2} = M_c$, with all three values relatively close for the possible range of γ_i's.

There are some complicating difficulties with such a view in the compressible-flow regime. Linear-stability analyses (*e.g.*, Gropengiesser 1970, Ragab & Wu 1988, Sandham & Reynolds 1990, and Zhuang *et al.* 1990) indicate the potential for several distinct "modes" of instability in unbounded flow, namely fast, central, and slow modes. This behavior differs from incompressible flow, where a single (central) mode is dominant and has been hypothesized to be a linear "embryo" of the two-dimensional coherent structures discussed above (Roshko 1976).

Schlieren/shadowgraph visualizations of supersonic, axisymmetric, turbulent jets indicate fast-mode existence (Lowson & Ollerhead 1968 and Tam 1971), as well as slow- and fast-mode coexistence (Oertel 1979), in the upstream, annular-shear-layer region. Lowson & Ollerhead (1968) remarked that the angle of the Mach waves generated by their axisymmetric jet indicated a large-scale structure convection speed, U_c, of about 70–80% of the jet-exit velocity; a value significantly higher than that inferred for incompressible jets. Following these observations, evidence of slow and fast modes in two-dimensional shear-layer flows were reported by Papamoschou (1989) and subsequently by Hall *et al.* (1993) and Papamoschou & Bunyajitradulya (1996). These (two-dimensional) shear-layer data appear to indicate, however, existence of either the slow *or* the fast mode in a given flow. Papamoschou (1989) suggested an empirical mode-selection rule, with a selection criterion based on the presence of subsonic lab-frame freestream flow. If a (lab-frame) criterion for mode selection is valid, or alternatively, if multiple-mode coexistence occurs, the fundamental idea of a purely convective-frame analysis must be questioned. A discussion of these issues is contained in Ch. 4.

Partially because of these difficulties, reports of shear-layer data have typically concentrated on behavior as a function of the total convective Mach number, M_c. This average compressibility measure lacks the rigor of incompressible-flow models, since turbulent features do not convect with the (central/isentropic)

speed implicit in Eq. 1.5, at least beyond low levels of compressibility. Additionally, flow-visualization data, *e.g.*, Clemens & Mungal (1995), are indicative of a relative reduction in well-organized, two-dimensional, coherent structure with increasing compressibility. Nevertheless, M_c, as well as the "relative Mach number" ($M_{rel} \equiv 2M_c$), has been widely used in assessing compressibility effects on, for example, growth rate. In particular, compressibility is usually assumed to act independently of freestream-velocity and -density ratios, yielding,

$$\frac{\delta/x}{\delta_0/x} \simeq \frac{\delta}{\delta_0}(M_c) \neq \text{fn}(r,s)\,. \tag{1.6}$$

Support for this type of scaling can also be found in the linear-stability analyses discussed above. There have been, however, experimentally-observed violations of Eq. 1.6, *e.g.*, in Hall *et al.* (1993), which are discussed in Ch. 6.

The growth rate measures the evolution of the largest (outer) length scale and can be regarded as the first step in a sequence of shear-layer mixing processes (Dimotakis 1991a). When a chemical reaction between two freestream constituents is of interest, *e.g.*, as in non-premixed combustion, then mixing processes at molecular scales must be addressed, since the (molecular-interaction) chemical processes/reactions occur at those scales. In particular, molecularly-mixed fluid is the end result of a multi-stage process that can be regarded to occur in a sequence of Lagrangian steps, *e.g.*, "stirring" then "mixing" (Danckwerts 1958). In such a process, parameters known to influence the largest scales of the flow, *i.e.*, inflow conditions, velocity and density ratios, and Mach number, must be augmented by variables that influence smaller spatial scales in the flow, *e.g.*, Schmidt number and (local) Reynolds number. Shear-layer mixing data indicate that even past the mixing transition, where a qualitative change in (small-scale) mixing occurs,** *i.e.*, for,

$$Re_\delta \equiv \frac{\rho \Delta U \delta}{\mu} \gtrsim 10^4, \tag{1.7}$$

there is a dependence of molecular mixing on Reynolds number. In particular, both experiments (Mungal *et al.* 1985, Frieler & Dimotakis 1988, and Bond & Dimotakis 1996), as well as models (Broadwell & Briedenthal 1982, Broadwell &

** A brief discussion of this transition can be found in Ch. 3. For a more complete discussion, see Dimotakis (1993).

Mungal 1991, and Dimotakis 1987) indicate a modest decrease in molecularly-mixed fluid, within the incompressible shear layer, as Reynolds number increases. Such a dependence suggests that if compressibility effects on molecular mixing are to be ascertained with any confidence, variations in Reynolds number, as well as other flow parameters, must be minimized. Experiments that observe this restriction are described in Ch. 5.

CHAPTER 2

Facility, instrumentation, and measurements

2.1 Facility overview

The GALCIT Supersonic Shear Layer (S^3L) Facility is a two-stream, blow-down, wind tunnel, capable of attaining freestream Mach numbers spanning from incompressible to highly-compressible gas-phase flow, in both chemically-reacting and non-reacting configurations. A brief overview of this facility is presented here for completeness. Additional details can be found in Hall & Dimotakis (1989), Hall (1991), and Bond (1998). Two major upgrades undertaken as part of this work, *i.e.*, extension to bi-supersonic flow and replacement of the surge tank, will be documented here.

The facility, shown schematically in Fig. 2.1, operates with a run time of $t_{\rm run} > t_{\rm dat} \simeq 2 - 4\,{\rm s}$, where $t_{\rm dat}$ is the data-recording time. Gas for the two freestreams is supplied by independent (high- and low-pressure, usually corresponding to high- and low-speed, respectively) flow systems charged by standard bottled-gas supplies prior to the experimental run. This facility can produce flows with fast-kinetic reactants, whose chemical reaction and associated temperature rise yields quantitative measurements of molecular-scale mixing in the shear-layer region. In such experiments, a dilute mixture of H_2 and NO is carried in the high-speed stream and a dilute concentration of F_2 is carried in the low-speed stream. The remaining diluent components are selected to control freestream thermodynamic properties, *e.g.*, densities, speeds-of-sound.

To provide the molecular number densities required for "fast" chemical reactions, large (unit) Reynolds numbers, and high optical-image cross sections, the test section operates at nominally-atmospheric static pressure. This is different from most other supersonic-flow facilities, in which test sections operate at lower-pressure conditions to ease demands on upstream flow-supply systems.

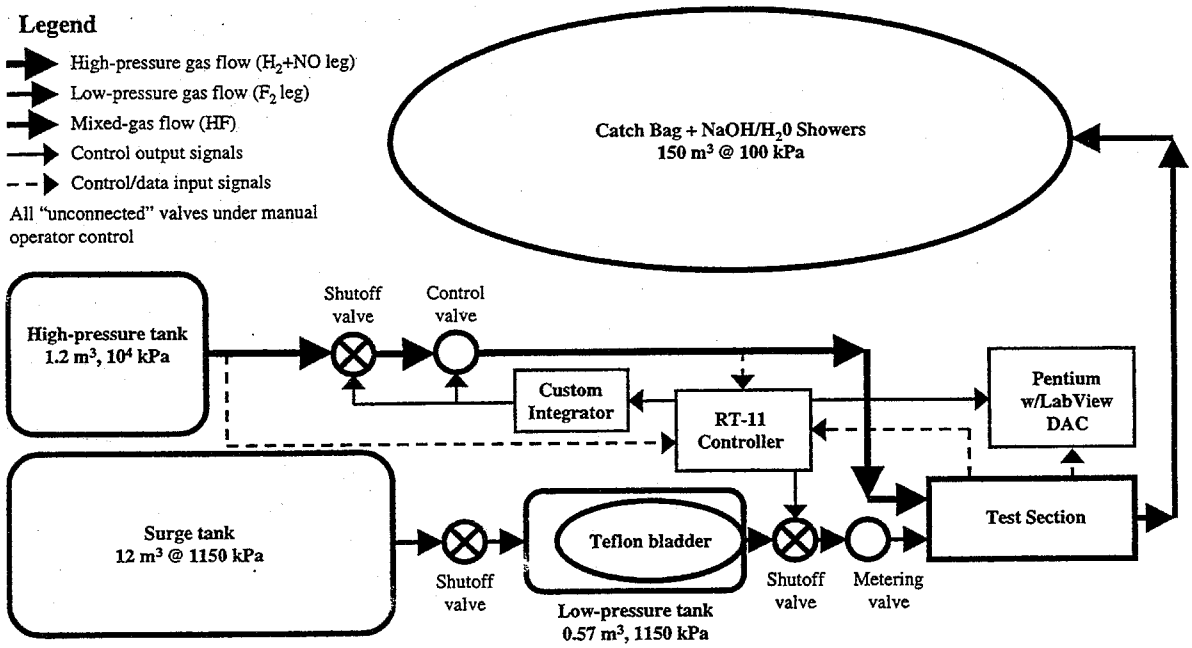

FIG. 2.1 Overall facility gas-flow schematic.

For the shear-layer flows investigated in these experiments, the high-pressure freestream speed is maintained by plenum-pressure control, operated in either an open-loop (program-control) configuration at low mass-flux conditions, *e.g.*, flows discussed in Ch. 3, or a closed-loop (nonlinear-feedback-control) configuration at moderate-to-high mass-flux conditions, *e.g.*, flows discussed in Ch. 4. Gas is supplied to this plenum from a $1.2\,\mathrm{m}^3$ pressure vessel, at a maximum pressure of $10^4\,\mathrm{kPa}$. During blowdown, vessel pressure can drop by as much as 50%, necessitating an active-control system. The gas in the vessel is maintained at a nearly constant temperature, however, by rolled aluminum screen (large heat capacity) that occupies the pressure-vessel volume.

The mass flux through the low-pressure plenum is set by a choked metering valve kept fixed during each run. Gas to this plenum is supplied from a $0.57\,\mathrm{m}^3$ vessel that encloses a bladder bag containing the F_2-laden charge. This vessel is

pressurized, in turn, by a N_2-filled, large-volume surge tank whose pressure falls by $3 - 5\%$ during a run. This nearly-isobaric arrangement obviates the need for low-pressure-side active control, greatly simplifying the flow-control process, as well as providing a relatively safe (teflon-buffered) method for handling extremely-corrosive fluorine gas.

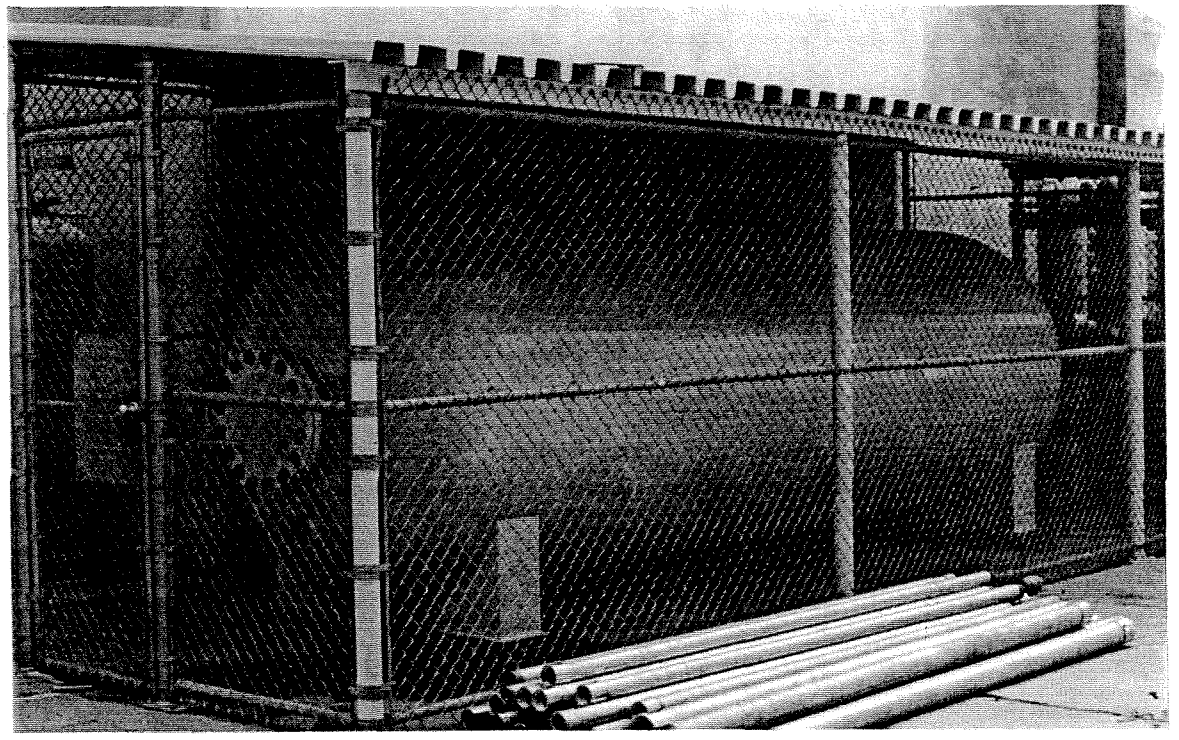

FIG. 2.2 Northeast view of the upgraded surge tank installation.

One major engineering upgrade undertaken during this work replaced the original (circa 1940) $12.7\,m^3$ surge tank and associated delivery piping with a higher-capacity system. The original system had a maximum working pressure of 700 kPa, limited by the tank pressure rating. This significant modification was necessitated by the planned demolition of the GALCIT 10-Foot Wind Tunnel during the summer of 1997, since the original surge tank resided adjacent to this tunnel, at both basement and sub-basement levels, in the center of the Guggenheim Building. The replacement surge tank, a custom $14.2\,m^3$ unit with a (maximum) working pressure of 1150 kPa, was installed in the Karman/Guggenheim courtyard (Fig. 2.2) and was connected to the low-pressure supply system in July of 1997. The upgraded system has since been successfully tested over a range of pressures and flowrates.

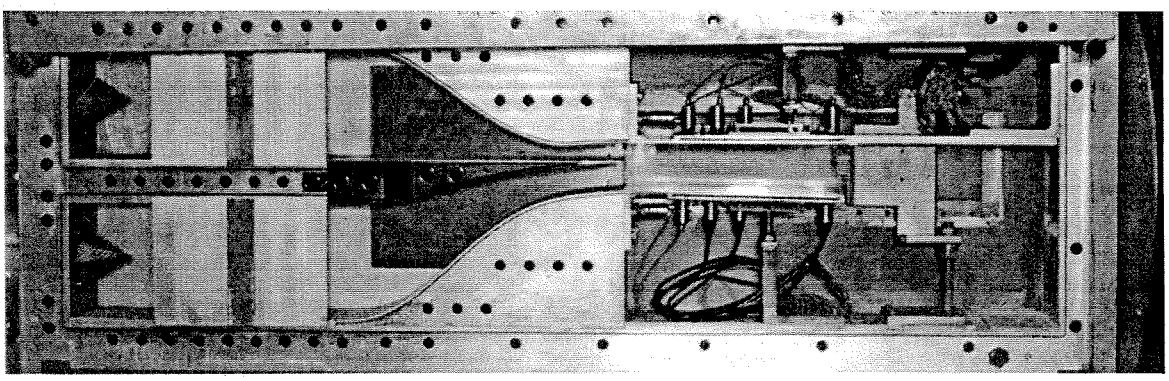

FIG. 2.3 Photograph of shear-layer flow-management and test-section regions. Gas flows from left to right. Image is approximately 2 m in length.

A photograph of the flow-management and test-section regions is shown in Fig. 2.3. Coarse-mesh-screen, honeycomb, and a series of fine-mesh-screen sections are used for turbulence management in the region upstream of the contractions. The two streams are separated in their respective plena by a splitter plate, which is flat on the top (high-speed) surface and curved on the bottom (low-speed) surface, as shown in Fig. 2.3. The splitter plate has a trailing-edge thickness of 0.13 mm, an included angle of 5°, and is estimated (using General Electric gauges) to have an average surface roughness of 0.4 μm.

For subsonic freestream flows, the modular "nozzle blocks" are configured as specially-machined contraction sections. Their shapes are described by 6^{th}-degree polynomials, which are iteratively optimized using a potential-flow solver (Pepin & Dimotakis 1989) to obtain the inviscid outer-flow solution, and the method of Thwaites (*e.g.*, White 1974) to obtain the boundary-layer thickness(es). The optimization endeavors to maximize flow uniformity and to minimize boundary-layer momentum thicknesses at the contraction exit, while ensuring suppression of any flow separation and three-dimensional Taylor-Görtler instabilities. This flow instability can occur in the boundary layers on the concave surfaces of both nozzle walls, as well as on the concave part of the lower splitter-plate surface. The design-iteration process minimizes the potential for this instability in all susceptible regions. For supersonic freestream flows, these nozzle blocks are configured as converging-diverging (Laval) nozzles, which employ similar contraction sections to the throat, mated to supersonic-expansion contours designed using the characteristic-capturing

method of Sivells (1978). As seen in Fig. 2.3, the 5° included angle of the splitter plate is matched on the bottom nozzle block, *i.e.*, the bottom-freestream flow enters the test section at a 5° angle relative to the top-freestream flow. Flow in the test section, downstream of the contractions/nozzles, is confined by top and bottom guidewalls, with optical windows serving as sidewalls, with a span, $b = 15.3\,\mathrm{cm}$. In these experiments, the upper guidewall is maintained horizontal (parallel to the top splitter-plate surface), with the lower guidewall adjusted, as necessary in each flow, to remove any mean streamwise pressure gradients.

Upon exiting the test section, the flow encounters a shower-tunnel and catch-bag containment, handling, and neutralization system. A set of shower heads inside the tunnel spray a H_2O/NaOH mixture into the exiting flow, simultaneously neutralizing and cooling the exhaust gases. The neutralization process transforms the exhaust into a mixture of non-toxic gases, more H_2O, and NaF, the active ingredient in many toothpastes. The $150\,\mathrm{m}^3$-volume, atmospheric pressure catch bag collects and contains the exhaust mixture downstream of the shower tunnel. An additional set of shower heads, within the bag, provides further neutralization and cooling of the exhaust products. Finally, in preparation for eventual venting, the catch bag allows for controlled dilution of any potentially-flammable gas mixtures to concentrations comfortably below ignition limits.

2.2 The upgrade to bi-supersonic flow

The original low-pressure freestream of the S^3L facility was limited in Mach number to subsonic flow ($M_2 \lesssim 0.5$) by the existing components. Consequently, an upgrade of these components was required to explore the regime of bi-supersonic flow, where both freestreams are supersonic in the laboratory frame. Two major modifications were required to allow bi-supersonic operation of the facility: a new control/regulation system, and a new nozzle block designed for an appropriate Mach number. Fortunately, the existing low-pressure side reservoirs (supply and surge tanks) were deemed capable of supplying enough gas for adequate run times at supersonic Mach numbers.

2.2.1 Low-pressure freestream control system

One might expect that an active-control valve, similar to the unit which regulates the high-pressure freestream flow, would be required to compensate for the anticipated stagnation-pressure drop during a run (35 kPa from the original surge-tank pressure of 700 kPa). However, since the existing high-pressure control valve can be pre-programmed, it is possible to achieve the desired pressure ratio across the splitter-plate tip throughout a run with fixed-area-valve metering of the low-pressure freestream. In order to accommodate increased mass fluxes associated with supersonic Mach numbers, an increase in (sonic) valve-orifice area was required. To provide this increase, a new sleeve was machined by the Aeronautics Machine Shop with approximately triple the choked-flow area of the original (subsonic) sleeve. These modular sleeves are easily interchanged, increasing the operating envelope of the S^3L facility to include bi-supersonic flow, in addition to high-mass-flux subsonic-flow conditions, *e.g.*, flows discussed in Ch. 5.

The existing passive-blowdown method of metering the low-pressure freestream has several significant advantages over an active-control scheme. In particular, this allows continued use of the original operating procedure and control algorithm/computer, minimizing changes to a well-tested facility. Additionally, all existing low-pressure "settings" remain valid, permitting low mass-flux runs to occur with a minimum of recalibration. Finally, omission of a complex valve assembly eliminates the significant safety considerations of long-term fluorine passivation and compatability.

2.2.2 Supersonic nozzle

A preliminary study indicated that a Mach number of less than approximately 1.13 would be achievable using existing reservoir components. This limit is dictated if a minimum allowable run time of 2 s is desired, *e.g.*, to provide adequate data-acquisition record lengths, and a nozzle-exit height of 38 mm is desired, *e.g.*, to admit the shear-layer growth expected over the test-section length. Near-sonic Mach numbers, however, dictate throat-to-expansion area ratios correspondingly close to unity. Considering uncertainties inherent in the displacement-thickness estimate† of 0.35 mm, as well as errors incurred in machining a large block of aluminum, it seemed wise to design a nozzle with a throat-to-exit expansion as large as possible, *i.e.*, a nozzle with as high a Mach number allowed by the above constraints. Consequently, a Mach 1.13 nozzle, with a throat-to-exit expansion of approximately 0.85 mm, was fabricated by Caltech Central Engineering Services and was used throughout the bi-supersonic flow experiments described in Ch. 4.

2.3 Method, instrumentation, and diagnostics

Three types of experimental results will be documented here: schlieren visualizations (both black-and-white and color), mean-temperature measurements, and mean-pressure measurements. Schlieren visualization records instantaneous, overall, spanwise-averaged (two-dimensional) structure in the layer, indicating whether the shear-layer growth is linear and also, depending on the selected sensitivity, whether any significant acoustic disturbances are present. Additionally, the visual-thickness growth rate, δ_{vis}/x, can be measured from such data. When configured correctly, color schlieren registers the additional dimension of information provided by color to record both components of line-of-sight-averaged index-of-refraction gradients in the flow (see Settles 1985 and Appendix A), as opposed to the single component recorded by traditional, black-and-white, knife-edge systems.

---

† Estimate provided by Spalding-Chi turbulent boundary-layer model internal to the Sivells nozzle-design code.

The temperature profiles are recorded by a rake of sixteen, 50 μm-diameter, chromel/alumel, exposed-junction thermocouples, that produce a running temporal average at the respective measurement locations. These probes have a response time estimated to be approximately 0.02 s. An adjacent rake of sixteen, 1.5 mm-diameter tubes record pitot pressures, with static pressures along both top and bottom guidewalls monitored by flush-mounted transducers. As with temperature data, pressure data represent running temporal averages at the various measurement stations. Both temperature and pressure measurements are recorded within 3 mm of the midspan plane, with the rakes positioned near the test-section exit (Fig. 2.3) to minimize probe-induced flow blockage.

These data are processed by a set of analog 3-pole Butterworth amplifier/filter banks with knee (−3 dB) frequencies set at 100 Hz. These are sampled at 200 Hz by a National Instruments analog-to-digital converter, operating under control of a Gateway-PC/LabView environment developed for these experiments. The data are post-processed by truncating the flow startup and shutdown periods, to obtain the steady-flow period of the run. This record is then divided into eight segments, each of which is individually processed to check for discrepancies with respect to the entire ensemble. An example of such an ensemble of (eighth-segment) temperature profiles is presented in Fig. 2.4. In this example, the maximum standard deviation of the mean (of 16 independent thermocouple records) is less than 2% of the mixture adiabatic-flame temperature rise, $\Delta T_{\rm f}$. The inferred mixed-fluid quantities described below, *e.g.*, Eq. 2.6, are based on the complete steady-flow ensemble, and are subject to a statistical uncertainty closer to 1% of $\Delta T_{\rm f}$.

Non-reacting flow temperatures are used to construct a "cold"-temperature profile for each flow condition. This profile serves as a reference, and when subtracted from reacting-flow mean-temperature measurements, yields the temperature rise, $\Delta T_i = \Delta T(x, y_i)$, at each measurement location. The resulting temperature rises are divided by the adiabatic flame temperature rise of the reacting mixture, $\Delta T_{\rm f}$, to yield normalized mean temperature-rise measurements, $\Delta T_i/\Delta T_{\rm f}$. These are least-squares fit with a functional form,

$$\Theta(y) \equiv \frac{\Delta T(y)}{\Delta T_{\rm f}} = \exp\left[-\left(p_0 + p_1\, y + p_2\, y^2 + p_3\, y^3 + p_4\, y^4\right)\right] , \qquad (2.1)$$

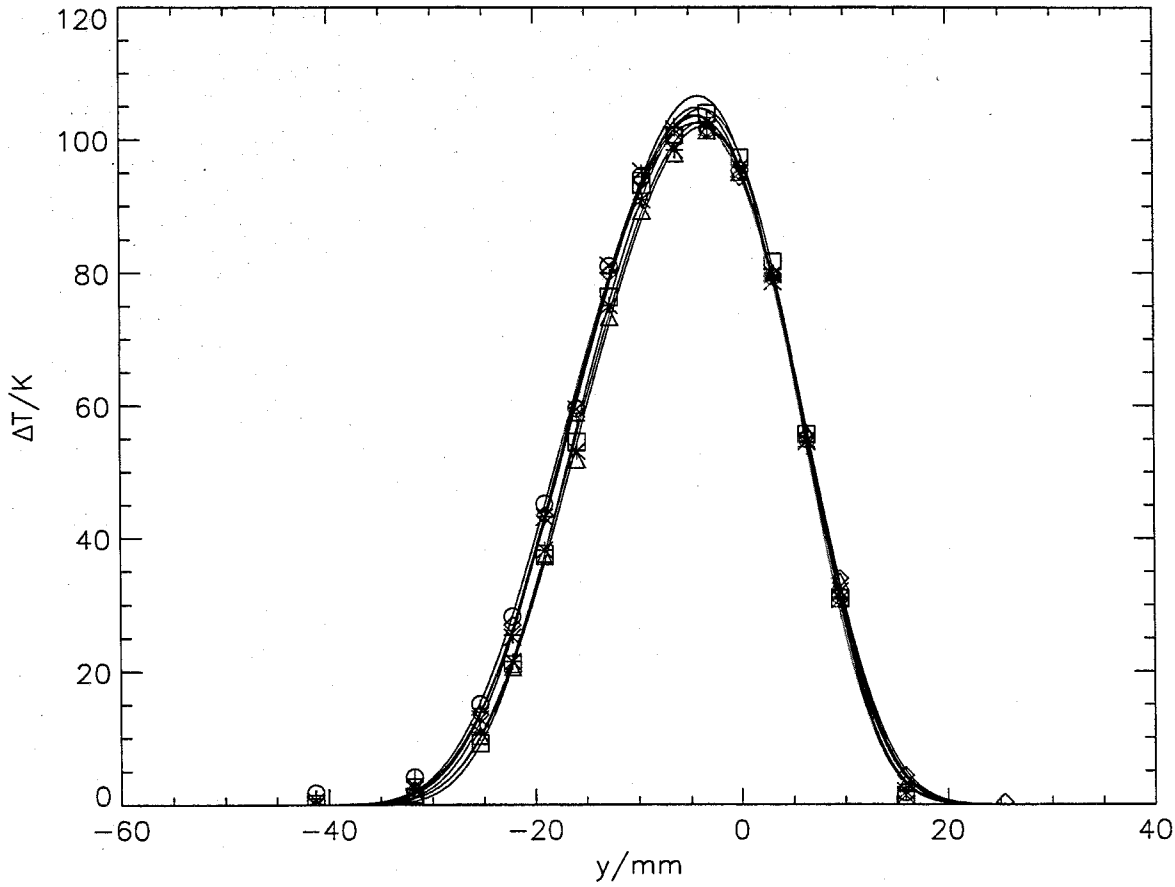

FIG. 2.4 Eight records of raw temperature data. Flow is (tripped) Case 3.1 conditions detailed in Ch. 3, below.

which is then used to estimate the quantities described below.

For incompressible-flow experiments, *e.g.*, flows discussed in Ch. 3, velocity data were deduced from direct pitot- and static-pressure measurements, as described in Hermanson & Dimotakis (1989),

$$U(y) \;=\; \sqrt{2\frac{P_{\rm p}(y) - P_{\rm g}}{\rho(y)}}\,, \tag{2.2}$$

where $P_{\rm p}(y)$ is the pitot-pressure measurement, $P_{\rm g}$ is the guidewall (static) pressure measurement and $\rho(y)$ is the density. Local values of density are estimated as,

$$\frac{\rho(y)}{\rho_0} \;=\; \frac{T_0}{T_0 + \Delta T(y),} \tag{2.3}$$

using the average temperature rise measured by the thermocouples, as well as the ambient temperature and density, T_0 and ρ_0, respectively. Velocity profiles are then least-squares fit with an analytical form,

$$U(y) \;=\; A \,+\, B\,\tanh\left(\,q_0 \,+\, q_1\,y \,+\, q_2\,y^2 \,+\, q_3\,y^3\,\right)\;. \tag{2.4}$$

For compressible-flow experiments, pitot-pressure measurements were only used to measure high- and low-speed freestream velocities, U_1 and U_2, respectively.

As alluded to above, the molecularly-mixed fluid was sampled using kinetically-fast chemical reactions to perform a "flip" experiment, *i.e.*, chemically-reacting flows at high Damköhler number,

$$Da \;\equiv\; \frac{\tau_{\rm mix}}{\tau_{\rm chem}} \;\gg\; 1\;, \tag{2.5}$$

where $\tau_{\rm mix}$ is the fluid-mechanical, molecular-mixing time and $\tau_{\rm chem}$ is the chemical-reaction (completion) time. A detailed summary of the rationale and measures employed in such an experiment is found in Dimotakis (1991a) and Bond (1998). A brief discussion is offered below.

In this high-Da regime, chemical-product formation and heat release (temperature rise) provide a resolution-insensitive probe of molecular mixing, mitigating the spatial-sampling/resolution difficulties of direct-measurement studies (*cf.* discussion in Breidenthal 1981, Koochesfahani & Dimotakis 1986, Dimotakis 1991a, and Karasso & Mungal 1996). In order to attain this fast-chemistry limit, in high-speed flows, use of the $(H_2 + NO)/F_2$ chemical system is required.

If the flow is of gases with uniform heat capacity, the normalization of the resulting temperature-rise profile, $\Delta T(y)$, at the measuring station, x, by the adiabatic flame temperature rise, $\Delta T_{\rm f}$, as in Eq. 2.1, yields a dimensionless chemical-product profile. As chemical-product formation can only take place where entrained fluids are mixed, this can be used to define the 1% shear-layer (temperature-rise) thickness, $\delta_{\rm T}$, as the span between the two points in the profile at 1% of the peak in $\Theta(y)$. This has been found to be in good agreement with alternative measures of the local shear-layer width, such as the visual thickness, $\delta_{\rm vis}$. This profile is also used to compute the chemical-product thickness,

$$\delta_{\rm p} \;\equiv\; \int_{-\infty}^{\infty} \Theta(y)\,{\rm d}y\;, \tag{2.6}$$

which represents the thickness of an equivalent layer that has uniformly-risen to the adiabatic-flame temperature. Finally, the product thickness is normalized by the 1% temperature-rise profile thickness, δ_T, to obtain the dimensionless product fraction, δ_p/δ_T, providing a measure of chemical-product formation that is insensitive to changes in the local shear-layer width.

Given product fractions at stoichiometric-mixture ratios, $\phi = \phi_0$ and $\phi = 1/\phi_0$, for large ϕ_0, the mixed-fluid fraction in the fast-kinetic regime can be estimated from,

$$\frac{\delta_m}{\delta_T} = \int_{-\infty}^{\infty} \int_{\epsilon_{\phi_0}}^{1-\epsilon_{\phi_0}} p(X,\eta)\, \mathrm{d}X\, \mathrm{d}\eta \simeq \frac{1}{1+1/\phi_0} \left[\left(\frac{\delta_p}{\delta_T}\right)_{\phi_0} + \left(\frac{\delta_p}{\delta_T}\right)_{1/\phi_0} \right] , \quad (2.7a)$$

where,

$$\eta \equiv \frac{y}{\delta_T} , \qquad \epsilon_{\phi_0} \simeq \frac{1}{2(1+\phi_0)} , \qquad e.g., \qquad \epsilon_8 \simeq 0.056 . \quad (2.7b)$$

In this expression, X is the high-speed freestream-fluid mole fraction, and $p(X,\eta)$ is its probability density function (pdf) at the normalized transverse coordinate, $\eta \equiv y/\delta_T$.

For a flow in the kinetically-fast regime, where chemical-product formation is mixing-rate-limited rather than kinetic-rate-limited, δ_m/δ_T serves as a resolution-insensitive measure of the mole fraction of molecularly-mixed fluid. Operationally, attainment of fast chemistry (high-Da) can be ascertained by demonstrating that the amount of chemical product remains unaltered as the chemical-kinetic rate is varied. This test was performed by proportionally changing the concentrations of all reactants, while holding ϕ_0 constant. This changes the kinetic rate by not only changing the number density of reactant species, but also the temperature and associated Arrhenius kinetics constants, resulting in an increase/decrease of τ_{chem}, while holding τ_{mix} constant.

Such measurements also yield the relative amounts of entrained freestream fluids that are molecularly mixed. In particular, the mixed-fluid composition (mole) ratio can be calculated as,

$$\mathcal{E}_n = \frac{(\delta_p/\delta_T)_{\phi_0}}{(\delta_p/\delta_T)_{1/\phi_0}} . \quad (2.8)$$

In the limit of large ϕ_0, this approaches the number of moles of high-speed freestream fluid, per mole of low-speed freestream fluid, that are molecularly mixed within the shear-layer region.

The predominant mixed-fluid composition, X_E, can be expected to reflect the mole ratio, E_n, of fluid entrained from the two freestreams at large scales (Dimotakis 1986, 1991b), *i.e.*,

$$X_E \simeq \frac{E_n}{E_n + 1} \ . \tag{2.9}$$

The mixed-fluid composition ratio, $\mathcal{E}_n$, as estimated above, however, will reflect the overall mixed-fluid composition and need not match E_n, as also indicated by various mixing models, *e.g.*, Broadwell & Breidenthal (1982), Broadwell & Mungal (1991), and Dimotakis (1987).

Effects of heat release on the flow were addressed by Hermanson & Dimotakis (1989). As was noted in those investigations, the most significant heat-release effect, at the values of $\Delta T_f/T_0$ in these experiments, is the dilatation-induced (displacement) flow acceleration in the confined-flow environment. In the present experiments, such effects were accommodated by adjusting the lower guidewall to maintain a zero streamwise pressure-gradient (no acceleration), for all cases, approximating an unbounded shear-layer flow, as noted above. Except for high heat-release conditions, *i.e.*, $\Delta T_f/T_0 \gtrsim 2$ or so, only small effects were observed on the mixed-fluid quantities. As noted by those authors, as well as Dimotakis (1991a), the adiabatic-flame-temperature rise is achieved in a relatively small fraction of the fluid within the layer, with an average temperature rise, distributed throughout the mixed fluid, that is significantly lower. This can can be seen directly in the mean temperature-rise data presented later, *e.g.*, Fig. 3.1.

CHAPTER 3

Effects of inflow conditions

This chapter details results from a set of incompressible-flow experiments, at high Reynolds number ($Re_\delta \equiv \rho \Delta U \, \delta(x)/\mu \simeq 2 \times 10^5$), in which inflow conditions of shear-layer formation were varied. These variations were effected by perturbing each, or both, of the boundary layers on the splitter plate separating the two freestream flows, upstream of shear-layer formation. Results of chemically-reacting flip experiments reveal that seemingly small changes in inflow conditions can have a significant influence on not only large-scale structure and shear-layer growth rate, as had been documented previously, but also on chemical-product formation and molecular mixing, far downstream of the inflow region.‡

‡ These results were reported in: Slessor, Bond, and Dimotakis (1998), *Turbulent shear-layer mixing at high Reynolds numbers: effects of inflow conditions*, GALCIT Report FM98–1, from which this Chapter largely derives.

3.1 Introduction

It is an implicit assumption of turbulence and dynamic-similarity theory that for high-enough Reynolds numbers and in regions of the flow sufficiently far from inflow boundaries, the behavior of the flow can be characterized by local-flow parameters, at least in a statistical sense (*e.g.*, Batchelor 1953). In free-shear layers and some other flows, however, it is known that the initial/inflow conditions of the flow can exert a significant influence on the far-field properties, even at Reynolds numbers that are considered high.

A comparison of two of the earliest turbulent "half-jet" experiments, by Liepmann & Laufer (1947) and Wygnanski & Fiedler (1970), for example, revealed a significantly-larger growth rate in the latter experiment, a discrepancy eventually attributed to differences in the flow upstream of the separation (shear-layer formation) region. In the former experiment, the boundary layer was laminar, while in the latter it was turbulent. This increase in half-jet growth associated with a turbulent splitter-plate boundary-layer initial condition was noted by Batt (1975), and confirmed by Oster *et al.* (1976). Interestingly, for non-zero velocity ratios, *i.e.*, in shear layers with a coflowing low-speed stream, Oster and coworkers found that a turbulent high-speed boundary layer had the opposite effect, *i.e.*, a reduced downstream growth rate. This behavior for co-flowing freestreams was confirmed by the subsequent work of Browand & Latigo (1979), Weisbrot *et al.* (1982), and Mungal *et al.* (1985). In much of this work, it was found that accompanying velocity-fluctuation (rms) and Reynolds-stress profiles were subject to significant changes, in response to perturbed inflow conditions.

Shear layers are not unique in exhibiting such behavior. Other examples of turbulent flows that depend on initial/inflow conditions have also been observed. Wygnanski *et al.* (1986) reported far-field properties of turbulent wakes that depended on the shape of the body that produced the wake, *e.g.*, airfoil, plate, *etc.* A sensitivity to initial conditions was also reported for wall-bounded flows by Coles (1965), in transitional Couette-flow experiments, a behavior corroborated by recent numerical simulations (Yao & Moulic 1995).

A requirement that the local Reynolds number must be appropriately large stems from the need to have Reynolds stresses dominate viscous stresses, but also such that sufficient small-scale three-dimensionality can have developed and be sustainable. In shear layers, a relatively-well-defined transition to a state of improved mixing was documented by Konrad (1976), in gas-phase shear layers, and subsequently confirmed in liquid-phase shear layers (Breidenthal 1978, Bernal *et al.* 1979, Koochesfahani & Dimotakis 1986, and subsequently others). This transition was documented to occur at the same minimum local Reynolds number, based on the local shear-layer thickness and velocity difference, for both gas- and liquid-phase layers, indicating that this requires, at a minimum,

$$Re_\delta \equiv \frac{\rho\,\Delta U\,\delta(x)}{\mu} \gtrsim 10^4 \ , \tag{3.1}$$

or so. Similar transitions, at comparable Reynolds numbers, have been documented in many other flows, so this behavior and the applicability of this criterion must be regarded as not limited to shear-layers (*cf.* Dimotakis 1993).

This minimum Reynolds number criterion must, however, be regarded as only necessary; good mixing and quasi-asymptotic behavior is documented to have additional requirements. Bradshaw (1966) indicated that shear-layer turbulence required a relatively long distance downstream to attain an asymptotic, quasi-self-similar state. In particular, he proposed that such a state required a minimum downstream distance, *i.e.*,

$$x/\theta \gtrsim 10^3, \tag{3.2}$$

where x is the distance downstream of separation, or splitter-plate trailing edge, and θ is the momentum thickness of the separating boundary layer; an inviscid criterion that can be varied independently of Reynolds number.

It was noted by Dimotakis & Brown (1976) that such a criterion could be recast in terms of a minimum number of large-scale-structure interactions (*e.g.*, pairings, or triplings, *etc.*), estimated by them to be approximately four, as measured in terms of an estimated number of mergings,

$$m(x) \;=\; \log_2\left(\frac{x}{\ell_0}\right) \;\gtrsim\; 4 \ , \tag{3.3}$$

that assumes that pairing interactions are dominant, *i.e.*, a measure of the downstream distance, x, as scaled by the initial-disturbance spacing, ℓ_0. They argued that this minimum distance and minimum number of interactions were required to amortize the effects of initial (inflow) conditions.

In subsequent work by Huang & Ho (1990), a similar scaling of the downstream distance was proposed,

$$P = \frac{1-r}{1+r}\left(\frac{x}{\ell_0}\right) \approx \frac{1-r}{1+r}\left(\frac{x}{30\,\theta_1}\right) , \tag{3.4a}$$

where $r \equiv U_2/U_1$ is the shear-layer freestream velocity ratio and θ_1 is the initial, high-speed boundary-layer momentum thickness. Huang & Ho argued that this parameter effectively described the approach to self-similarity for a variety of shear-layer flows, *i.e.*, for different velocity ratios, r (*cf.* also Ho & Huerre 1984). They suggested that a minimum value of 8 was required for self-similarity of the peak turbulence level in gas-phase flows, *i.e.*,

$$P_{\mathrm{HH}} \gtrsim 8 , \tag{3.4b}$$

corresponding to the location of the *second* large-structure pairing, according to their estimate, *i.e.*, a criterion more relaxed than the one suggested by Dimotakis & Brown. These authors also noted that the properties of this self-similar state appeared to be influenced, if not determined by, the initial conditions of turbulence formation, regardless of the distance from separation.

We note that the velocity-ratio scaling factor in Eq. 3.4 is proportional to the local, normalized, large-scale spacing, $\ell(x)/x$, independently of the freestream density ratio (*cf.* Dimotakis 1986), and, therefore, as a measure, the Huang & Ho parameter, P, is proportional to $\ell(x)/\ell_0$, rather than x/ℓ_0.

Much of the previous work included measurements of shear-layer growth rates, Reynolds stresses, *etc.* Only limited data are available, however, regarding the response and sensitivity of the shear-layer concentration field and its mixing properties to changes in inflow conditions. Given the large-scale effects observed in the work cited above, one might also expect significant influences in the small-scale behavior of the flow, which is important in molecular/diffusion-scale mixing processes.

Indeed, hints of such behavior can be found in other flows. By way of example, far-field jet-fluid concentration-fluctuation statistics, in the far field of a turbulent jet, were found to be strongly influenced by small (when scaled by the jet-exit velocity) velocity fluctuations in the reservoir fluid that the jet discharged into (Miller 1991).

Some recent work on scalar mixing in a shear-layer flow was reported by Karasso & Mungal (1996). These authors found the Huang & Ho (1990) scaling parameter useful in their analysis of their measured estimates of the concentration-field probability-density function (pdf). Dubbing P the "pairing parameter" (Eq. 3.4), they proposed a minimum value for a converged mixed-fluid state (scalar pdf) of $P \simeq 22$, corresponding to a distance between the average locations of third and fourth vortex interaction; more closely in accord with the original proposal of Dimotakis & Brown (1976). Despite expressing reservations about the accuracy of their direct-measurement, laser-induced fluorescence results, on which their pdf experimental-estimates relied, they suggested that this value determined the transition between a "non-marching" pdf, where the most-probable concentration is nearly-independent of the transverse coordinate, y, and a "tilted" pdf, in which the composition is correlated with the local mean, *i.e.*, a function of y. In particular, they proposed that the former would be observed for $P \lesssim 22$, while the latter for $P \gtrsim 22$, *i.e.*, that self-similarity can be expected for,

$$P_{\mathrm{KM}} \gtrsim 22 \ . \tag{3.4c}$$

Karasso & Mungal also studied the effects of tripping the initial boundary layers, stating that the effect of tripping was to decrease the (absolute) distance, x, required to reach self-similarity, in accord with the behavior reported by Bell & Mehta (1990), who stated that, "The distance required to achieve self-similarity was distinctly shorter in the tripped case, ..." Karasso & Mungal further suggested that beyond this distance, inflow conditions were "forgotten" by the turbulence, with a unique far-field configuration, that only depends on the (local) freestream-velocity and -density ratios. Since tripping the boundary layer(s) can be expected to result in an increase in the initial momentum thickness(es), it would appear that this observation is not in accord with a minimum-threshold criterion based on the pairing parameter P, or any other measure of distance downstream scaled by initial boundary-layer thickness scales.

3.2 Experiments

Experiments were performed at a single nominal flow condition, with freestream speeds,

$$U_1 \simeq 100\,\mathrm{m/s} \quad \text{and} \quad U_2 \simeq 40\,\mathrm{m/s}\ , \qquad i.e.,\quad r \equiv \frac{U_2}{U_1} \simeq 0.4\ , \tag{3.5a}$$

and a density ratio of,

$$s \equiv \frac{\rho_2}{\rho_1} \simeq 1.0\ . \tag{3.5b}$$

The velocity and density ratios were chosen to facilitate a comparison with previous work on (incompressible) chemically-reacting flows, at similar freestream conditions (*e.g.*, Mungal *et al.* 1985, Frieler & Dimotakis 1988, Hermanson & Dimotakis 1989, Bond & Dimotakis 1996), as well as Island (1997), who investigated molecular mixing in shear-layers at different conditions, however, using a fluorescence-quenching ("cold-chemistry") technique.

The pressure and temperature profiles in these experiments were recorded at a single measuring station, $x = 0.365\,\mathrm{m}$, where x is measured from the location of the splitter-plate tip. Profiles were measured as a function of the transverse coordinate, y, that is also referenced to the splitter-plate tip. The resulting shear layers have a local Reynolds number at the measuring station in the range,

$$1.8\times 10^5 \lesssim Re_\delta = \frac{\rho\,\Delta U\,\delta(x)}{\mu} \lesssim 2.4\times 10^5\ , \tag{3.6}$$

where $\Delta U \equiv U_1 - U_2$ is the freestream velocity difference, and ρ and μ are the mixed-fluid density and viscosity, respectively. These are calculated using the properties of a gas mixture with a high-speed fluid mole fraction given by X_E (Eq. 2.9), assuming conservation of (total) enthalpy to estimate the mixed-fluid density, ρ, and the method of Wilke (1950) to estimate the mixed-fluid (shear) viscosity, μ. These parameters were kept nominally fixed to isolate effects of variable inflow conditions, as each is known to influence shear-layer growth, entrainment, and mixing. The range in Eq. 3.6 arises primarily from variations in local shear-layer thickness, $\delta(x)$, in each case, as will be documented below.

	θ/mm	$Re_\theta \equiv \rho U\theta/\mu$	x/θ	P (Eq. 3.4)
High-speed side:	0.11	640	3.3×10^3	47
Low-speed side:	0.17	400	2.1×10^3	-

Table 3.1: Untripped (natural) splitter-plate boundary-layer flows.

Changes in inflow conditions were effected through various combinations of trip wires on the splitter plate. For freestream conditions in these experiments, estimated boundary-layer properties at the splitter-plate tip ($x = 0$) are listed in Table 3.1. As described in Ch. 2, three sets of experimental runs were performed to create a "flip experiment". These relied on chemically-reacting flows, with stoichiometric-mixture ratios of $\phi = \phi_0$ and $\phi = 1/\phi_0$, for $\phi_0 = 8$, in addition to non-reacting flows ("cold" runs). Table 3.2 lists the flow conditions and freestream fluid compositions for these runs.

3.1 - Fluorine-rich ($\phi = 8$, $\Delta T_f \simeq 171\,\mathrm{K}$):

$U_1 \simeq 100\,\mathrm{m/s}$: 8.00% Ar, 15.07% He, 0.93% H_2, 0.14% NO, 75.86% N_2
$U_2 \simeq 40\,\mathrm{m/s}$: 16.00% He, 8.00% F_2, 76.00% N_2 .

3.2 - Hydrogen-rich ($\phi = 1/8$, $\Delta T_f \simeq 267\,\mathrm{K}$):

$U_1 \simeq 100\,\mathrm{m/s}$: 8.00% Ar, 4.00% He, 12.00% H_2, 0.75% NO, 75.25% N_2
$U_2 \simeq 40\,\mathrm{m/s}$: 6.45% Ar, 16.00% He, 1.55% F_2, 76.00% N_2 .

3.3 - Hydrogen-rich, reduced concentration ($\phi = 1/8$, $\Delta T_f \simeq 171\,\mathrm{K}$):

$U_1 \simeq 100\,\mathrm{m/s}$: 8.00% Ar, 8.00% He, 8.00% H_2, 0.50% NO, 75.50% N_2
$U_2 \simeq 40\,\mathrm{m/s}$: 6.97% Ar, 16.00% He, 1.03% F_2, 76.00% N_2 .

3.4 - Non-reacting:

$U_1 \simeq 100\,\mathrm{m/s}$: 8.00% Ar, 16.00% He, 76.00% N_2
$U_2 \simeq 40\,\mathrm{m/s}$: 8.00% Ar, 16.00% He, 76.00% N_2 .

Table 3.2: Freestream speeds and compositions.

The local Reynolds numbers for the shear layers investigated, at the $x = 0.365\,\mathrm{m}$ measuring station (Eq. 3.6), are higher than in the previous shear-layer, molecular-mixing work by Mungal *et al.* (1985), which included an exploratory investigation of inflow effects. In the facility used for the present experiments, it was possible to increase flow speeds (and measuring-station Reynolds numbers), such that the natural (unperturbed) flow boundary layers could be expected to remain laminar, but at high-enough Reynolds numbers to permit a transition to turbulent boundary-layers, if tripped. For higher Reynolds numbers yet, the naturally-occurring splitter-plate boundary layers would be transitional, or naturally turbulent, and purposely altering inflow conditions by tripping would not be expected to have as large an effect.

3.3 Results and discussion

Normalized temperature-rise profile measurements for the natural (untripped) flow conditions (Cases 3.1–3) are plotted in Fig. 3.1. The corresponding velocity-profile data are plotted in Fig. 3.2.

To ensure that the flows were in the kinetically-fast, high-Da limit (*cf.* Eq. 2.5 and associated discussion), reactant concentrations for the kinetically-slower of the two cases (H_2-rich, $\phi = 1/8$ case) were reduced to those listed under Case 3.3 (Table 3.2). Da's associated with the F_2-rich ($\phi = 8$) case of the flip experiment are higher than those of the H_2-rich ($\phi = 1/8$) case, with higher concentrations of the rate-limiting (free) fluorine atoms in the former case. The Da ratio for the two $\phi = 1/8$ cases is computed to be larger than 3, if a homogeneous-composition, constant-pressure, "balloon" reactor (Dimotakis & Hall 1987) is used to estimate the reaction-completion times: $\tau_{\mathrm{chem}} = 0.45\,\mathrm{ms}$ and $1.50\,\mathrm{ms}$, respectively (*cf.* Eq. 2.5). As can be seen in Fig. 3.1, the two $\phi = 1/8$ temperature-rise profiles, corresponding to the already kinetically-slower of the two ϕ's, are within typical experimental reproducibility, demonstrating that the flows are in the high-Da regime.

The values of the adiabatic-flame temperature rise, ΔT_{f}, for these runs are all in a regime where dilatation and other heat-release effects have been documented to

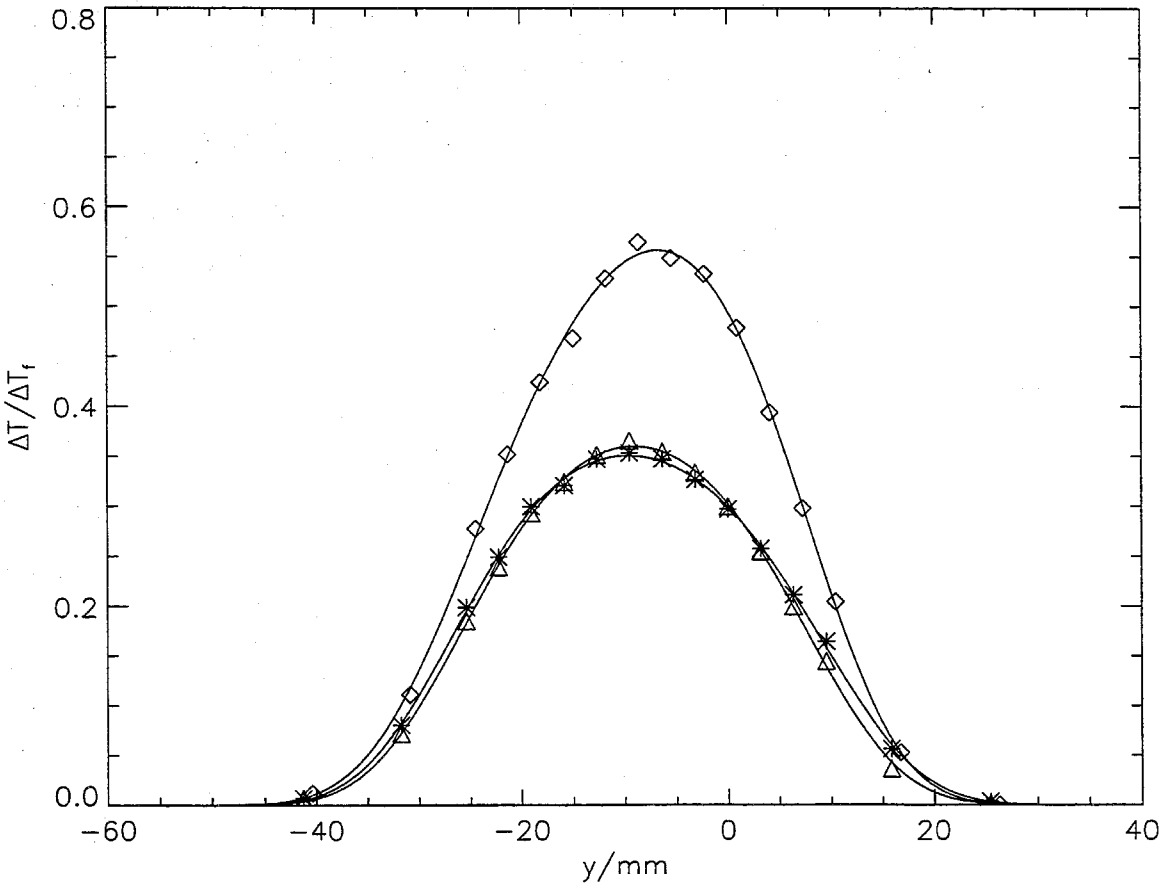

FIG. 3.1 Normalized temperature-rise data with natural (untripped) boundary layers. Diamonds: Case 3.1, $\phi = 8$. Triangles: Case 3.2, $\phi = 1/8$. Asterisks: Case 3.3, $\phi = 1/8$, reduced chemical-kinetic rate.

be small (Hermanson & Dimotakis 1989), once displacement effects from dilatation are removed, as was done here (see discussion in Ch. 2, above). This can be directly confirmed by comparing the temperature-rise profiles, and 1% thicknesses, δ_T, of Case 3.1 runs with those of Case 3.2 runs, for which $\Delta T_f/T_0$ is substantially different, by comparing Case 3.2 with Case 3.3 runs, since both are in the fast-kinetic regime. This collapse demonstrates that heat-release effects are weak; the adiabatic flame temperature rise, ΔT_f, was lower by over a factor of 1.5 for the kinetically-slower case (*cf.* Table 3.2). No significant heat-release effects are manifest in the velocity profiles either, with differences typical of the small run-to-run variations.

Acoustic forcing is known to exert an important influence on both large-scale

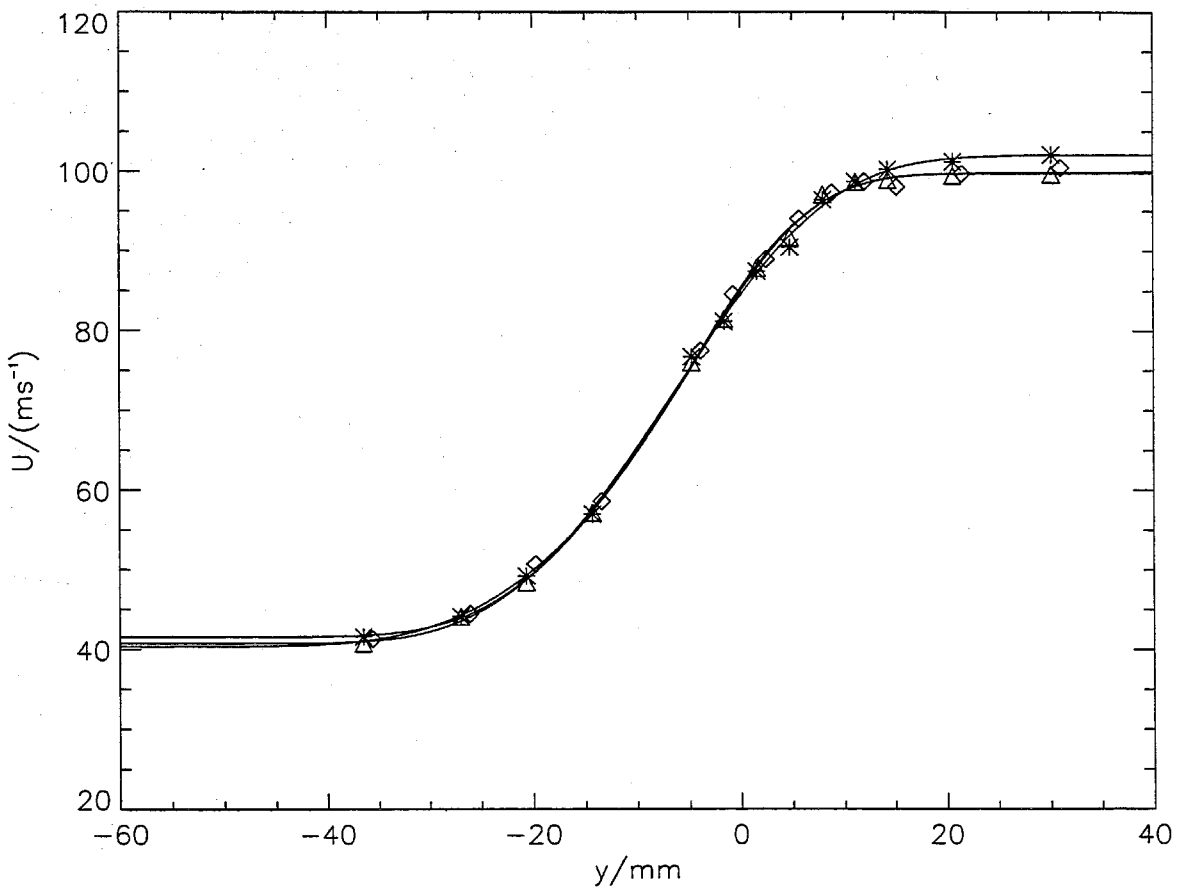

FIG. 3.2 Velocity profiles for natural (untripped) flows. Legend as in Fig. 3.1.

entrainment (*e.g.*, Koochesfahani & MacKinnon 1991), as well as on turbulent-fluctuation profiles (*e.g.*, Wygnanski *et al.* 1979). Acoustic forcing resonant with some local, large-scale-passage frequency at an intermediate downstream location would result in non-linear shear-layer growth rates (*e.g.*, Wygnanski *et al.* 1979, Oster & Wygnanski 1982, Ho & Huang 1982, Ho & Huerre 1984, Dziomba & Fiedler 1985, Roberts 1985, and Roberts & Roshko 1985).

All shear layers investigated in the present experiments exhibit a very-nearly-linear growth rate, *i.e.*, $\delta(x) \propto x$, as seen in the flow-visualization data reproduced in Fig. 3.3. Such data represent instantaneous flow visualizations, *i.e.*, are not time averaged. They are subject, however, to an evolving aspect ratio, $b/\delta(x)$, where $b = 15.3\,\mathrm{cm}$ is the fixed span, while $\delta(x) \propto x$, as the layer grows. Any three-dimensional structure of the flow will be scaled by the linearly-increasing local width,

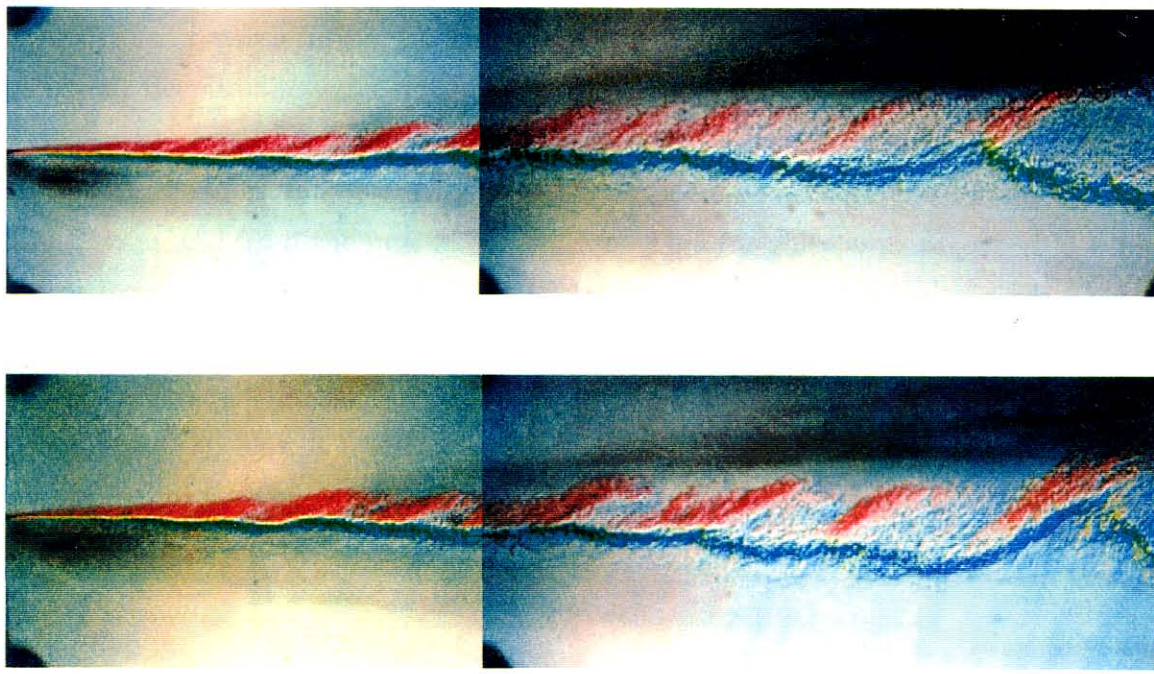

FIG. 3.3 Composite color-schlieren images of untripped (natural), Case 3.2 flows. Note linear growth and similar large-scale structure, indicating self-similar flow.

$\delta(x)$, at its largest scales. As a consequence, an apparent evolution in "coherence", *i.e.*, an artifact of the visualization, can be expected to make the flow look as if it is becoming increasingly two-dimensional with increasing downstream distance.

The temperature-rise data in Fig. 3.1 were used to compute the various quantities described above. In particular, for this natural (untripped) flow:

$$\begin{aligned} &\text{Case 3.1:} \quad \phi = 8 \ , \quad \delta_T/x = 0.178 \ , \quad \delta_p/\delta_T = 0.277 \ ; \\ &\text{Case 3.2:} \quad \phi = 1/8 \ , \quad \delta_T/x = 0.177 \ , \quad \delta_p/\delta_T = 0.184 \ , \end{aligned} \tag{3.7a}$$

where δ_T is the temperature-rise profile 1% thickness and δ_p is the product thickness (Eq. 2.6). These numbers are determined with a precision for each flow of $\lesssim 1\%$, with a run-to-run reproducibility, at these flow conditions, in the range of $1\% - 3\%$. The reproducibility of the local shear layer width, δ_T/x, between different runs is indicative of this behavior. These can be used to compute the mixed-fluid fraction (Eq. 2.7),

$$\delta_m/\delta_T \ = \ 0.410 \ . \tag{3.7b}$$

As can be seen in Fig. 3.1, the locations of the peak temperature rise are nearly aligned, despite the extreme shift in stoichiometric-mixture ratio (from $\phi = 1/8$ to $\phi = 8$). Such behavior is indicative of a "non-marching" pdf, *i.e.*, a pdf that is nearly independent of y, corresponding to local compositions that do not favor fluid entrained from the nearest freestream. These profiles were recorded in a high local Reynolds number ($Re_\delta \sim 2 \times 10^5$) shear-layer flow, far downstream ($x/\theta_1 \simeq 3.3 \times 10^3$), and corresponding to a high value of the pairing parameter ($P \simeq 47$). As discussed in the Introduction, by any of the measures employed to characterize such flows (*cf.* Eqs. 3.1, 3.2, and 3.3 and 3.4a-c), these data were recorded in an environment that must be regarded as representing fully-developed turbulent shear flow.

The implied mixed-fluid composition at these conditions is at variance with the report by Karasso & Mungal (1996). As discussed by these authors, one might expect some spatial "flip" shift in the two temperature-rise peaks, *i.e.*, that the F_2-rich ($\phi = 8$) case would have a peak temperature shifted towards the lean-reactant, H_2-bearing freestream, and vice-versa for the H_2-rich ($\phi = 1/8$) case, at least in high Reynolds number shear-layer flows. Examples of such behavior are found in the references cited above (*cf.* data and discussion in Dimotakis 1991a), and are indicative of a pdf that is "marching", as it has become known, in which mixture composition favors the fluid of the closer of the two freestreams and is a weak function of the transverse coordinate, y. An absence of flip shift, similar to that seen here, was observed in the lower-Re, liquid-phase, chemically-reacting shear-layer flows of Koochesfahani & Dimotakis (1986). Such behavior has been attributed to Schmidt number effects, Lagrangian-time-frame delays in mixing, or finite chemical-kinetic rate effects in discussions of the BBM model (*cf.* Broadwell & Mungal 1991). Alternatively, Rogers & Moser (1992, 1994) have attributed this to a higher degree of two-dimensional organization in the flow. In their simulations of temporally-developing shear layers, these authors found a correlation between the degree of two-dimensionality of conditions used to initialize the simulation and the characteristics of the pdf that persists for the duration of the simulation time. In particular, for initial conditions dominated by two-dimensional disturbances, the flow structure largely maintained the two-dimensionality, yielding a scalar field described by a non-marching pdf. When initialized by a more three-dimensional

disturbance field, however, the flow evolved differently, yielding a marching pdf. These temporal-flow simulations were conducted at $Re_\delta \lesssim 2 \times 10^4$, *i.e.*, just past the mixing transition (Eq. 3.1). As noted by the authors, the flow did not appear to have reached a self-similar state during the simulation time, at least for the strongly-two-dimensional case.

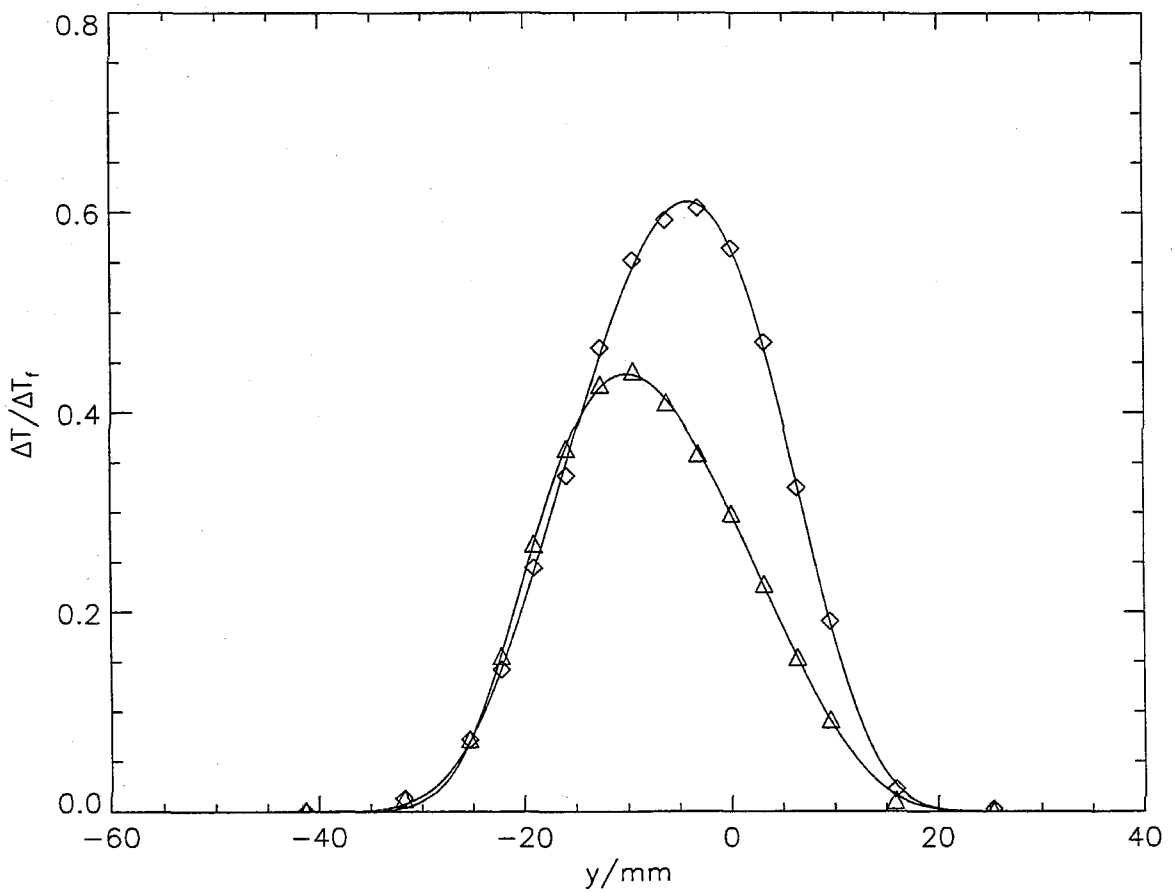

FIG. 3.4 Normalized temperature-rise data with tripped high-speed boundary layers. Diamonds: Case 3.1 ($\phi = 8$). Triangles: Case 3.2 ($\phi = 1/8$).

To explore the sensitivity to inflow conditions, a 0.8 mm-diameter trip wire was placed on the upper (high-speed) face of the splitter plate, 50 mm upstream of the splitter-plate trailing-edge. The naturally-occurring boundary-layer is estimated to be laminar, with a momentum thickness of 0.095 mm at the trip location (trailing-edge values in Table 3.1), estimated using the method of Thwaites. The trip-wire size and position matched those employed by Mungal *et al.* (1985), in the

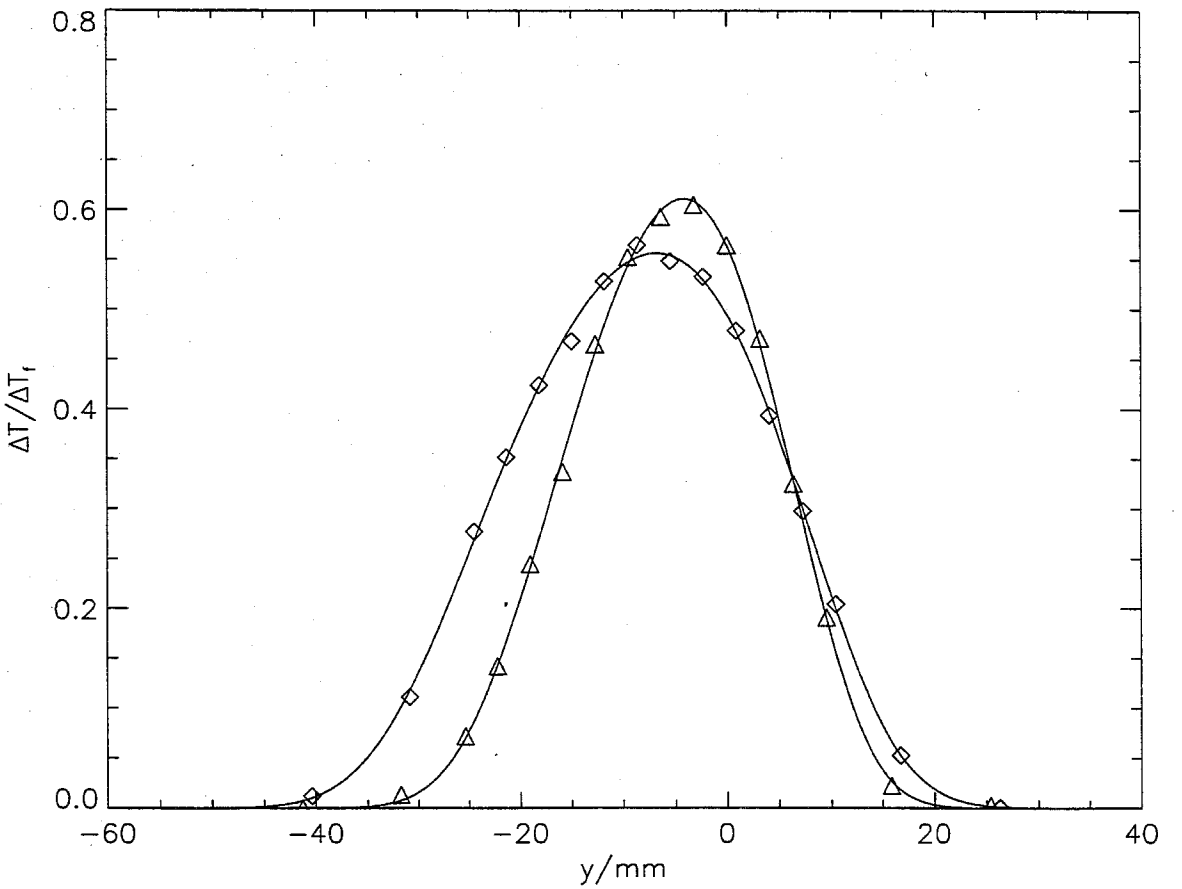

FIG. 3.5 Normalized temperature-rise data for tripped and untripped boundary layers at $\phi = 8$. Both experiments with Case 3.1 reactant concentrations. Diamonds: untripped high-speed boundary layer, triangles: tripped high-speed boundary layer.

previous (subsonic) version of this facility. White (1974) recommends a Reynolds number based on wire diameter in excess of 0.85×10^3 to ensure transition (in a receptive boundary layer). The trip wire Reynolds number in this flow is estimated to be 4.6×10^3. The resulting temperature-rise and streamwise-velocity profile data, corresponding to those plotted in Figs. 3.1 and 3.2, are plotted in Figs. 3.4 and 3.7, respectively, with schlieren data reproduced in Fig. 3.8. In addition, a direct comparison of the normalized temperature-rise profiles in the untripped and tripped flows is found in Figs. 3.5 and 3.6, for the F_2-rich ($\phi = 8$) and H_2-rich ($\phi = 1/8$) stoichiometries, respectively.

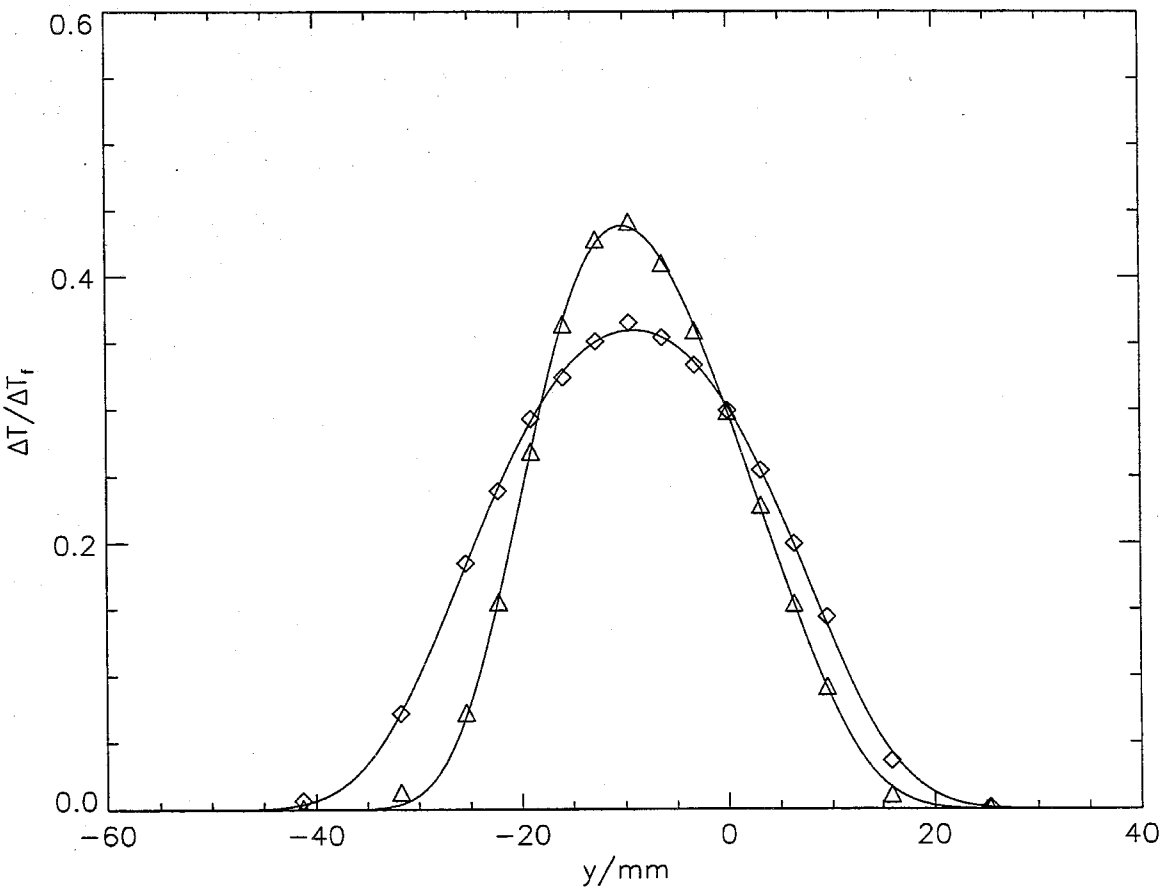

FIG. 3.6 Normalized temperature-rise data for tripped and untripped splitter-plate boundary layers at $\phi = 1/8$. Both experiments with Case 3.2 reactant concentrations. Legend as in Fig. 3.5.

The temperature-rise profiles in Fig. 3.4 are measured 0.415 m, or, approximately, 500 trip-wire diameters, downstream of the trip location; in the "far-field" of this perturbation. The untripped flow, at the same location, satisfies all previously-proposed criteria for fully-developed flow. In the case of the tripped boundary-layer flow, even if the boundary layer (momentum thickness) was assumed to increase to 1/3 the trip-wire diameter, the same criteria would still be satisfied.

The shear-layer growth and mixed-fluid quantities, for the flows with the high-speed boundary-layer tripped, were also derived from these temperature-rise profile

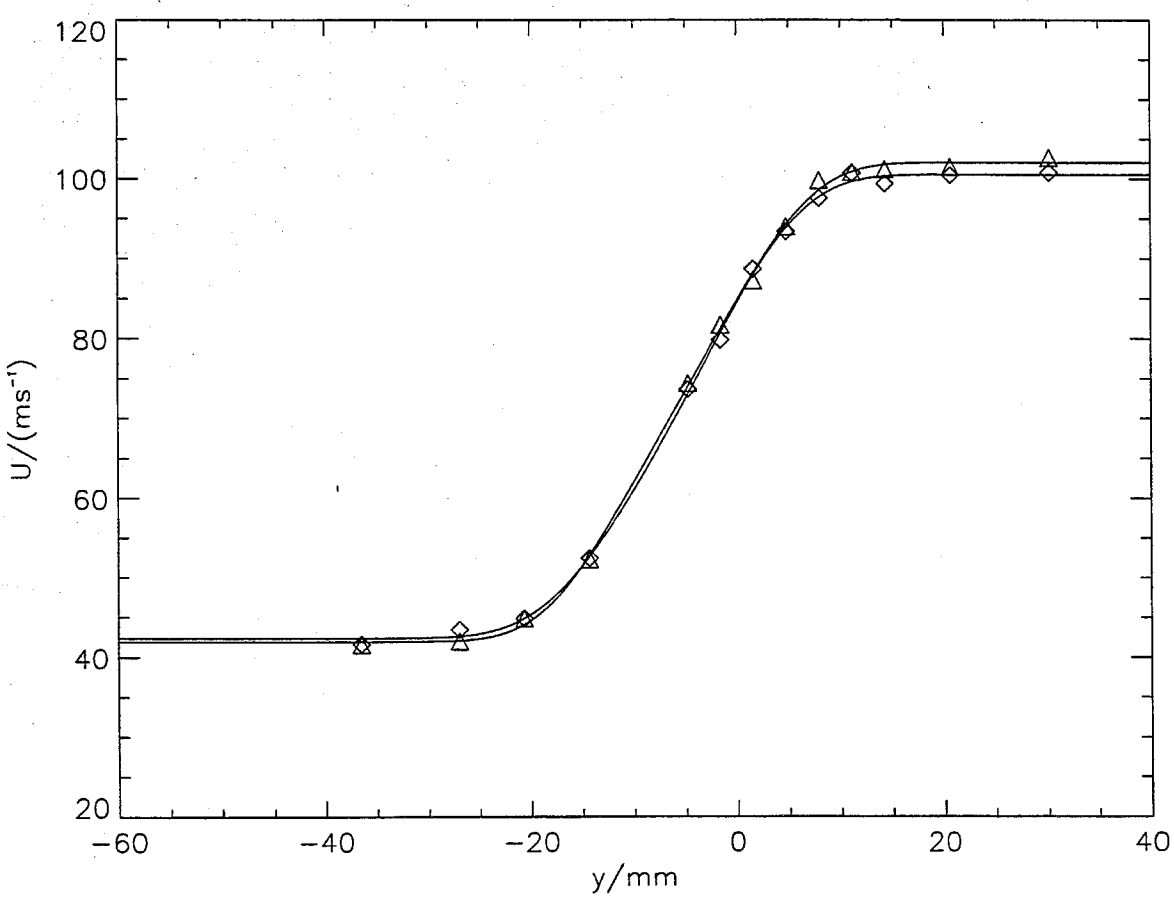

FIG. 3.7 Velocity profiles for the flows with tripped high-speed side boundary layers. Legend as Fig. 3.4.

data,

$$\begin{aligned} &\text{Case 3.1:} \quad \phi = 8\ , \quad \delta_{\mathrm{T}}/x = 0.140\ , \quad \delta_{\mathrm{p}}/\delta_{\mathrm{T}} = 0.293\ ; \\ &\text{Case 3.2:} \quad \phi = 1/8\ , \quad \delta_{\mathrm{T}}/x = 0.138\ , \quad \delta_{\mathrm{p}}/\delta_{\mathrm{T}} = 0.211\ , \end{aligned} \tag{3.8a}$$

yielding a mixed-fluid fraction of,

$$\delta_{\mathrm{m}}/\delta_{\mathrm{T}} \ = \ 0.448\ . \tag{3.8b}$$

Comparing with the untripped boundary-layer data (Eq. 3.7), tripping the high-speed boundary layer can be seen to have resulted in a growth rate, $\delta(x)/x$, that is lower by $21\% \pm 1.5\%$. This must be regarded as a substantial reduction considering that this flow should have attained quasi-asymptotic behavior, *i.e.*, one in which

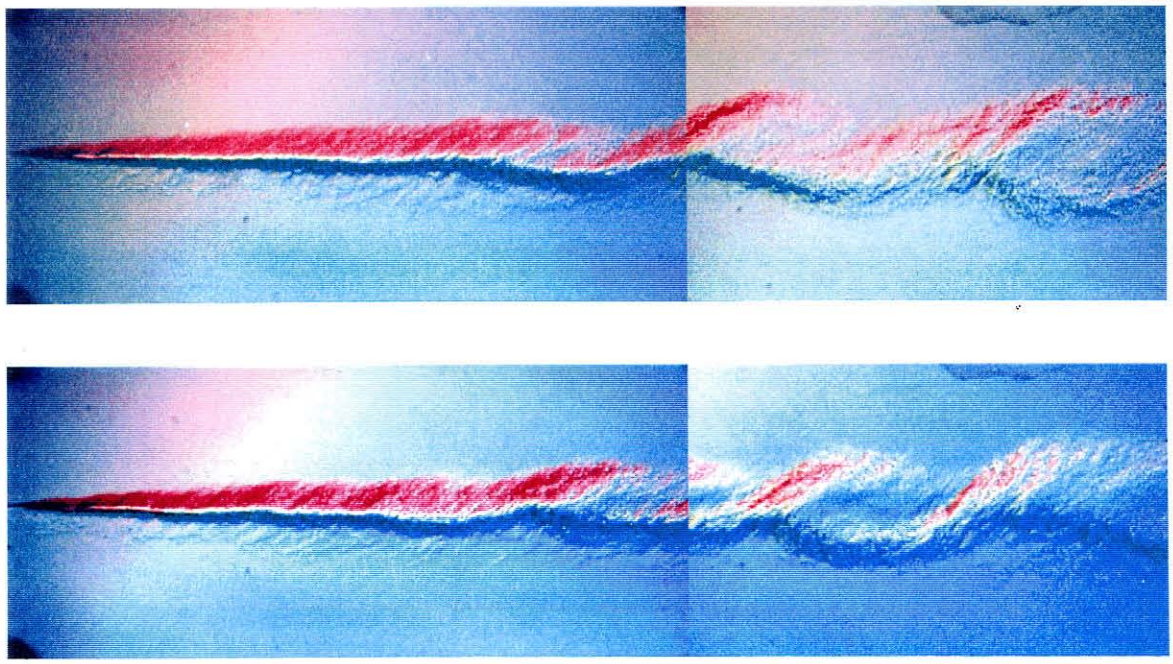

FIG. 3.8 Composite color-schlieren images of tripped (0.8 mm wire on high-speed side), Case 3.2 flows. Note linear growth and geometrically-similar large-scale structures.

inflow/initial conditions are expected to exert a minimal influence, if any. This reduction, however, is in qualitative accord with previous investigations, at lower Re_δ, of two-stream (as opposed to half-jet) shear layers, as discussed in the Introduction.

Significantly, the temperature-rise data for the tripped high-speed boundary-layer exhibit a "flip" shift, indicating that a transition to a "tilted" molecularly-mixed-fluid pdf has occurred, *i.e.*, the mixed-fluid composition is now a function of the transverse coordinate, y. If this is to be expected of turbulence in a "more-developed" state, as suggested by Karasso & Mungal (1996), it cannot be attributed to an increase in Reynolds number. The 21% reduction in local thickness, $\delta(x)$, induced by tripping the high-speed side boundary layer, *decreases* the local Reynolds number, Re_δ, by the same amount. The data are also at variance with the proposed Karasso & Mungal criteria for pdf evolution and behavior, in terms of the change in x/θ_1. The tripped flow has a slightly-thicker high-speed boundary layer, *i.e.*, a higher θ_1, and, therefore, a lower scaled downstream distance, x/θ_1, as well as pairing parameter, P. Changes in this direction should have had the opposite effect, *i.e.*, taken a "non-marching" pdf, characteristic of "undeveloped" flow, to a

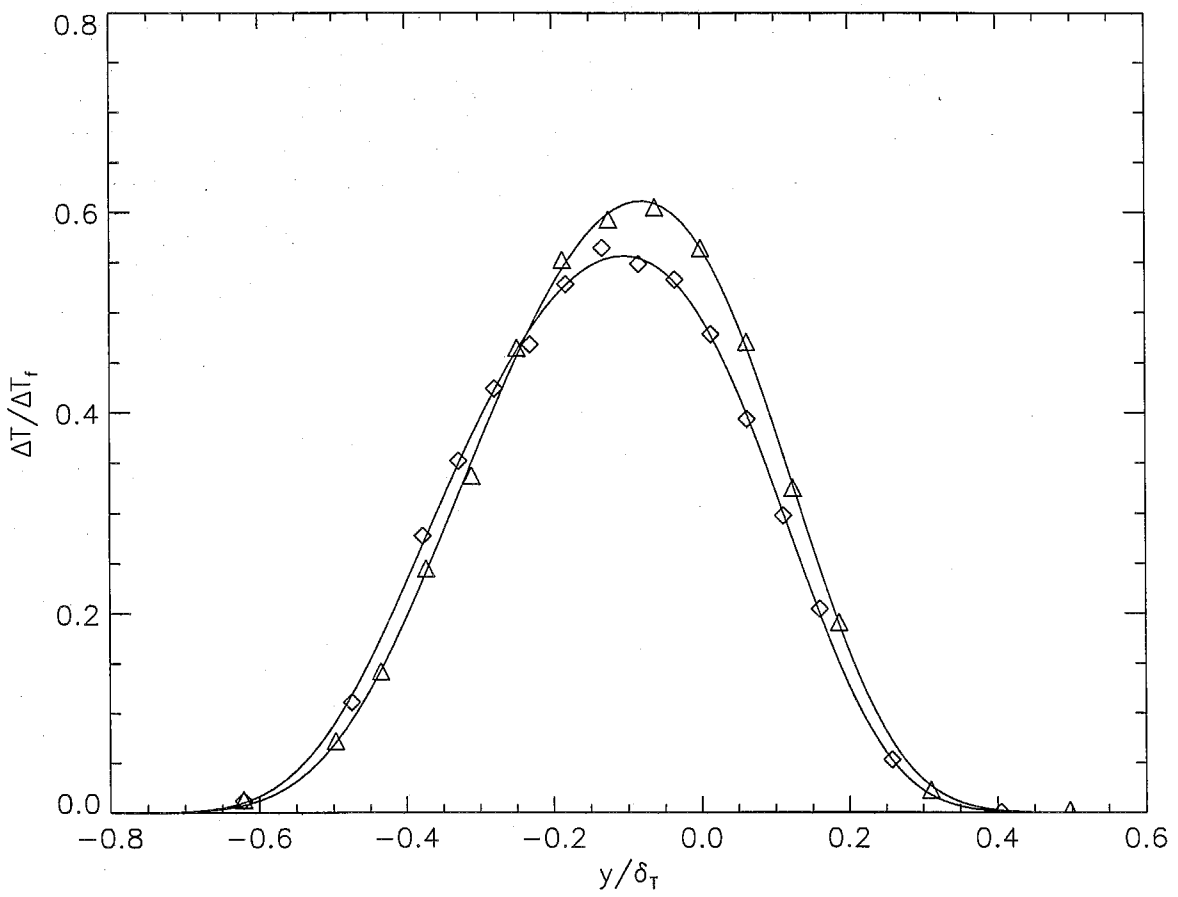

FIG. 3.9 Normalized temperature-rise data for tripped and untripped splitter-plate boundary layers at $\phi = 8$. Transverse coordinate normalized by δ_T. Diamonds: untripped high-speed side, triangles: tripped high-speed side.

"marching" pdf, characteristic of "developed" flow, according to these authors.

Tripping reduced entrainment and shear-layer growth far downstream of the change in inflow conditions. Interestingly, it also produced more vigorous stirring and effective molecular mixing. The latter can be ascertained by plotting the data, scaling the transverse coordinate by the local width, *i.e.*, y/δ_T, as in Figs. 3.9 and 3.10. It is in these units that the computation of the mixed-fluid fraction, δ_m/δ_T, is performed (Eq. 2.7). The increase in chemical product and molecular mixing within the shear layer, in each case, is clear. As can be seen by comparing the product fractions, δ_p/δ_T, for the two cases (Eqs. 3.7 *vs.* 3.8), the increase is approximately 6% in the $\phi = 8$ flow and 16% in the $\phi = 1/8$ flow.

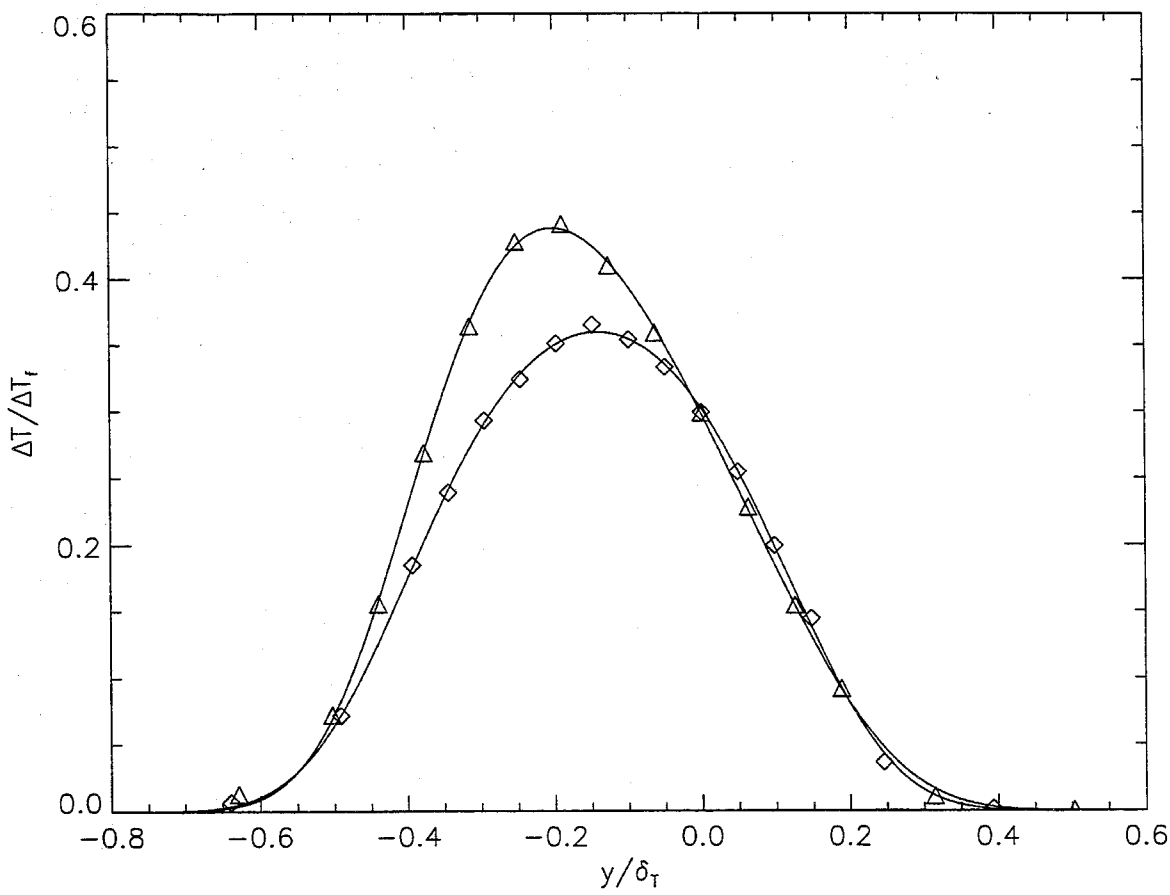

FIG. 3.10 Normalized temperature-rise data for tripped and untripped boundary layers at $\phi = 1/8$. Transverse coordinate normalized by δ_T. Legend as Fig. 3.9.

Comparing the schlieren image data in Fig. 3.3 and Fig. 3.8 reveals that tripping the high-speed-side boundary layer has not only changed the growth rate, but also the large-scale structure, far downstream. For the tripped flow, a decrease in two-dimensional organization of the flow is evident, with spanwise optical integration obscuring local large-scale-structures in the upstream half of the flow. The inferred "marching" scalar pdf behavior for this flow is observed along with this decrease in two-dimensional organization, as also noted by Rogers & Moser (1994) in their numerical simulations. In the context of large-scale-entrainment models for this flow (Dimotakis 1986, 1991b), a change in the entrained-fluid mole ratio, E_n, is expected. While this was not measured, one can infer the mixed-fluid molar composition ratio, estimated with Eq. 2.8. The two ratios, E_n and $\mathcal{E}_n$, need not have the same value.

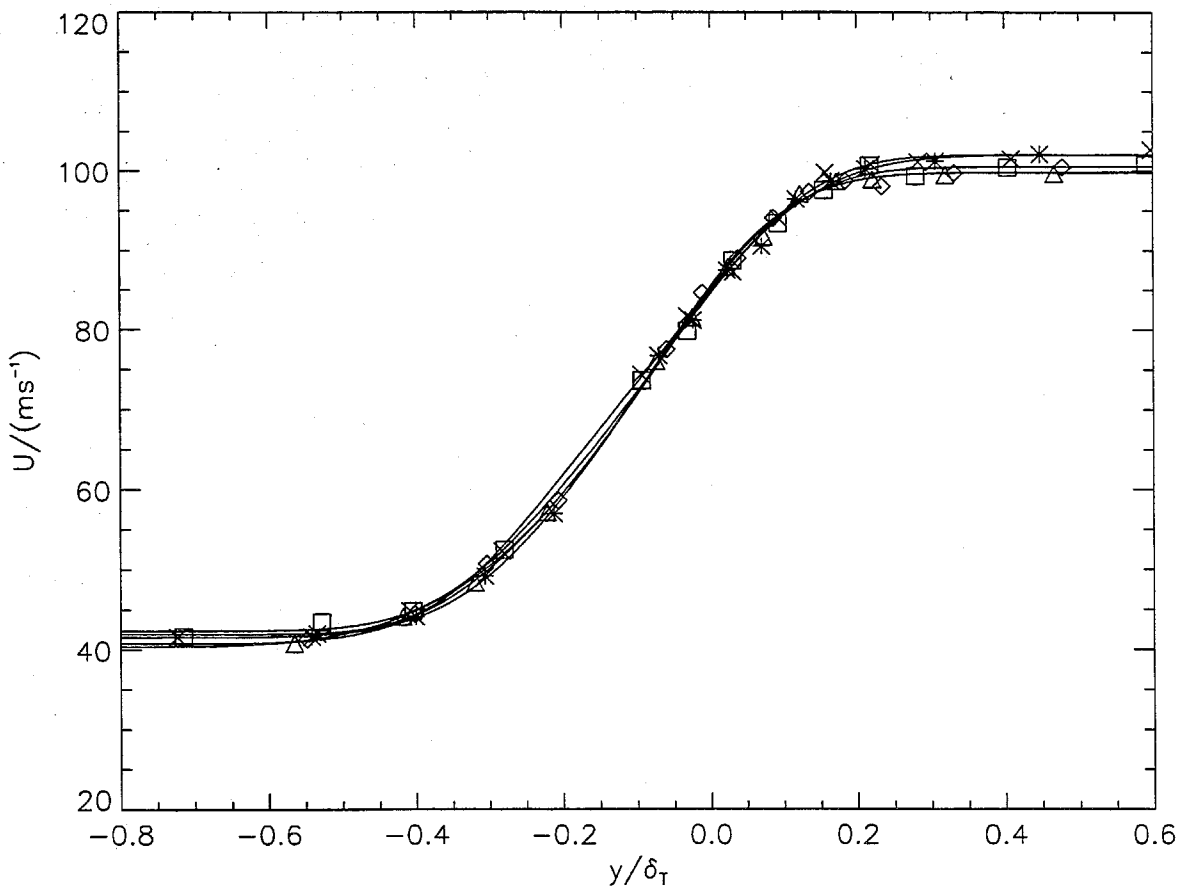

FIG. 3.11 Velocity profiles for both untripped and tripped flows. Transverse coordinate normalized by 1% temperature-rise thickness.

The former measures the entrained-fluid ratio, at the largest scales of the flow, whereas the latter measures the mixed-fluid ratio. Using the tripped and untripped shear layer temperature-rise measurements, we find (Eq. 2.8),

$$(\mathcal{E}_{\rm n})_{\rm untripped} \simeq 1.52 \ , \qquad vs. \qquad (\mathcal{E}_{\rm n})_{\rm tripped} \simeq 1.39 \ , \tag{3.9}$$

i.e., a shift to a lower mixed-fluid ratio (closer to symmetric). Interestingly, the increase in the large-scale-structure spacing-to-position ratio induced by tripping, evident in the schlieren data, suggests that the change in $E_{\rm n}$ is towards larger values, *i.e.*, in the opposite direction.

The velocity profiles for the untripped and tripped flows examined thus far are plotted in Fig. 3.11, *vs.* the normalized transverse coordinate, $y/\delta_{\rm T}$, for comparison.

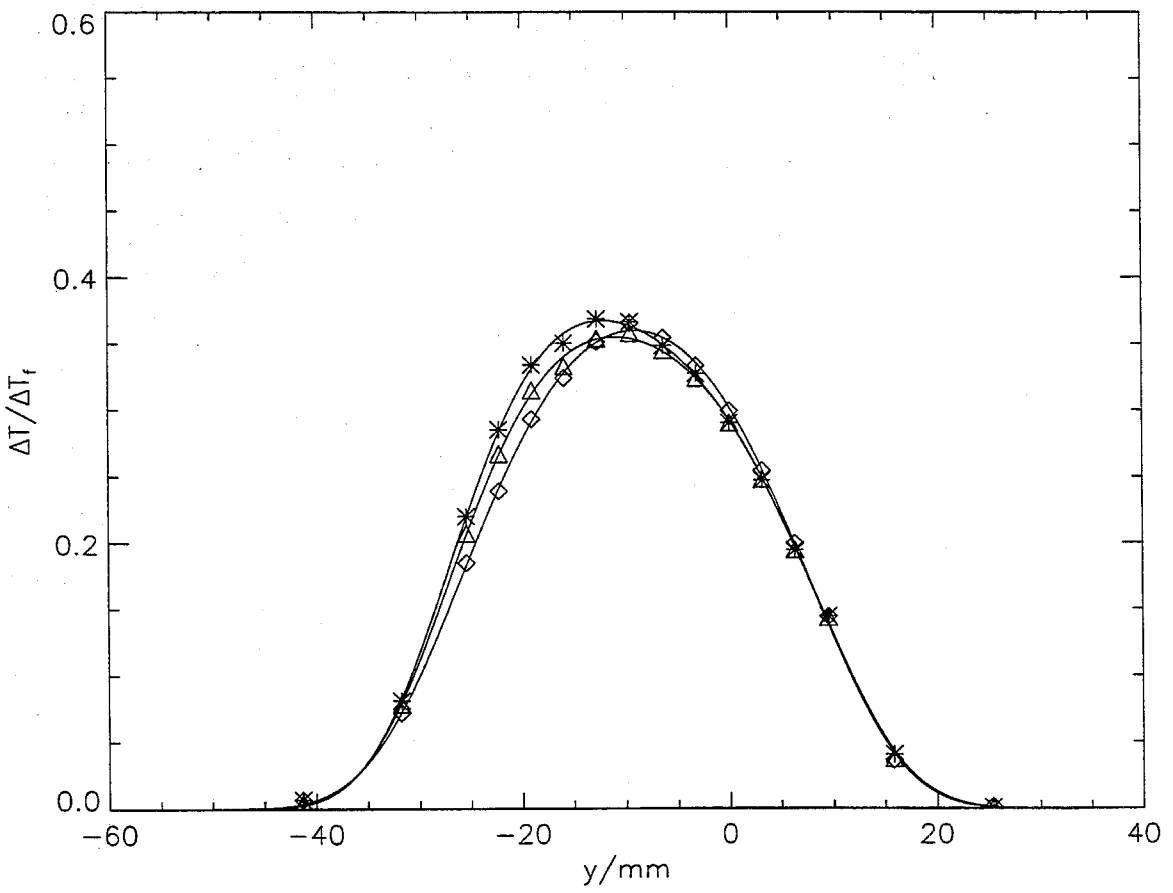

FIG. 3.12 Normalized temperature-rise data with various low-speed boundary layer trips. All flows with Case 3.2 reactant concentrations. Diamonds: Untripped flow. Triangles: 0.8 mm trip wire. Asterisks: 1.6 mm trip wire.

This scaling can be seen to produce a substantial collapse of the mean, streamwise velocity profile at the measuring station, despite the differences between tripped and untripped flows discussed above. This collapse also demonstrates that the transverse length scale, as estimated on the basis of mixed-fluid/temperature-rise data, also scales the velocity field, *i.e.*, that $\delta_{\mathrm{u}}(x) \simeq \delta_{\mathrm{T}}(x)$, where $\delta_{\mathrm{u}}(x)$ would be some appropriate velocity-profile-based transverse width. Finally, the collapse in the scaled profiles in Fig. 3.11 indicates that the mean velocity is largely insensitive to the processes responsible for the changes in entrainment and mixing. Accordingly, it would be surprising if shear-layer-entrainment and -mixing models based on mean-velocity profiles, *e.g.*, of eddy-viscosity-type, could accommodate, let alone predict, the observed mixing dependence on inflow conditions.

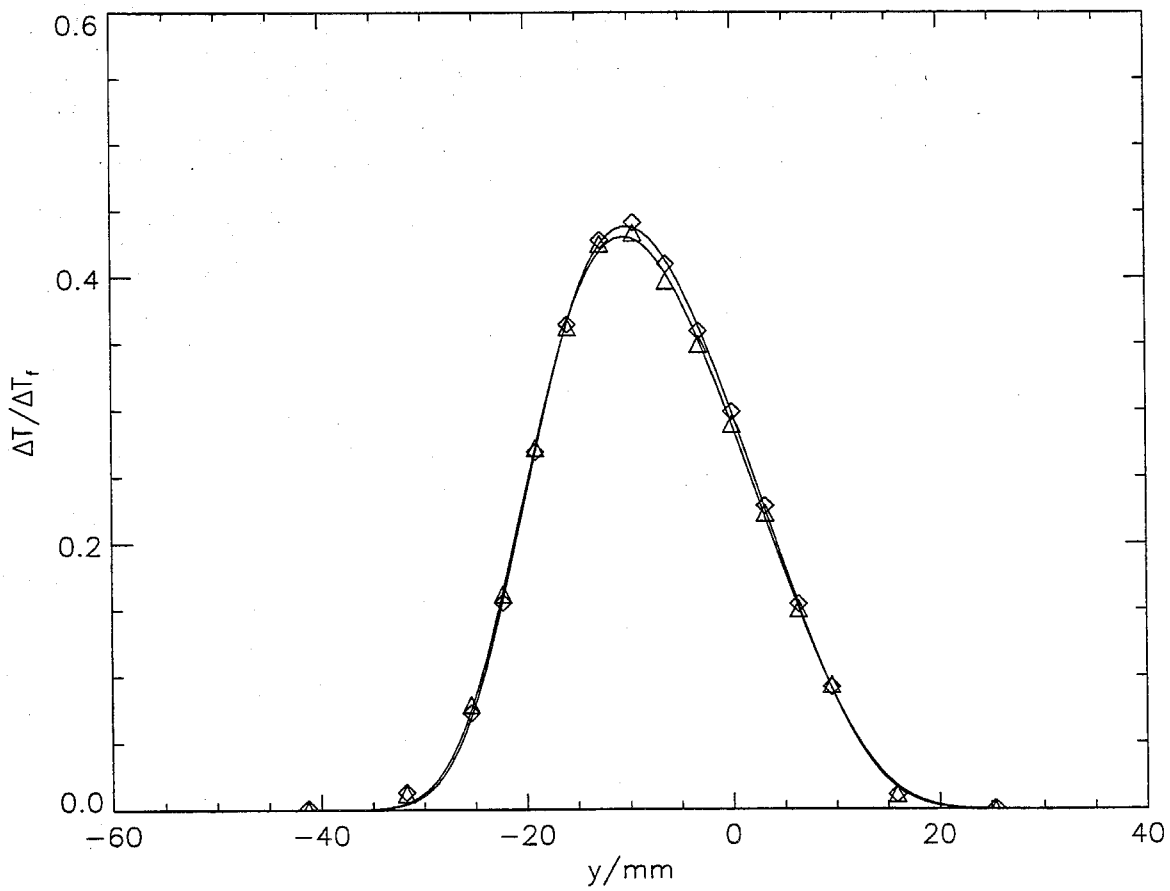

FIG. 3.13 Normalized temperature-rise data recorded with various boundary layer trips. Both flows employ Case 3.2 reactant concentrations, and 0.8 mm-diameter trip wires. Diamonds: Both sides tripped, triangles: High-speed side tripped.

Additional experiments were performed to explore the effects that other near-field perturbations might have, at these nominal conditions. Guided by the results of Lang (1985), in which a large low-speed-side momentum defect (wake) was found to significantly increase the shear-layer growth rate at a freestream speed ratio of $r \simeq 0.5$, two different trip wires were employed on the low-speed side of the splitter plate, with diameters of 0.8 mm and 1.6 mm, also at $x = -50$ mm. The natural low-speed side boundary layer is estimated to be laminar and to have a momentum thickness of 0.15 mm at this trip location. As seen in Fig. 3.12, these low-speed-side perturbations have little, if any, influence on the far-field growth of the layer, in contrast to the significant changes induced by tripping the high-speed splitter plate

boundary layer, and only a weak effect on mixing.

A possible reason for the lack of low-speed-side boundary-layer trip influence is that the naturally-occurring (untripped) boundary layer is already turbulent. The low-speed side splitter plate has concave curvature over a portion of its length (Fig. 2.3), and may be susceptible to Taylor-Görtler vortex formation. At the conditions of these experiments, however, the Taylor number is estimated to be, approximately, 4, significantly less than the stability limit of 7 proposed by Liepmann (1945; *cf.* also discussion in Schlichting 1968). This indicates that the untripped low-speed boundary layer did not support Taylor-Görtler vortices and was likely laminar.

As a further exploration, both splitter-plate boundary-layers were tripped to see if additional effects could be detected (*cf.* Fig. 3.13). In this case, the temperature-rise profile is nearly indistinguishable from that of the flow in which only the high-speed side layer was tripped.

The lack of shear-layer sensitivity to low-speed side perturbations, relative to that seen for high-speed perturbations, is likely due to the stability characteristics of the near-field flow. In particular, linear-stability analyses of wake-like profiles exhibit a "resonance" phenomenon, similar to that found in quantum mechanics (Koochesfahani & Freiler 1989). In their study of density-ratio effects on wake-like flows, these authors found substantial increases in amplification of the "wake" mode, relative to the usually-amplified "shear-layer" mode, for particular choices of the mean profile corresponding to such a resonance condition. A similar effect may be present in this $s \simeq 1$ flow, where the relative amplification of various modes might be substantially altered by a change in the initial velocity profile (tripping). In particular, the profile for the high-speed-tripped flow may be closer, in a state-space sense, to such a resonance than the low-speed-tripped profile. If such a mode were amplified to the non-linear regime, the flow might find itself in a different "basin of attraction", a behavior observed in low-dimensional dynamical systems, *e.g.*, Wiggins (1990).

Table 3.3 summarizes the various computed quantities for each of the natural, or tripped, inflow boundary layer configurations.

Mixture, perturbation	δ_T/mm	δ_p/mm	δ_p/δ_T	$Re_\delta/10^5$
Case 3.1, untripped:	65.0	18.0	0.277	2.3
Case 3.1, 0.8 mm HSS trip:	51.1	15.0	0.293	1.8
Case 3.2, untripped:	64.6	11.9	0.184	2.3
Case 3.2, 0.8 mm HSS trip:	50.5	10.7	0.211	1.8
Case 3.2, 0.8 mm LSS trip:	63.7	12.0	0.189	2.2
Case 3.2, 1.6 mm LSS trip:	63.7	12.4	0.195	2.2
Case 3.2, 0.8 mm trips (both):	51.3	10.6	0.206	1.8
Case 3.3, untripped:	67.4	12.3	0.181	2.4

$(\delta_m/\delta_T)_{untripped} \simeq 0.410$ $\qquad$ $(\delta_m/\delta_T)_{tripped} \simeq 0.448$

$(\mathcal{E}_n)_{untripped} \simeq 1.52$ $\qquad$ $(\mathcal{E}_n)_{tripped} \simeq 1.39$

Table 3.3: Chemically-reacting flow data for various inflow conditions.

3.4 Conclusions

In the shear-layer flows investigated, the measuring station is well downstream of the minimum recommended distance, as scaled by the initial boundary-layer(s) momentum thickness, the values of the "pairing parameter" (Eq. 3.4) are well in excess of previously-proposed minimum values, and the local Reynolds numbers are well beyond the "mixing transition", *i.e.*, $Re_\delta \gg 10^4$, as indicated for asymptotic, self-similar behavior, mixing, and chemical-product formation. In this flow environment, the shear-layer growth rate, $\delta_T(x)/x$, the mixed-fluid mole fraction, δ_m/δ_T, as well as the mixed-fluid composition ratio, $\mathcal{E}_n$, were all found to depend on inflow conditions. The present results corroborate previously-documented findings regarding inflow (boundary-layer) effects on shear-layer growth. They also demonstrate, however, that inflow conditions influence small-scale (molecular) mixing in shear layers, far downstream and at high values of the local Reynolds number. Interestingly, scaling the velocity profiles downstream by shear-layer thickness leaves no other effect of inflow conditions on these profiles, concealing the conspicuous effects on (molecular) mixing.

The data presented here, as well as in previous investigations, indicate that

while a quasi-self-similar state can be achieved, at high Reynolds numbers, in a relatively short fraction of the downstream distance, this state is a function of the inflow conditions. The flow at high Reynolds numbers and away from inflow boundaries is not found to be a unique function of local-flow parameters, such as freestream-velocity and -density ratios, local Reynolds number, *etc.* No support for the existence of a universal, local-parameter-defined flow could be gleaned from these investigations. Indeed, the apparent discrepancies between the new results and previous reports, as well as inconsistencies between numerous previous reports, are probably attributable to interpretations that have implicitly assumed that an inflow-independent, quasi-asymptotic state exists.

CHAPTER 4

Compressibility and dynamics

This chapter details results from a set of non-reacting experiments in the transonic- and supersonic-flow regime. Interactions between pressure waves, both stationary and traveling in the laboratory frame, and turbulence are present in all flows investigated. Freestream Mach numbers were varied to produce both bi-supersonic and bi-subsonic flows, to explore what effect, if any, the presence of (lab-frame) subsonic regions might have on the flow. Among other findings, turbulent-structure convection speeds were observed to violate an empirical mode-selection rule that was based on the presence of a subsonic freestream. In addition, a sensitivity of the global flowfield to various boundary conditions was observed, due primarily to transonic-flow sensitivity to imposed area changes.

4.1 Introduction

Compressibility is an important parameter of turbulent shear-layer flows. As described in Ch. 1, experimental evidence demonstrates that an increase in velocity difference between the two freestreams, as scaled by a representative speed of sound, is correlated with a decrease in shear-layer growth rate, when normalized by the corresponding incompressible value for the same freestream-velocity and -density ratios (*e.g.*, Bogdanoff 1983, Chinzei *et al.* 1986, Papamoschou & Roshko 1988, Samimy & Elliott 1990, Goebel & Dutton 1991, Clemens & Mungal 1992a, and Hall *et al.* 1993).

Compressible-flow data also indicate that the two-dimensional, coherent structures observed in subsonic shear layers do not persist as compressibility is increased. In particular, Clemens & Mungal (1992a, 1995) noted that their images, obtained using Mie scattering from an alcohol condensate as well as nitric-oxide planar induced fluorescence, indicate strong (large-scale) three-dimensionality, for $M_c \gtrsim 0.62$. These experiments, however, covered a streamwise extent in the early portion of the shear-layer flow, with guidewalls separated by a vertical distance, $h/\delta(x) \gg 1$, *i.e.*, large when scaled by the local shear-layer width. In this regime, the shear layer can be expected to approach unbounded-flow behavior. Data recorded at $M_c \simeq 0.5$ (Hall *et al.* 1993, Figs. 10a–c) indicate a smooth transition from a flow close to the splitter plate, where $h/\delta(x) \gg 1$, in which spanwise (two-dimensional) organization is absent, to one further downstream, where $h/\delta(x) \sim 1$, where a two-dimensional, large-scale organization emerges. Similar behavior is exhibited in the downstream part of the higher-M_c spanwise-integrated image data in Clemens & Mungal (1995, Fig. 31). The degree of spanwise coherence can be further enhanced downstream *via* the interaction with a strong, 2-D wave system, especially when a resonant-wave condition is encountered between large-scale-structure spacings and streamwise round-trip distances of wall-reflected waves (Tam & Hu 1989; and Hall *et al.* 1993, Figs. 11). The experimental data are, however, subject to an evolving aspect ratio, $b/\delta(x)$, as the shear-layer grows (see discussion in Ch. 3), an effect that would favor visualization of an apparent enhanced coherence at large x, *i.e.*, small $b/\delta(x)$.

Linear-stability analyses of unbounded flows show suppression of the growth

of two-dimensional, spanwise-coherent modes and a relative increase in the growth of three-dimensional, oblique waves for $M_c \gtrsim 0.6$. In the presence of (reflecting) walls, however, where most of these flows have necessarily been experimentally investigated, the amplification of two-dimensional disturbances can be dominant (*e.g.*, Tam & Hu 1989, and Zhuang *et al.* 1990).

As described in Ch. 1, one of the characteristics of moderate-to-high compressibility shear-layer flows are supersonically-convecting features that produce Mach-wave radiation in the freestreams. One such convected-wave system was captured by Hall *et al.* (1993, see Fig. 5 and related discussion), in the subsonic freestream of a high-compressibility shear layer. They estimated (by measuring the wave-system Mach angles) a convective Mach number of the supersonic disturbance with respect to the low-speed freestream, in the range,

$$2.1 \lesssim M_{c2} \lesssim 2.6 , \qquad \text{at} \qquad M_c \simeq 0.96 , \tag{4.1}$$

indicating the presence of a fast-mode disturbance in the flow. As noted by those authors, the waves are essentially acoustic in nature (near-specular reflection from the lower guidewall) and do not appear to be associated with a two-dimensional, spanwise-coherent, large- (δ-) scale structure. Despite the relative lack of flow structure observed in direct-visualization experiments at similar conditions, these waves are evidently produced by a large-scale, long-lived (temporally-coherent) disturbance, as they are seen to emanate with a characteristic spacing scaled by the local outer scale, $\delta(x)$, and propagate for long distances in a near-linear manner.

It has been recently proposed that these waves are a result of bounding-wall influences (*e.g.*, Umemura *et al.* 1996 and Smits & Dussuage 1996). To explore this possibility, we refer to the original visualizations of Hall *et al.* (1993), where the waves are seen to be generated immediately following the splitter-plate tip, where the flow is essentially unbounded, *i.e.*, $h/\delta(x) \gg 1$. The radiation is continually emitted by the layer to the test-section exit, where the flow is likely to be partially influenced by the walls, since $h/\delta(x) \sim 1$ there. The characteristic Mach angle of the emitted waves remains approximately constant over this large range of h/δ, indicating that the convection speed of the wave-generating turbulent features is independent of the bounding-wall geometry, at least in that flow.

We also note that such a wave system does not preclude the mode coexistence observed by Oertel (1979), since the fast mode would likely be the only source of turbulence-generated acoustic radiation in this flow (Dimotakis 1991b). Preliminary data reported in Dimotakis & Leonard (1991), recorded at high-compressibility conditions ($M_c \simeq 1.5$), appear to indicate the presence of two distinct modes, each radiating into a separate freestream.

As indicated by Eq. 4.1, observations of turbulent-structure convection speeds, or equivalently, convective Mach numbers, are at variance with (central-mode) isentropic-recovery estimates, *e.g.*, Eq. 1.5. Instead, features are found to convect with a speed close to one of the freestream speeds. Proposals by both Papamoschou (1991) and Dimotakis (1991a,b) indicated that the ability of shear-layer structures to support convected shock waves could be responsible for this asymmetry. The proposal of Dimotakis included a model calculation of convective Mach numbers that took total-pressure (shock) losses into account, and was found to be in quantitative accord with existing data.

Papamoschou (1989) proposed that this convection-speed bifurcation is governed by the presence (or absence) of a laboratory-frame subsonic freestream, *i.e.*,

$$\text{Supersonic/subsonic flow} \iff \text{fast-mode convection speed, } i.e., \; M_{c1} \ll M_{c2},$$

and

$$\text{Bi-supersonic flow} \iff \text{slow-mode convection speed, } i.e., \; M_{c1} \gg M_{c2}.$$

Subsequent supporting data, *e.g.*, Hall (1991), led to the coining of this proposal as a "stream-selection rule" by Dimotakis (1991b), who, however, noted its difficulty with respect to Galilean invariance. Obviously, a (purely) convective-frame description of the flow cannot capture a criterion of this nature.

We also note, with regard to downstream-to-upstream communication, *e.g.*, from the exit region of the test-section to the splitter-plate tip, that an elliptic (subsonic) freestream provides an acoustic-feedback path, possibly coupling the near-field of shear-layer development to disturbances generated far downstream. The precise effect of such feedback is not clear. However, as discussed by Dimotakis

& Brown (1976), it potentially exercises a considerable influence in incompressible flows. This communication path is absent in a bi-supersonic configuration, effectively decoupling upstream (inflow) conditions from the facility outflow conditions.

4.2 Experiments

Experimental flow conditions for this part of the study are listed in Table 4.1. Evident in many of the bi-supersonic flow visualizations, *e.g.*, Fig. 4.1, are spatially-varying freestream conditions close to the test-section inlet, at small x. These variations are due to differences between freestream static pressures and flow directions at the splitter-plate tip, in addition to (discontinuous) changes in flow direction induced by shear-/mixing-layer displacement thicknesses. In a bi-supersonic configuration, the flow can only avail itself of these differences through a system of shock and expansion waves. Measurements presented in Table 4.2, *e.g.*, δ_{vis}/x, are recorded in the far field, once the two freestream flows have "equilibrated", however, the mechanisms and dynamics of this near-field equilibration are often noteworthy. As before, guidewalls were adjusted to provide non-accelerating freestream flows in the downstream measurement region.

	Gas 1	Gas 2	γ_1	γ_2	M_{1e}	M_{2e}
Case 4.1:	N_2	N_2	1.40	1.40	1.14	0.65
Case 4.2:	N_2	N_2	1.40	1.40	1.42	1.13
Case 4.3:	Ar	N_2	1.67	1.40	1.47	1.22
Case 4.4:	He	N_2	1.67	1.40	1.39	1.12
Case 4.5:	He	$(N_2/C_2H_4)^1$	1.67	1.30	0.9	0.5

[1] In equal (molar) proportions.

Table 4.1: Freestream gas properties and nominal flow conditions.

The term "mixing layer" is used to describe some flows, since low-shear ($r \sim 1$) layers are likely influenced, at least in early regions of development, by the

splitter-plate wake (Zhuang & Dimotakis 1995). Additionally, when used to describe pressure waves, the terms "stationary" and "traveling" refer to a laboratory-fixed reference frame.

As indicated in Eq. 1.6, presentation of compressibility effects on growth rate requires normalization by an estimate of the corresponding (same r, s) incompressible-flow growth rate. This normalization is provided by Eq. 1.2, appropriate for the spatially-developing layers investigated here.

4.3 Results and discussion

4.3.1 Low-compressibility flows

To explore bi-supersonic flow, *i.e.*, flow with two laboratory-frame supersonic freestreams, a set of runs was initially performed at low-compressibility, *i.e.*, $M_c \simeq 0.1$. Significant dynamical differences from bi-subsonic flow are inherent to this regime, namely the absence of downstream-to-upstream feedback and the presence of refractive interactions between stationary pressure waves and turbulence. Such interactions are disallowed, *i.e.*, are purely reflective, in supersonic/subsonic flow.

To investigate Case 4.1, the facility was configured to produce a subsonic top freestream and a supersonic bottom freestream at the test-section inlet plane. Both gases were pure N_2. As seen in the schlieren image in Fig. 4.1, this configuration results in a flow different from all others presented here; the lower freestream is the high-speed stream. Evident in this visualization is the interaction of the mixing layer with a fan from the 5° expansion corner at the (upstream) test-section inlet. The subsequent turning of the instantaneous dividing streamline initially causes a reduction in the cross-sectional area of the top, subsonic freestream and a corresponding increase in the cross-sectional area of the bottom, supersonic freestream, effectively producing an aerodynamic Laval nozzle.

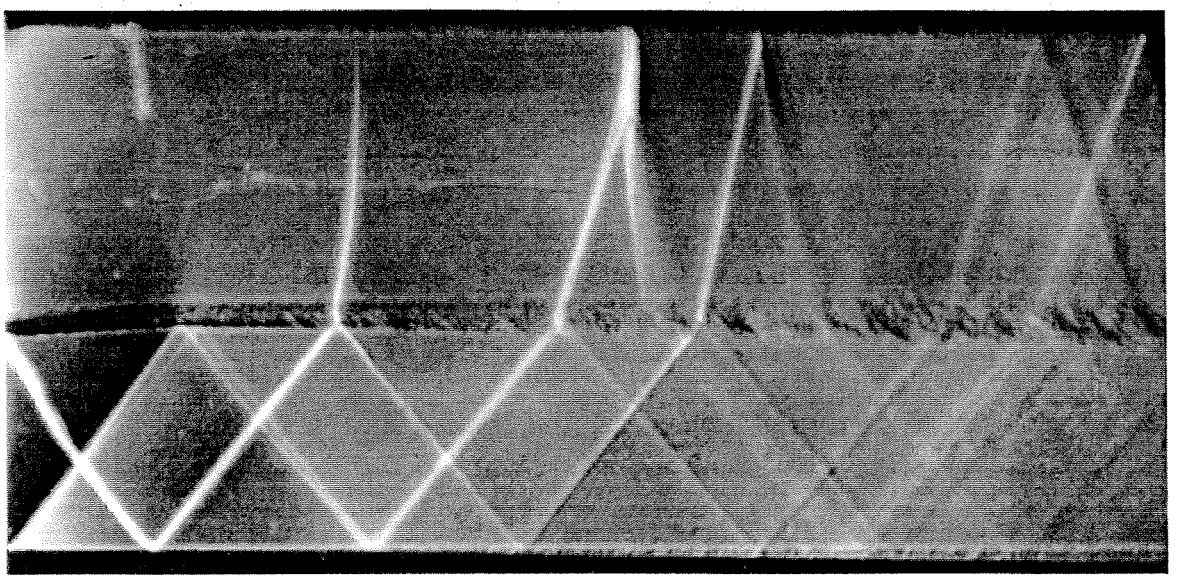

FIG. 4.1 Schlieren (vertical knife-edge) visualization of Case 4.1 mixing-layer flow.

As predicted by quasi-one-dimensional gasdynamics, the Mach numbers and, consequently, the velocities of *both* freestreams are increased in this situation. There is, however, no gain in total momentum flux, as the increase in dynamic pressure is offset by a corresponding decrease in static pressure, as required by momentum considerations. Although the top freestream is subsonic at the inlet plane, it accelerates to a supersonic condition, as evidenced by the near-vertical wave transmitted into the top freestream. This top-freestream acceleration continues for several wave reflections, until the freestream static pressures and flow directions equilibrate, to form a bi-supersonic flow.[♯] The turbulence does not appear to be influenced by the transition from a subsonic to supersonic freestream region, other than (minor) growth-rate variations attributable to local freestream-velocity variations.

An interesting shockwave-interaction phenomenon is seen in the top freestream, downstream from the transition to supersonic flow. A reflection of a compression wave from the top guidewall appears to be a Mach reflection. However, as discussed by various authors, *e.g.*, Hornung (1986), such a configuration is disallowed by the

[♯] This hybrid freestream condition was originally dubbed a "bi-sonic" flow, until Dr. Julian Tishkoff pointed out that the experiment had nothing to do with the large animals that once roamed the plains.

classic (3-shock) von Neumann theory, at this (local) freestream Mach number of 1.13. The resolution of this "von Neumann paradox" is a matter of current study and debate. Proposed explanations concentrate on the triple-point region, with modifications to the three-shock theory including slipstream displacement effects (Kobayashi *et al.* 1995), finite-curvature effects (Colella & Henderson 1990, and Brio & Hunter 1992), and, perhaps the most likely explanation, the addition of a fourth, centered-expansion wave (Guderley 1947, see discussion in Sandemann 1997). The wave reflection observed in Fig. 4.1 is an example of such an interaction in steady flow, in contrast to pseudo-steady (self-similar in mixed spatio-temporal variables) flows generated in shock-tube experiments.

A second set of low-compressibility mixing-layer flows are visualized in Figs. 4.2. These flows are distinguished from Case 4.1 above, in that both freestreams are supersonic at the nozzle-exit plane. Evident in the visualization of Case 4.2a (Fig. 4.2a), however, is a near-normal, stationary, compression shock in the bottom freestream, located slightly downstream of the nozzle-exit plane. An oblique Mach wave incident on the normal-wave front is seen to terminate there, as demanded by post-shock subsonic (wave-frame) flow. The flow is then accelerated by the effective freestream-area change produced by the combination of mixing- and boundary-layer displacement thicknesses. Notably, the mixing layer presents a negative displacement thickness to the bottom freestream flow, while the boundary layer presents a positive displacement. The net effect is a transition back to supersonic flow a short distance downstream of the normal wave, as is evident from the refractive interaction of a (stationary) Mach wave with the mixing layer, at that downstream location. This post-shock acceleration is a product of the same mechanism, *i.e.*, an aerodynamic Laval nozzle, by which the top freestream of Case 4.1 transitioned to a bi-supersonic configuration.

This response to local displacement thicknesses is a consequence of the large effect that small cross-sectional-area changes can have in transonic flow, and is largely due to the sensitivity of the quasi-one-dimensional Mach number-area relationship in this regime (*e.g.*, Figure 5.2 of Liepmann & Roshko 1957). An excellent example of this sensitivity is contained in the transonic-airfoil experiments of Liepmann (see sequence 245–248 in Van Dyke 1982), where small differences between displacement

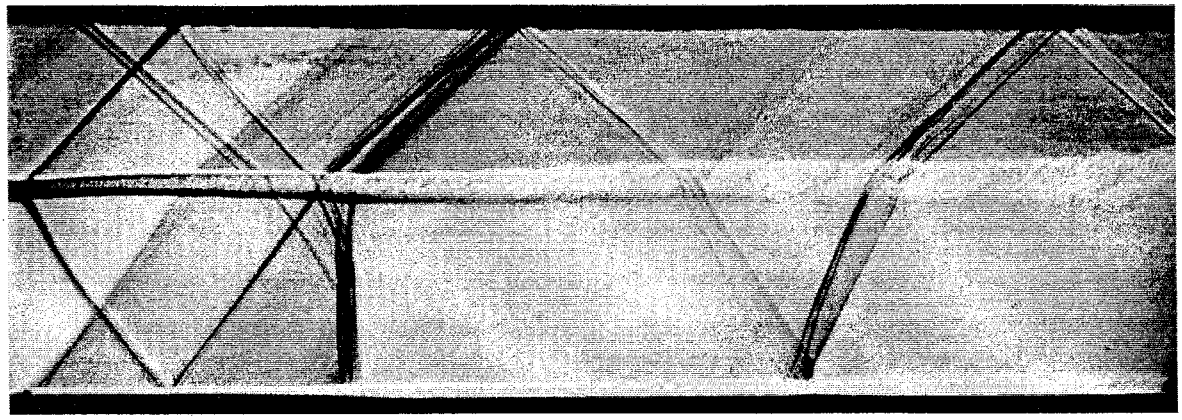

FIG. 4.2a Schlieren (oblique knife edge) visualization of bi-supersonic Case 4.2a mixing-layer flow.

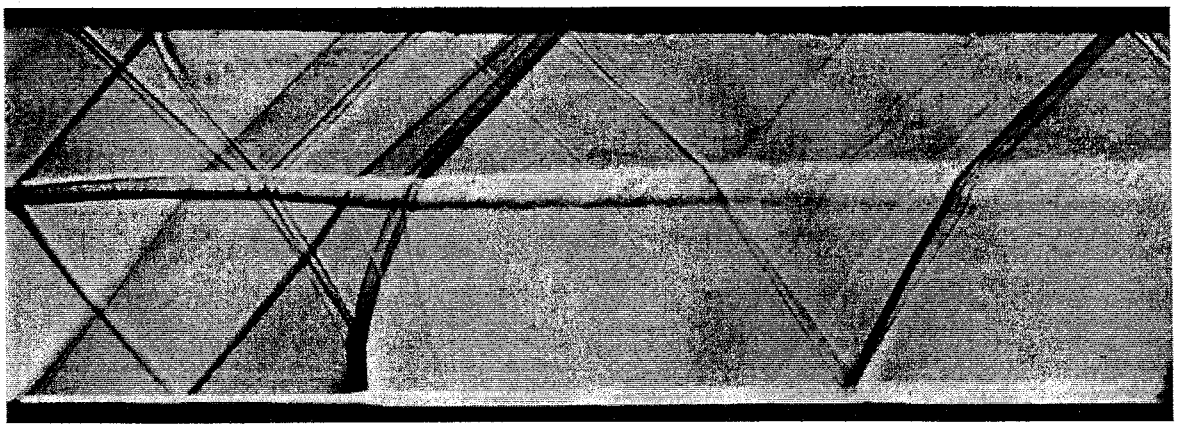

FIG. 4.2b Schlieren (oblique knife edge) visualization of bi-supersonic Case 4.2b mixing-layer flow.

thicknesses of laminar and turbulent boundary layers produce large changes in the global airfoil flowfield.

In Case 4.2a, there is a transition from supersonic to subsonic, and eventually back to supersonic, flow. This generates a subsonic (lab-frame) freestream region in a fashion similar to the Case 4.1 flow, but here the subsonic region is separated from the inflow conditions. Once again there is no qualitative change in turbulence properties associated with transitions between supersonic and subsonic lab-frame freestream flow.

A perturbation of Case 4.2a flow conditions results in Case 4.2b. The latter is produced with a slightly-lower (5%) high-speed freestream stagnation pressure. This

perturbation of the inlet-plane "boundary condition" results in a flow configuration shown in Fig. 4.2b, where the normal shock observed previously is now "unfolded" into a Mach reflection from the bottom guidewall. Visualizations recorded in a sequence of decreasing stagnation pressures exhibit a gradual shortening of the Mach stem, until regular reflection is attained. As illustrated by Case 4.2 flows, it is possible to manipulate the strength of these waves by adjusting upstream boundary conditions, *e.g.*, stagnation pressures. Because of the discontinuous jump in displacement thicknesses at the splitter-plate tip, however, such a wave system will always be generated, even as an infinitesimally-weak N-wave.

These flow configurations, *i.e.*, two moderately-supersonic, acoustically-similar gas streams, provide a unique diagnostic capability. As noted above, bi-supersonic flow permits refraction of stationary waves by/through the mixing layer. In the flows discussed above, turbulence-generated index-of-refraction (density) gradients are relatively weak in comparison to wave-generated gradients. As observed in Fig. 4.2a, for example, this discrepancy in the two types of gradients provides instantaneous visualizations of wave-turbulence interactions. Given that many of these waves are well-approximated as infinitesimal (acoustic) disturbances, such data serve as passive measurements of the instantaneous Mach number field. Interestingly, this field appears to be nearly discontinuous in many cases, *i.e.*, waves are "kinked". This suggests an instantaneous Mach number field quite different from the smoothly-varying mean field, a behavior also observed in incompressible flow (Dimotakis *et al.* 1981).

In the case where these interactions are of finite strength (non-acoustic), the potential for baroclinic-vorticity generation exists. Such vorticity would be aligned with the mixing-layer vorticity, either augmenting or diminishing it, depending on the density gradient. This interaction geometry is purely two-dimensional, in contrast to the experiment of Clemens & Mungal (1992b) in which enhanced (spanwise-integrated) layer growth was observed as a result of a three-dimensional shock-wave/shear-layer interaction. In such interactions, the baroclinically-generated vorticity is not parallel to that of the original mixing layer, and alters (direction and magnitude) the vorticity field, creating a substantially-different flowfield.

In N_2/N_2 flows above, the potential for vorticity generation was not large, as

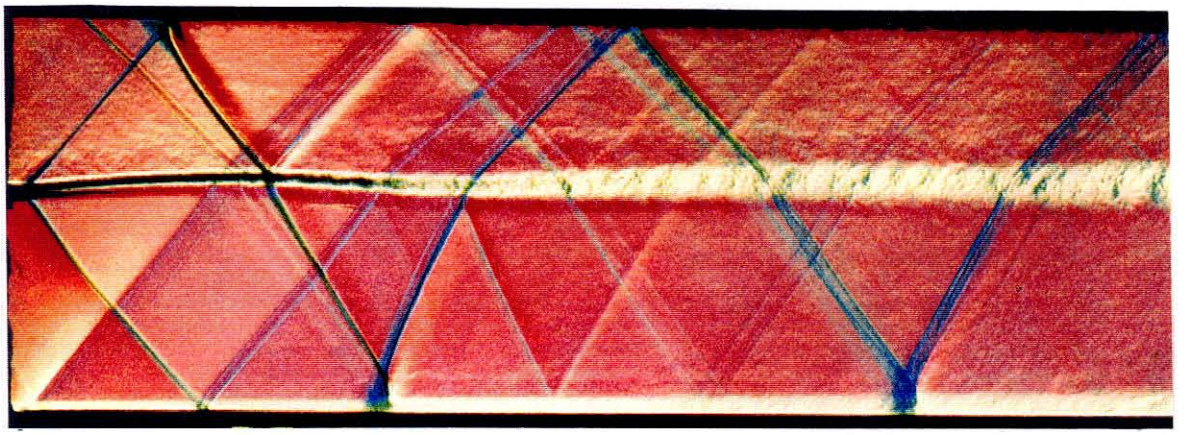

FIG. 4.3 Color schlieren photograph of Case 4.3 mixing-layer flow.

freestream-density gradients are close to unity. To explore the effects on a layer that supports a significant density gradient, a flow similar to Case 4.2 was investigated, but with a high-speed freestream of Ar, instead of N_2. The low-speed freestream in Case 4.3 was still N_2, resulting in freestream conditions of $s \simeq 0.54$ and $r \simeq 0.98$ (at the shock-impingement location), conditions that could result in significant (fractional) augmentation of mixing-layer vorticity. However, as seen in the color schlieren photograph in Fig. 4.3, there is no discernible shock-induced change in the mixing-layer growth rate. It should be noted that the unperturbed vorticity field in this flow is probably wake-like in nature, as the relative shear is low. This finding is in accord with (two-dimensional) shock-wave/mixing-layer interaction experiments of other investigators, *e.g.*, Shau *et al.* (1993), who concluded that a similar interaction had little net effect on large scales in the flow.

4.3.2 Moderate-compressibility flows

In contrast to the low-compressibility flows discussed above, Case 4.4 and 4.5 flows were produced with helium high-speed freestreams. In Case 4.4, for example, the relatively-high speed of sound of helium yields a higher compressibility than that of Case 4.2, at the same nominal freestream Mach numbers (Table 4.1). This feature was originally exploited, in this facility, by Hall (1991) and Hall *et al.* (1993).

Two distinct pressure-wave systems are evident in Case 4.4 (Figs. 4.4ab) flow visualizations, a stationary-wave system similar to that found in low-compressibility flows, and a traveling-wave system in the low-speed freestream, similar to that observed by Hall *et al.* (1993). As in Case 4.1–4.3 flows, the stationary-wave/shear-layer interaction does not significantly modify the growth rate, although this interaction is estimated to produce vorticity of relatively small magnitude and of opposite sign to the unperturbed shear-layer vorticity. In addition, this wave system does not appear to be resonant with any two-dimensional structure in the flow; the enhanced two-dimensional structure observed in the downstream region by Hall *et al.* (1993) is not observed here (Fig. 4.4b). We note, however, that the values of h/δ in this flow are less than those for enhanced-structure flow, and Case 4.4 may approximate unbounded-flow conditions.

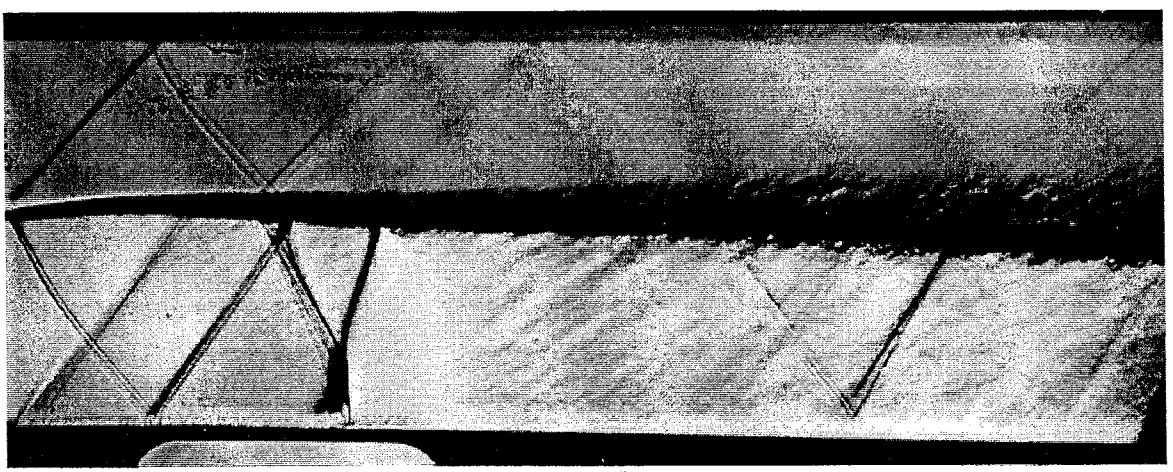

FIG. 4.4a Schlieren (oblique knife edge) photograph of the upstream region of bi-supersonic Case 4.4 shear-layer flow.

As in the Hall *et al.* (1993) analysis (Eq. 4.1), a convective Mach number with respect to the low-speed freestream is inferred from the image data as,

$$\text{Case 4.4}: \qquad M_{c2} \simeq 1.70 \pm 0.10 \;\Rightarrow\; M_{c1} \simeq 0.29 \pm 0.017. \tag{4.2}$$

This is in general accord with the previously-observed asymmetry, *i.e.*, $M_{c1} \neq M_{c2}$, as shown in Fig. 4.5. Only measurements recorded in two-dimensional shear-layer flows, *i.e.*, no data from annular-shear-layer/turbulent-jet flows, are presented here. Recent evidence indicates that geometrical differences are likely to be important (Freund *et al.* 1997).

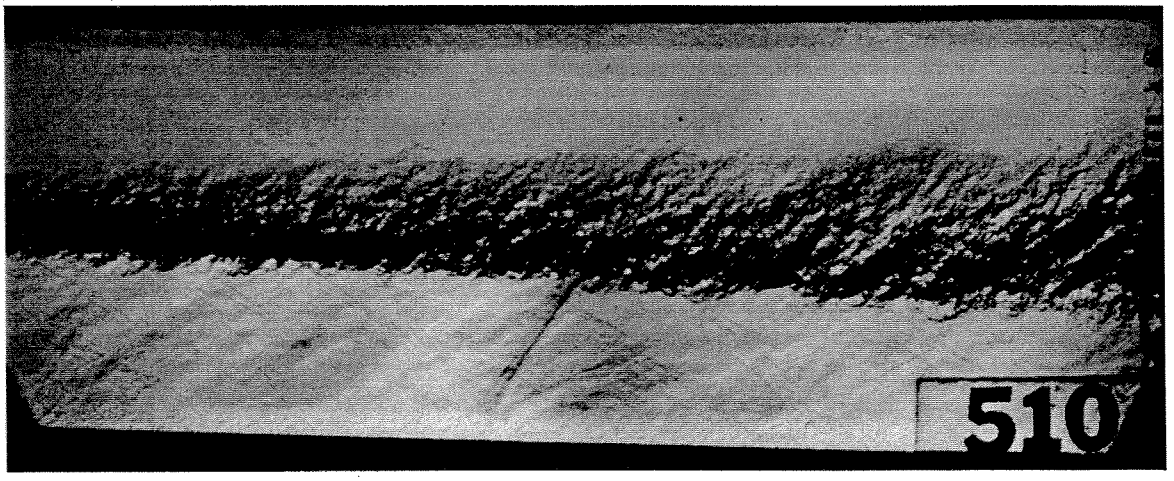

FIG. 4.4b Schlieren (oblique knife edge) photograph of downstream region of bi-supersonic Case 4.4 flow. Same nozzle-exit conditions as those recorded in Fig. 4.4a.

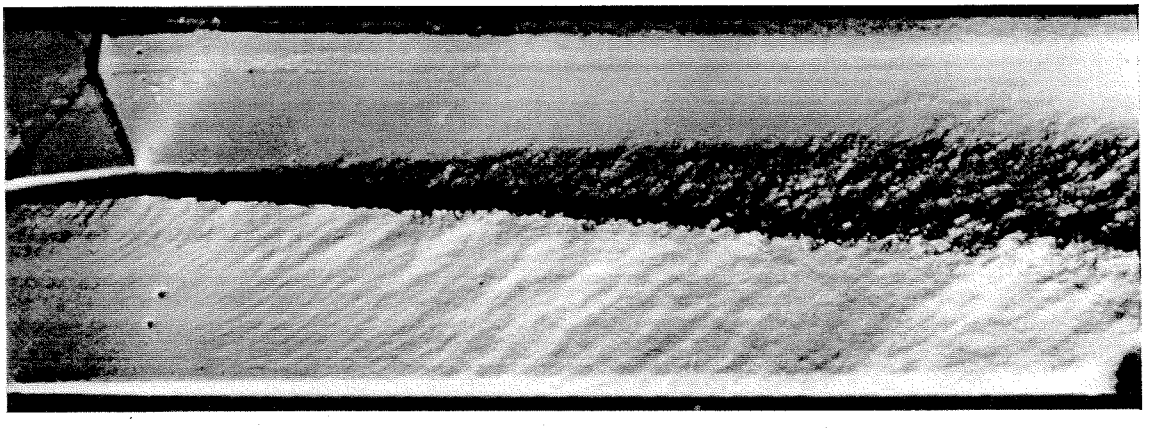

FIG. 4.4c Schlieren (oblique knife edge) photograph of off-design (now bi-subsonic) Case 4.4 flow.

Although in general agreement with the asymmetry, Case 4.4 exhibits a fast-mode convection speed in bi-supersonic flow; a result at variance with the stream-selection rule originally proposed by Papamoschou (1989). An exception to this empirical rule is also in the original Papamoschou data (1989, Case N31N17), however, at an ambiguously-low level of compressibility.

This measurement provides direct evidence, at a moderate-to-high level of compressibility ($M_c \simeq 0.7$), that the (empirically-based) "stream-selection rule", a criterion based solely on laboratory-frame conditions, does not provide an accurate

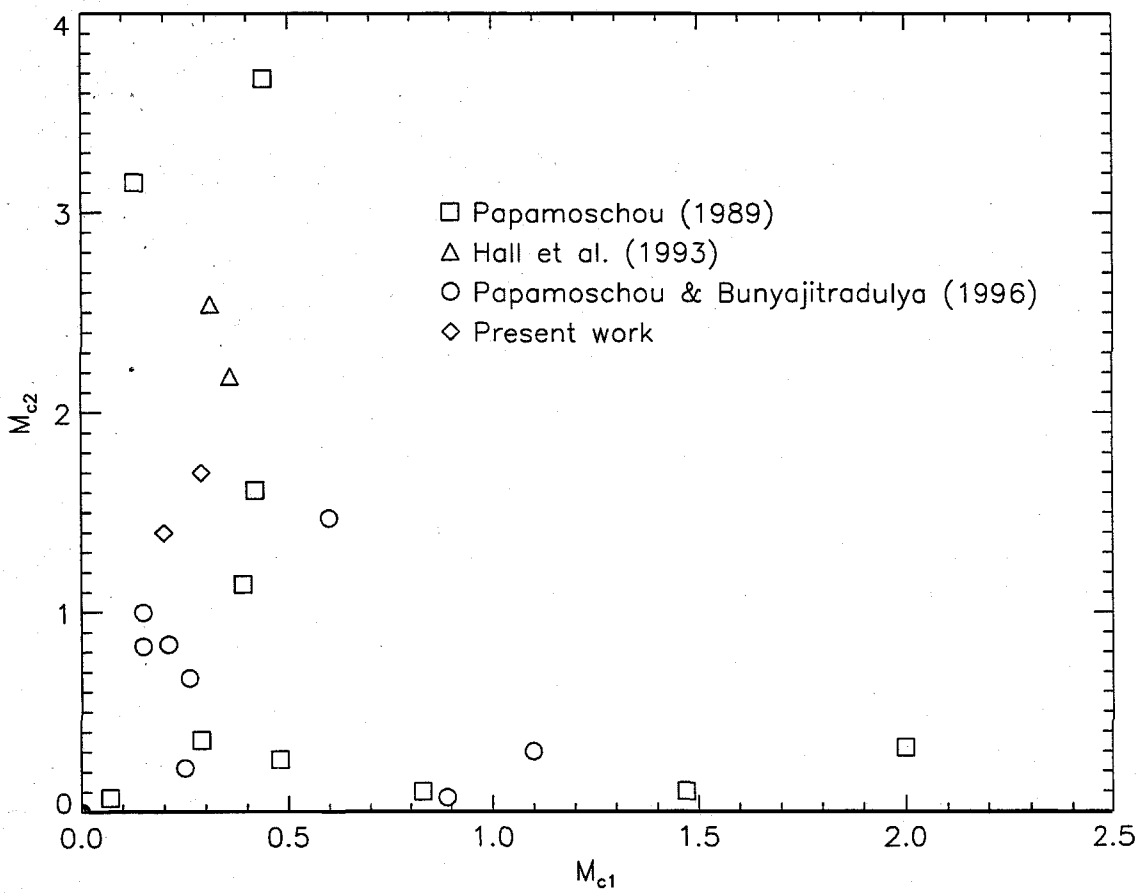

FIG. 4.5 Observed turbulent-feature convection speeds. Isentropic-recovery model predicts a line with near-unity slope, *i.e.*, $M_{c1} \simeq M_{c2}$.

description of the convection-speed behavior. This is manifest in Fig. 4.6, where the data have been split into groups according to whether the freestream flows are supersonic, or not. As with the low-compressibility results discussed earlier, the presence of (here, the lack of) a subsonic laboratory-frame freestream region does not govern large-scale dynamics in turbulent shear/mixing layers. Several possible alternative criteria, *e.g.*, an analog of the regular-/Mach-reflection "information condition" of Hornung *et al.* (1979), were also tested against the data with no success.

The sensitivity to imposed freestream boundary conditions exhibited by the low-compressibility flows was also observed here. In particular, the flow conditions shown in Fig. 4.4c were recorded during the multiple-run iterative procedure required to produce (on-design) bi-supersonic Case 4.4 flow conditions. This flow was

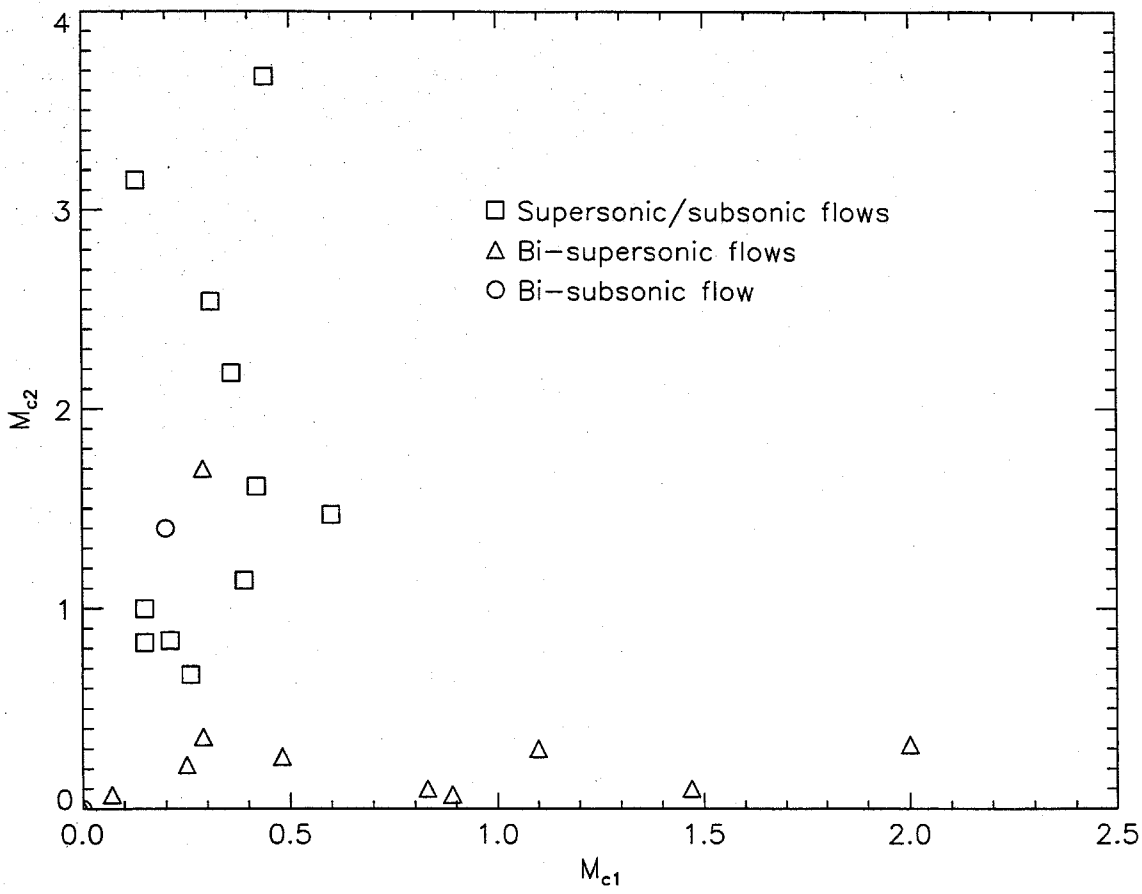

FIG. 4.6 Stream-selection data. Case 4.4: bi-supersonic flow on vertical (fast-mode) branch.

produced with the same (nominal) nozzle-/contraction-plenum pressures, but at a non-diverging guidewall angle, *i.e.*, 0° as opposed to 1.2° divergence for on-design Case 4.4, as is evident from the comparison of Fig. 4.4c and Figs. 4.4ab, respectively. The flow is almost completely subsonic in this off-design configuration, having been shocked by a three-wave structure near the test-section inlet. Interestingly, a traveling wave system is again present in the low-speed freestream, similar to that observed in bi-supersonic Case 4.4 flow.

The possibility for supersonically-convecting turbulent structures in bi-subsonic flow is further addressed by Case 4.5 conditions. As seen in Fig. 4.7, there is indeed a traveling (oblique) pressure-wave system in the bottom (low-speed) freestream,

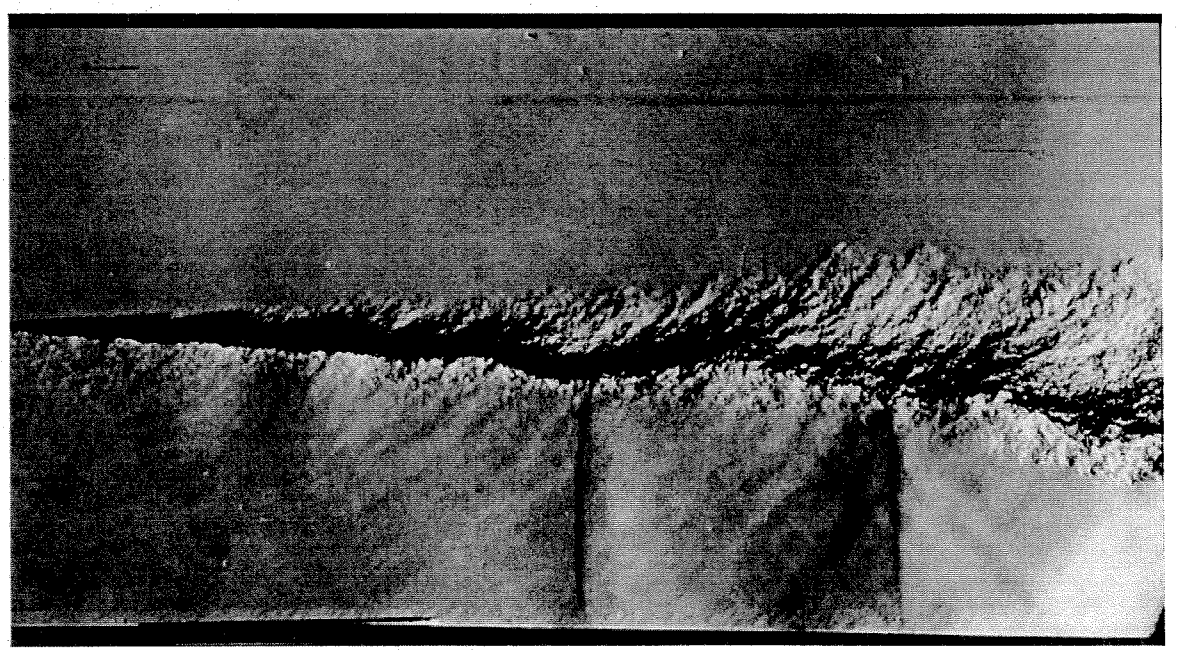

FIG. 4.7 Schlieren (vertical knife edge) photograph of Case 4.5 bi-subsonic shear-layer flow.

indicative of a disturbance with convective Mach numbers,

$$\text{Case 4.5 :} \qquad M_{c2} \simeq 1.40 \pm 0.25 \;\Rightarrow\; M_{c1} \simeq 0.20 \pm 0.036. \tag{4.3}$$

There is also an upstream-traveling, *i.e.*, right-to-left, set of near-normal pressure waves, similar to those observed by Hall (1991) in the same facility. These disturbances are the signature of a downstream-to-upstream feedback mechanism which exploits subsonic flow. The probable origin of this acoustic feedback is the large-scale-structure communication described by Dimotakis & Brown (1976). As noted by these authors, this feedback is present in any subsonic-flow facility, coupling outflow (downstream) conditions to those in the inflow region.

Normalized growth rates for these two flows, as well as those of two low-compressibility flows (Cases 4.1 and 4.2), along with previous data, are presented in Table 4.2 and Fig. 4.8. Only data recorded in two-dimensional shear-layer experiments are plotted, for the same geometrical reasons detailed for convection-speed data. Absolute growth rates of Case 4.1 and 4.2 flows are extremely small, and as a consequence, have significant fractional uncertainties associated with them, because of near-unity values of the velocity ratio, r. Case 3.3 is excluded from this

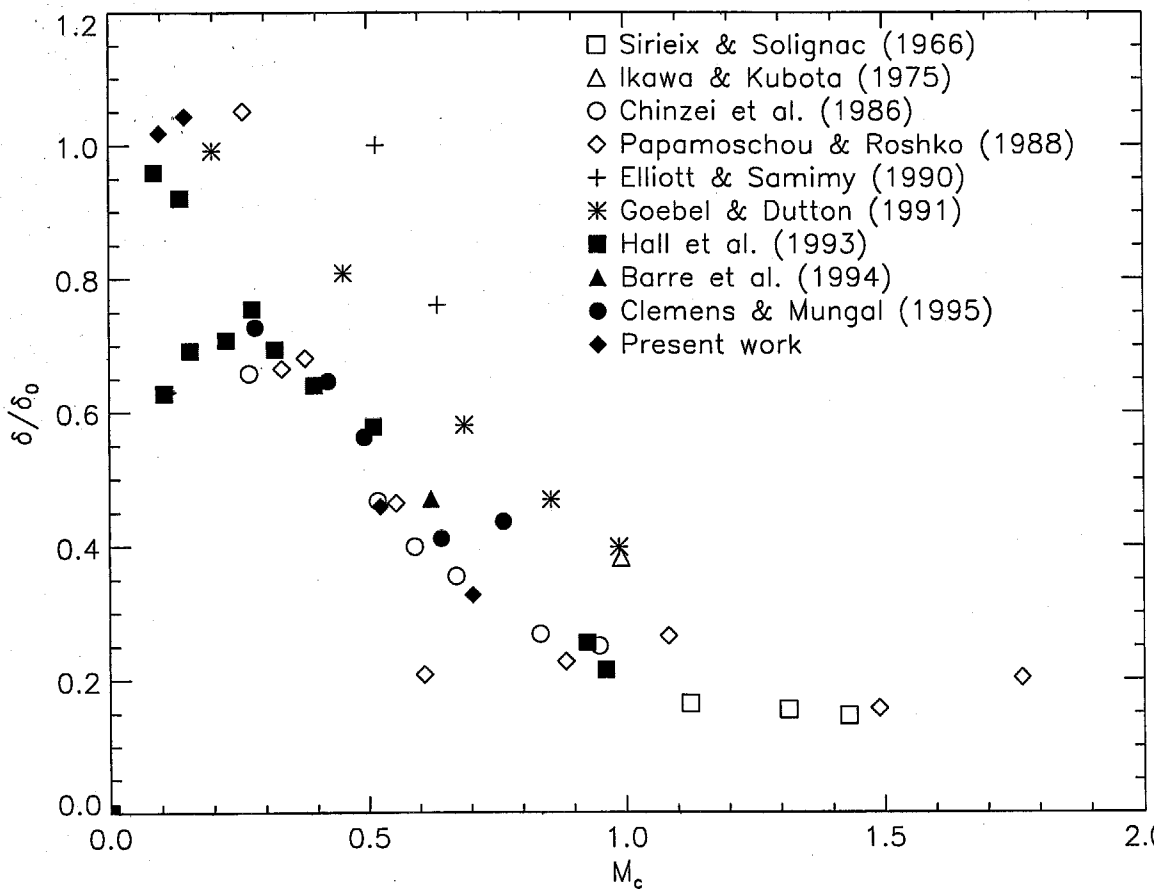

FIG. 4.8 Normalized compressible shear-layer growth rates as parameterized by the total convective Mach number, M_c (Eq. 1.5). Normalization provided by Eq. 1.2, with C_δ's as suggested (when documented) by the various investigators.

presentation, as it is more accurately classified as a wake than a shear-layer. The data are seen to be in good overall agreement with those of previous investigations, suggesting that the presence of subsonic/supersonic freestream-flow regions does not have a significant effect on growth rate.

	M_1	M_2	r	s	M_c	δ_0/x	δ_{vis}/x	δ_{vis}/δ_0
Case 4.1:	1.31	1.06	0.85	0.91	0.097	0.0275	0.028	1.02
Case 4.2:	1.41	1.09	0.82	0.94	0.15	0.034	0.035	1.04
Case 4.3:[1]	1.44	1.26	0.98	0.54	–	–	–	–
Case 4.4:	1.49	1.27	0.34	5.30	0.70	0.072	0.22	0.33
Case 4.5:	0.9	0.5	0.21	5.80	0.52	0.150	0.33	0.46

[1] Conditions at shock-impingement location.

Table 4.2: Far-field (equilibrated) flow properties.

4.4 Conclusions

Non-reacting shear-/mixing-layer flows, in the transonic regime, have been investigated. Interactions between pressure waves and turbulence are manifest in schlieren visualizations. Three flows, with transonic laboratory-frame freestreams, but at low levels of mixing-layer compressibility ($M_c \simeq 0.1$), were found to be sensitive to imposed boundary conditions. Both bi-supersonic and bi-subsonic flows, at $M_c \simeq 0.7$ and $M_c \simeq 0.5$, respectively, are found to exhibit turbulent-structure convection speeds that violate a previously-proposed rule for mode selection. The moderate-compressibility, bi-supersonic flowfield was also observed to be sensitive to imposed boundary conditions, further demonstrating the potential for global-flowfield manipulation, with significant control authority, in this transonic-flow regime.

Normalized growth rates measured in these flows are in qualitative accord with existing data; regardless of whether the flow is bi-supersonic, bi-subsonic, or a hybrid-flow condition. Along with the violation of the stream-selection rule, a criterion based on lab-frame Mach numbers, this suggests that the presence, or absence, of laboratory-frame subsonic freestream regions does not significantly affect free-shear turbulence.

CHAPTER 5

Compressibility and mixing

This chapter describes experimental results regarding compressibility effects on turbulent shear-layer mixing. Two chemically-reacting "flip" experiments were performed, while holding freestream-velocity and -density ratios, Reynolds number, and reactant concentrations nominally fixed. An increase in compressibility, while holding these other parameters fixed, is associated with a decrease in growth rate, in accord with previous investigations. The increase in compressibility is also associated with an increase in the peak (normalized) temperature rise, and to a lesser degree, the mixed-fluid fraction. This change in small-scale mixing is solely attributable to compressibility.

5.1 Introduction

It is often stated that the effect of compressibility on turbulent shear-layer flows is to suppress *mixing*, *e.g.*, Martens *et al.* (1994). Such an inference is likely made on the basis of data concerning the suppression of the (large-scale) growth rate by compressibility. However, as discussed by various authors, *e.g.*, Dimotakis (1986), high-Reynolds-number mixing processes can be conceptually broken into three separate stages: large-scale entrainment, intermediate-scale stirring, and small-scale diffusion/mixing, with each stage important to the overall molecular mixing of the two, initially-separated, freestream constituents.

This sequence can be expressed in terms of the quantities that are accessible to the measurement techniques employed here, *i.e.*,

$$\frac{\delta_{\rm m}}{x} = \left(\frac{\delta}{x}\right) \times \left(\frac{\delta_{\rm m}}{\delta}\right) . \tag{5.1}$$

The first term represents the first stage of mixing, while the second represents the process at all of the remaining spatial scales, down to the diffusion, or Batchelor, scale. The behavior of δ/x as a function of compressibility is relatively well known; the behavior of $\delta_{\rm m}/\delta$ (here $\delta_{\rm m}/\delta_{\rm T}$) is a matter of some controversy.

The partition in Eq. 5.1 indicates that we should expect a *net* decrease in the amount of molecularly-mixed fluid, at least at moderate-to-high compressibility conditions. This expectation stems from two experimental facts (Dimotakis 1991a): the large-scale growth rate is approximately 1/2 of the incompressible value by $M_{\rm c} \simeq 0.5$ (*e.g.*, Ch. 4), and the mixed-fluid fraction is approximately 1/2 at incompressible-flow conditions (*e.g.*, Ch. 3).

There have been several recent reports on molecular mixing in compressible shear-layer flows, *i.e.*, Hall *et al.* (1991), Clemens & Paul (1995), Island (1997), and Freund *et al.* (1997), with an almost equal number of differing conclusions. The techniques employed in these studies are threefold: chemically-reacting flip experiments (this work, and Hall *et al.* 1991), cold-chemistry (fluorescence-quenching) flip experiments (Clemens & Paul 1995, Island 1997), and direct numerical simulation (Freund *et al.* 1997). This variety of techniques, in addition to differing measures of $\delta_{\rm m}/\delta$ employed in each case, renders direct comparison difficult.

Hall *et al.* (1991) concluded that the amount of molecularly-mixed fluid decreased with increasing M_c, Clemens & Paul (1995) concluded that it increased, Island (1997) concluded no change or a slight increase, and Freund *et al.* (1997) observed an increase. The three sets of experimental data are, however, subject to several caveats. In particular, changes in M_c are accompanied by associated changes in velocity ratio, density ratio, and/or Reynolds number. As a result, interpretations of the data are often ambiguous, with (strong) assumptions required. A typical example of such an ambiguity is found in the Island (1997) interpretation, where it is unclear whether observed increases in δ_m/δ are attributable to compressibility effects, or Reynolds-number effects, or even possible large-scale effects, *e.g.*, streamwise pressure gradient, and/or velocity/density ratio. The Hall *et al.* (1991) and Clemens & Paul (1995) data are also subject to similar ambiguities. The numerical simulations of Freund *et al.* (1997) are free of such difficulties, as all parameters except Mach number were held nominally fixed. The Reynolds number of the simulated flow is however, very low because of computational constraints. In particular, the simulated-flow Reynolds numbers of $Re \simeq 2.5 \times 10^3$ (based on jet radius) make direct comparison with experimentally-generated flows difficult, as the experiments are conducted at Reynolds numbers well in excess of the mixing transition.

Collectively, this evidence suggests that if compressibility effects, as measured by the convective Mach number, M_c, are to be assessed with any confidence, we must hold as many of these parameters as constant as possible. Such a set of shear-layer flip experiments is described below.

5.2 Experiments

These experiments were performed at two nominal sets of freestream conditions, a low-compressibility flow with $M_c \simeq 0.25$ (Cases 5.Xa) and a moderate-compressibility flow with $M_c \simeq 0.47$ (Cases 5.Xb).

Freestream-velocity and -density ratios were chosen to facilitate a comparison with the existing body of chemically-reacting data (see discussion in Ch. 3, and

5.1a - Fluorine-rich ($\phi = 8$, $\Delta T_f \simeq 171\,\mathrm{K}$):

$U_1 \simeq 280\,\mathrm{m/s}$: 8.00% Ar, 15.07% He, 0.93% H_2, 0.14% NO, 75.86% N_2
$U_2 \simeq 110\,\mathrm{m/s}$: 8.00% Ar, 8.00% He, 8.00% F_2, 76.00% N_2.

5.2a - Hydrogen-rich ($\phi = 1/8$, $\Delta T_f \simeq 311\,\mathrm{K}$):

$U_1 \simeq 280\,\mathrm{m/s}$: 8.00% Ar, 14.00% H_2, 0.88% NO, 77.12% N_2
$U_2 \simeq 110\,\mathrm{m/s}$: 14.20% Ar, 8.00% He, 1.80% F_2, 76.00% N_2.

5.3a - Hydrogen-rich, increased concentration ($\phi = 1/8$, $\Delta T_f \simeq 355\,\mathrm{K}$):

$U_1 \simeq 280\,\mathrm{m/s}$: 8.00% Ar, 16.00% H_2, 1.00% NO, 75.00% N_2
$U_2 \simeq 110\,\mathrm{m/s}$: 13.94% Ar, 8.00% He, 2.06% F_2, 76.00% N_2.

5.4a - Non-reacting:

$U_1 \simeq 280\,\mathrm{m/s}$: 8.00% Ar, 16.00% He, 76.00% N_2
$U_2 \simeq 110\,\mathrm{m/s}$: 16.00% Ar, 8.00% He, 76.00% N_2.

Table 5.1a: Low-compressibility flow: freestream speeds and compositions.

references therein), *i.e.*,

$$r \equiv \frac{U_2}{U_1} \simeq 0.4\,, \quad \text{and} \quad s \equiv \frac{\rho_2}{\rho_1} \simeq 1.0\,. \tag{5.2}$$

Low-compressibility data were recorded in flows with freestream speeds,

$$U_1 \simeq 280\,\mathrm{m/s} \quad \text{and} \quad U_2 \simeq 110\,\mathrm{m/s} \quad \Rightarrow \Delta U \simeq 170\,\mathrm{m/s}\,, \tag{5.3a}$$

and moderate-compressibility data in flows with,

$$U_1 \simeq 525\,\mathrm{m/s} \quad \text{and} \quad U_2 \simeq 210\,\mathrm{m/s} \quad \Rightarrow \Delta U \simeq 315\,\mathrm{m/s}\,. \tag{5.3b}$$

In both flows, freestream compositions documented in Tables 5.1 were tailored to offset the various density changes associated with compressible-flow freestreams, *i.e.*, a freestream molecular-mass ratio of unity does not imply $s = 1$. In addition, the flip-experiment mixture ratio, ϕ_0, was held constant at $\phi_0 = 8$.

5.1b - Fluorine-rich ($\phi = 8$, $\Delta T_f \simeq 179\,\mathrm{K}$):

$U_1 \simeq 525\,\mathrm{m/s}$: 41.07% He, 0.93% H_2, 0.14% NO, 57.86% N_2
$U_2 \simeq 210\,\mathrm{m/s}$: 20.00% Ar, 14.00% He, 8.00% F_2, 58.00% N_2 .

5.2b - Hydrogen-rich ($\phi = 1/8$, $\Delta T_f \simeq 329\,\mathrm{K}$):

$U_1 \simeq 525\,\mathrm{m/s}$: 28.00% He, 14.00% H_2, 0.88% NO, 57.12% N_2
$U_2 \simeq 210\,\mathrm{m/s}$: 26.20% Ar, 14.00% He, 1.80% F_2, 58.00% N_2 .

5.3b - Hydrogen-rich, increased concentration ($\phi = 1/8$, $\Delta T_f \simeq 375\,\mathrm{K}$):

$U_1 \simeq 525\,\mathrm{m/s}$: 26.00% He, 16.00% H_2, 1.00% NO, 57.00% N_2
$U_2 \simeq 210\,\mathrm{m/s}$: 25.94% Ar, 14.00% He, 2.06% F_2, 58.00% N_2 .

5.4b - Non-reacting:

$U_1 \simeq 525\,\mathrm{m/s}$: 42.00% He, 58.00% N_2
$U_2 \simeq 210\,\mathrm{m/s}$: 28.00% Ar, 14.00% He, 58.00% N_2 .

Table 5.1b: Moderate-compressibility flow: freestream speeds and compositions.

With reference to Eq. 5.3, it might appear that the Reynolds number of the moderate-compressibility flow would be significantly higher than that of the low-compressibility flow. As discussed above, such an increase has been a shortcoming of previous investigations. The present experiment was designed to exploit the compressibility-induced reduction in growth rate (for example, in Fig. 4.8), to produce minimal changes in Reynolds number as compressibility was changed. There are also relatively small changes in mixture density and viscosity associated with lower (static) temperatures in the moderate-compressibility flow.

Profiles of the temperature rise from chemical reaction were recorded at a downstream station of $x = 0.365\,\mathrm{m}$, as before. Splitter-plate boundary layers in these flows are thinner (higher Re_θ) than for flows described in Ch. 3, which were themselves seen to comfortably satisfy all indicated criteria for fully-developed, self-similar flow. The resulting shear layers have a local Reynolds number range at this

measuring station of,

$$7.6 \times 10^5 \lesssim Re_\delta \lesssim 7.9 \times 10^5 , \tag{5.4a}$$

for Case 5.Xa flows and,

$$9.8 \times 10^5 \lesssim Re_\delta \lesssim 10 \times 10^5 , \tag{5.4b}$$

for Case 5.Xb flows. The slight (1/10-decade) change in Re_δ is due to imposed requirements discussed above, *i.e.*, constant r, s, and ϕ_0.

The increase in velocity does, however, result in a substantial increase of the total convective Mach number, from,

$$M_c \simeq 0.25 , \tag{5.5a}$$

for Case 5.Xa flows, to,

$$M_c \simeq 0.47 , \tag{5.5b}$$

for Case 5.Xb flows. As a consequence of this restriction of the parameter space, any changes in mixed-fluid properties can be attributed solely to the change in compressibility.

5.3 Results and discussion

Normalized temperature-rise profile measurements for low-compressibility flow conditions (Cases 5.1a–5.3a) are plotted in Fig. 5.1.

A procedure similar to that detailed in Ch. 3 was employed to ensure that the flows were in the kinetically-fast regime. In this case, however, reactant concentrations for the kinetically-slower H_2-rich flows were increased, in contrast to the reduction employed in Ch. 3 flows. The Da ratios for the $\phi = 1/8$ cases, in both low- and moderate-compressibility flows, are computed to be larger than 1.5. Once again, Damköhler numbers associated with the F_2-rich ($\phi = 8$) part of the flip experiment are considerably higher than those of the H_2-rich ($\phi = 1/8$) part.

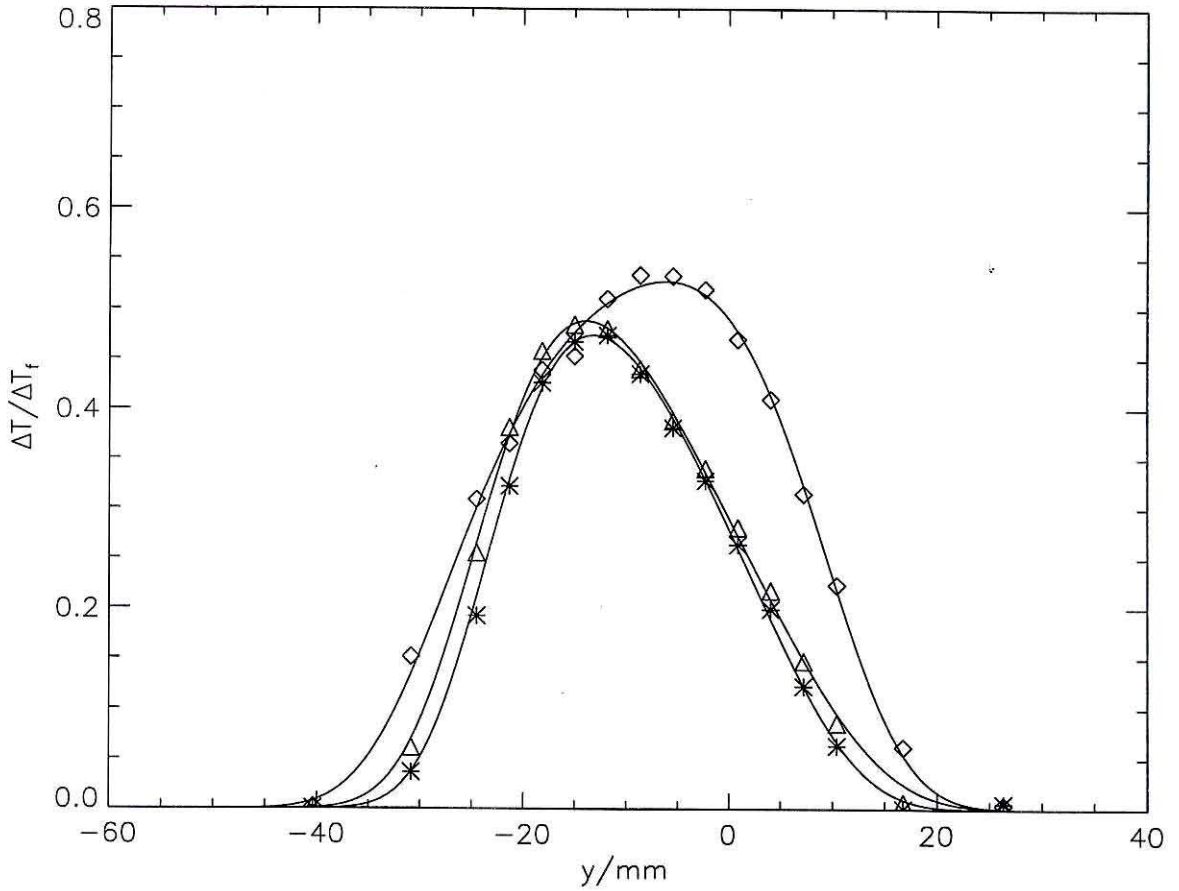

FIG. 5.1 Normalized temperature-rise data for the low-compressibility flow ($M_c \simeq 0.25$). Diamonds: Case 5.1a, $\phi = 8$. Triangles: Case 5.2a, $\phi = 1/8$. Asterisks: Case 5.3a, $\phi = 1/8$, increased chemical-kinetic rate.

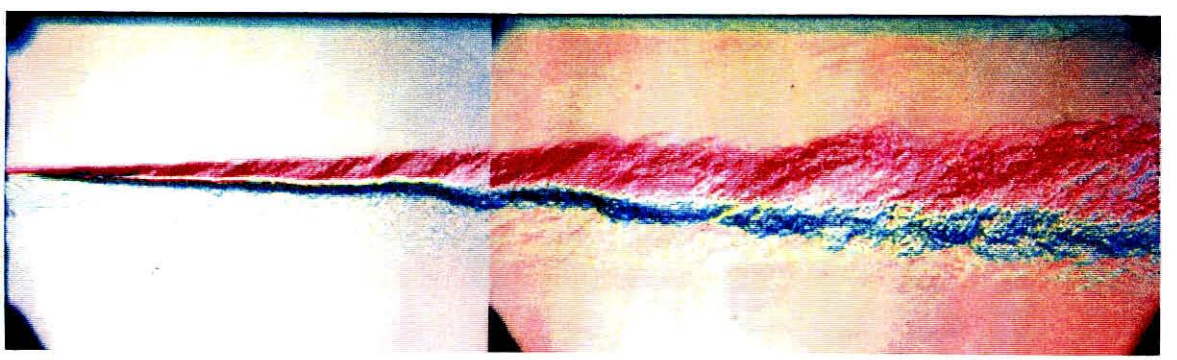

FIG. 5.2 Composite color-schlieren image of Case 5.2a flow. Note linear growth and similar large-scale structure.

The lower-concentration compositions were used to estimate the mixed-fluid quantities, to alleviate concerns regarding the effects of heat release. In particular,

at these high-speed conditions, mixing times, $\tau_{\rm mix}$, are substantially reduced from those in Ch. 3 flows, requiring a commensurate reduction in chemical times, $\tau_{\rm chem}$, to remain in the fast-kinetic regime. This is accomplished by increasing reactant concentrations in the H_2-rich ($\phi = 1/8$) case. There are, of course, associated increases in adiabatic flame temperatures and consequent levels of heat release. As seen in Fig. 5.1, there may be slight heat-release effects at work; the temperature profile recorded for (higher-concentration) Case 5.3a concentrations is reduced in both width and height relative to that recorded for Case 5.2a, indicative of slight reductions in both shear-layer growth and product fraction, respectively. These reductions are in accord with those observed by Hermanson & Dimotakis (1989), at similar heat-release levels.

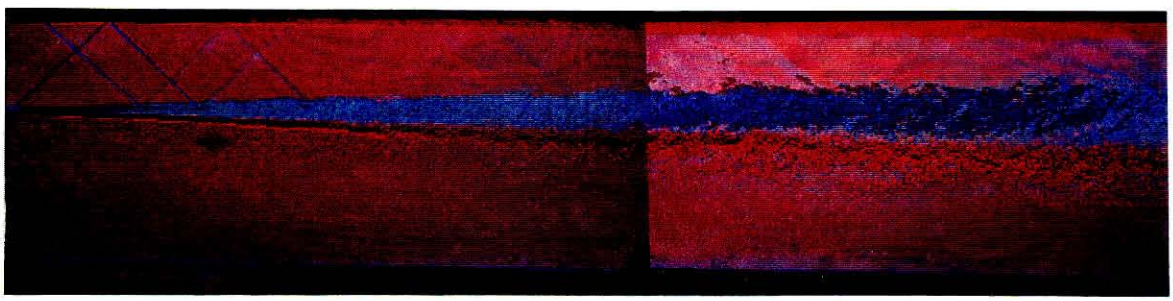

FIG. 5.4 Composite color-schlieren image of Case 5.2b flow.

The temperature-rise data in Fig. 5.1 were used to compute the various quantities described above. In particular, for this low-compressibility flow,

$$\begin{aligned} &\text{Case 5.1a:} \quad \phi = 8\ , \quad \delta_{\rm T}/x = 0.174\ , \quad \delta_{\rm p}/\delta_{\rm T} = 0.287\ ; \\ &\text{Case 5.2a:} \quad \phi = 1/8\ , \quad \delta_{\rm T}/x = 0.164\ , \quad \delta_{\rm p}/\delta_{\rm T} = 0.229\ , \end{aligned} \tag{5.6a}$$

which in turn yield a mixed-fluid (mole) fraction,

$$\delta_{\rm m}/\delta_{\rm T} \ = \ 0.459\ , \tag{5.6b}$$

and a mixed-fluid composition ratio,

$$\mathcal{E}_{\rm n} \ = \ 1.25\ . \tag{5.6b}$$

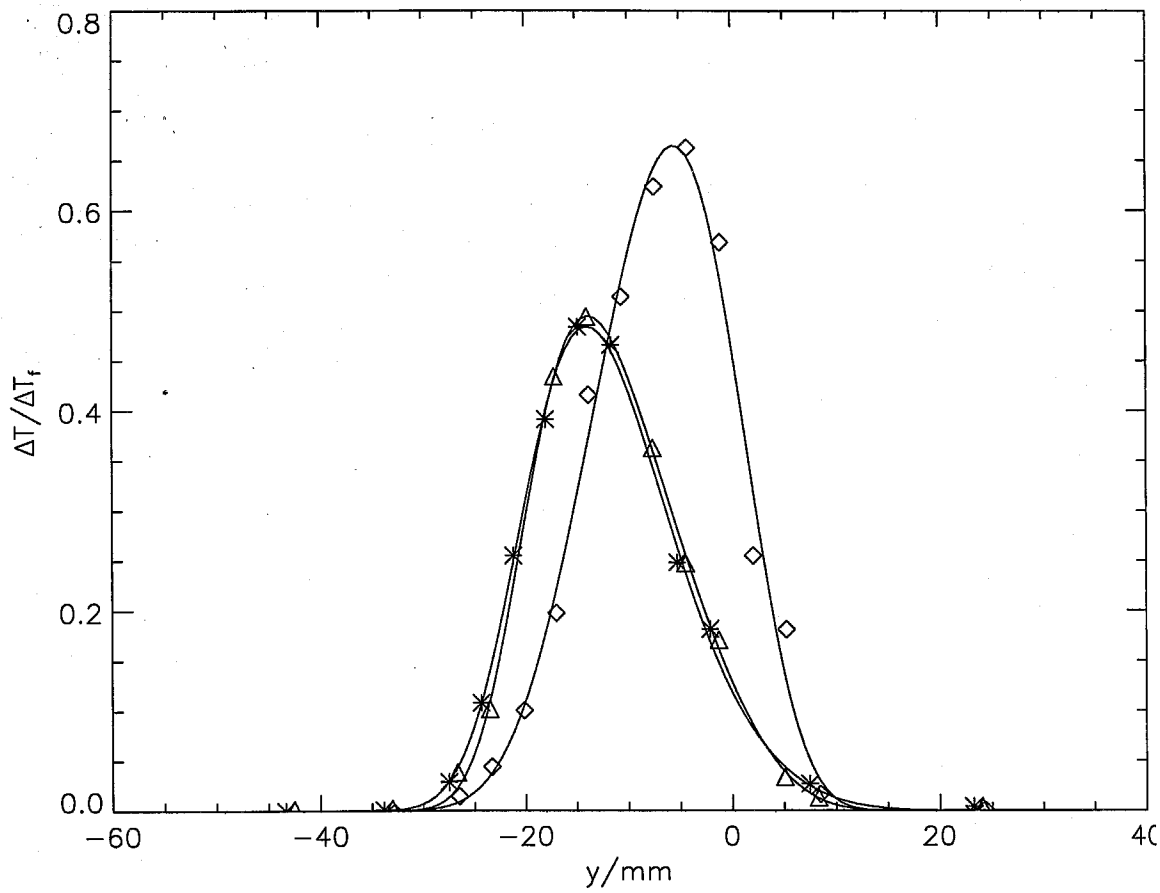

FIG. 5.3 Normalized temperature-rise data for moderate-compressibility flow ($M_c \simeq 0.47$). Same scale as in Fig. 5.1, above, to allow direct comparison of the profiles. Diamonds: Case 5.1b, $\phi = 8$. Triangles: Case 5.2b, $\phi = 1/8$. Asterisks: Case 5.3b, $\phi = 1/8$, increased chemical-kinetic rate.

Normalized temperature-rise measurements for moderate-compressibility flow conditions (Cases 5.1b–5.3b) are plotted in Fig. 5.3. Several differences relative to low-compressibility flow (Fig. 5.1) are noted. In particular, the shear-layer is seen to be thinner, *i.e.*, δ/x has been reduced, at this higher level of compressibility, in quantitative agreement with previous investigations (Fig. 4.8). For the H_2-rich ($\phi = 1/8$) parts of the flip experiment, the maximum normalized temperature rises are comparable in both low- and moderate-compressibility flows. However, the maximum attained in the F_2-rich ($\phi = 8$) part is significantly (25%) higher than in low-compressibility flow, reaching nearly 70% of the adiabatic flame temperature. This behavior was also observed in moderately-compressible flows with freestream-

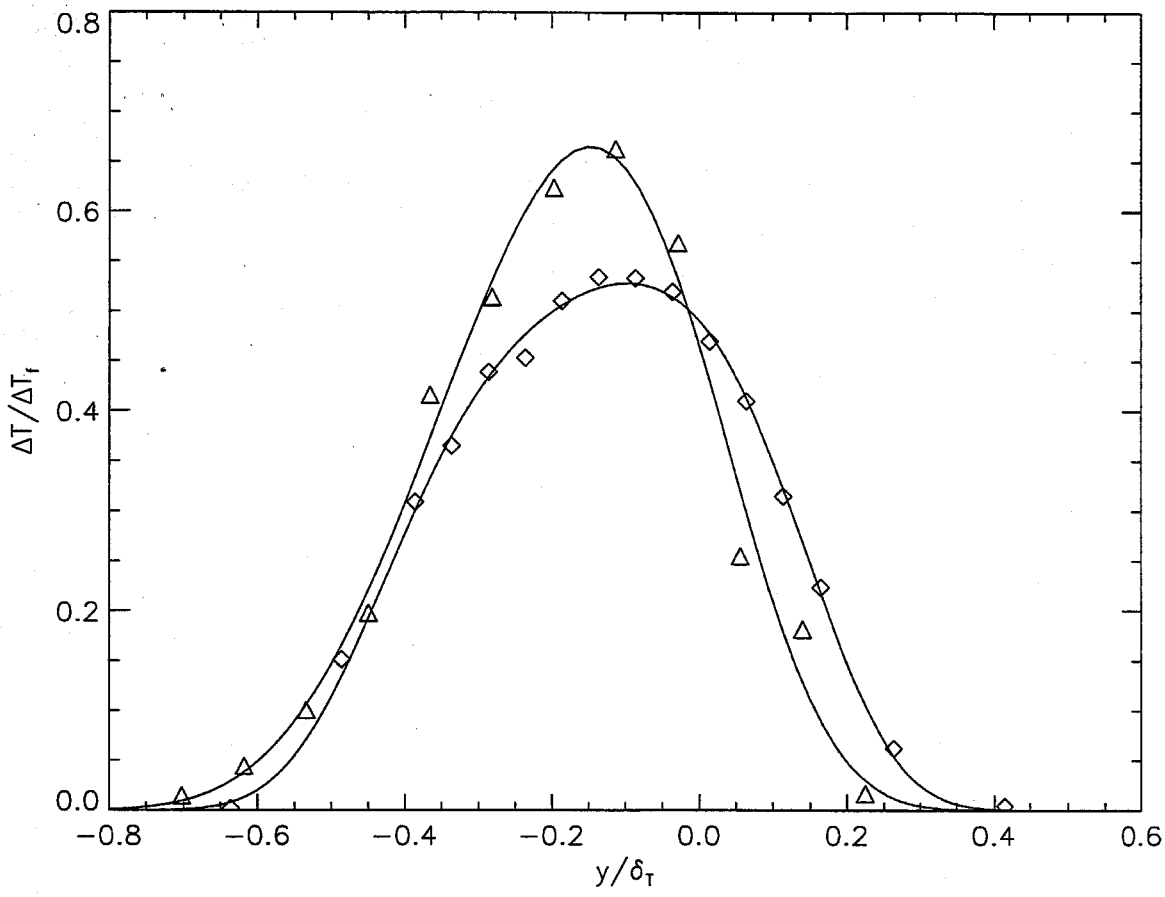

FIG. 5.5 Normalized temperature-rise data for F_2-rich ($\phi = 8$) flows. Diamonds: low-compressibility ($M_c \simeq 0.25$) flow, triangles: moderate-compressibility flow ($M_c \simeq 0.47$).

diluent mixtures of helium and argon (Bond 1996, private communication).

As in Eqs. 5.6 above,

$$\begin{aligned} &\text{Case 5.1b:} \quad \phi = 8 \ , \quad \delta_T/x = 0.103 \ , \quad \delta_p/\delta_T = 0.303 \ ; \\ &\text{Case 5.2b:} \quad \phi = 1/8 \ , \quad \delta_T/x = 0.107 \ , \quad \delta_p/\delta_T = 0.221 \ , \end{aligned} \tag{5.7a}$$

which in turn yield a mixed-fluid fraction,

$$\delta_m/\delta_T \ = \ 0.466 \ , \tag{5.7b}$$

and a mixed-fluid composition ratio,

$$\mathcal{E}_n \ = \ 1.37 \ . \tag{5.7b}$$

These data, despite the significant increase in normalized temperature-rise at $\phi = 8$, show a only a modest increase in chemical product fraction, and consequently, mixed-fluid fraction, associated with the increase in M_c. This finding reflects a change in the shape of the temperature-rise profile, and consequently, the mixed-fluid structure. Figure 5.5 provides a direct comparison of the F_2-rich temperature-rise profiles, with the transverse coordinate normalized by δ_T (see discussion in Ch. 3. Changes are also observed in the instantaneous flow visualizations in Figs. 5.2 and 5.4, where qualitative differences in visualized structure are evident A modified flow structure is also indicated provided by the change in the mixed-fluid composition ratio, which is seen to increase for moderate-compressibility flow, favoring the high-speed fluid to a greater extent than in low-compressibility flow.

5.4 Conclusions

Effects of compressibility on molecular mixing were investigated with the use of chemically-reacting flip experiments at two different freestream-flow conditions. These conditions are characterized by nominally-fixed local-flow Reynolds numbers, freestream-velocity and -density ratios, and reactant compositions, but, a change in convective Mach number from $M_c \simeq 0.25$ to $M_c \simeq 0.47$.

This (isolated) increase in flow compressibility allows the observed changes in shear-layer growth and mixing to be attributed solely to the increase in M_c. A 25% increase in the peak normalized temperature rise was recorded in the F_2-rich part of the flip experiment. However, compressibility has also altered the molecularly-mixed fluid structure, as indicated by changes in temperature-rise profile shapes, as well as in the mixed-fluid composition ratios. As a result, the associated increase in mixed-fluid fraction is small.

CHAPTER 6

An alternative compressibility parameter

A new shear-layer flow compressibility parameter is proposed as an alternative to the (total) convective Mach number, M_c. This parameter is derived from consideration of compressibility as an energy transformation (kinetic to thermal, and *vice versa*) mechanism, and differs from M_c at non-unity freestream-density (speed-of-sound) ratios. Experimentally-observed growth rates are well represented by this new parameter.

6.1 Introduction

Compressibility effects on shear-layer growth are often presented in terms of the total convective Mach number, in the form indicated by Eq. 1.6. This scaling captures the overall reduction in growth rate with increasing M_c, as discussed earlier. Figure 4.8 is reproduced below as Fig. 6.1a, for reference. A fair degree of "scatter" is evident in the data. However, as noted by Clemens & Mungal (1995), among others, the scaling exhibited by many individual sets of experimental data, *e.g.*, Chinzei *et al.* (1986), is reasonably consistent. This behavior is reminiscent of that documented in Ch. 3, *i.e.*, an influence of inflow (or other facility-dependent) conditions that result in the range of values exhibited by Eq. 1.3. Such a variance is not typically addressed in reports of compressible shear-layer growth rates, where a value for C_δ may (often) be chosen to match experimental data, *e.g.*, of Brown & Roshko (1974). An additional complicating difficulty is presented by the use of different measures of the local thickness, δ, *i.e.*, pitot thickness, visual thickness, *etc.*, that comprise the data shown in Fig. 6.1a, and the ill-defined relationships between various measures (Papamoschou 1986).

In an attempt to reconcile experiments performed in various facilities, the constant C_δ is re-evaluated for each individual experimental data set. This procedure, and the resulting values for C_δ, are documented in Appendix B. As seen in Fig. 6.1b, this renormalization provides a substantial reduction in the overall scatter.

It has further been suggested by Sandham and Reynolds (1989), and subsequently discussed by others, *e.g.*, Hall *et al.* (1993), that M_c does not provide a universal compressibility measure, even within a set of experiments performed in a given facility. Examples of this non-universality are evident in Fig. 6.1b, in reduced values of δ/δ_0 reported by Papamoschou & Roshko (1988) and Hall *et al.* (1993).* These low-growth-rate data were recorded in flows characterized by extreme freestream density ratios, *e.g.*, $s \simeq 0.058$ for the argon/helium Case 9 flow of Hall *et al.* (1993). Lu & Lele (1994) have suggested that this behavior indicates that the departure from a universal collapse is a systematic deviation, and not due

* See, by way of example, Case 9 of Papamoschou & Roshko (1988) and Cases 7-9 of Hall *et al.* (1993)

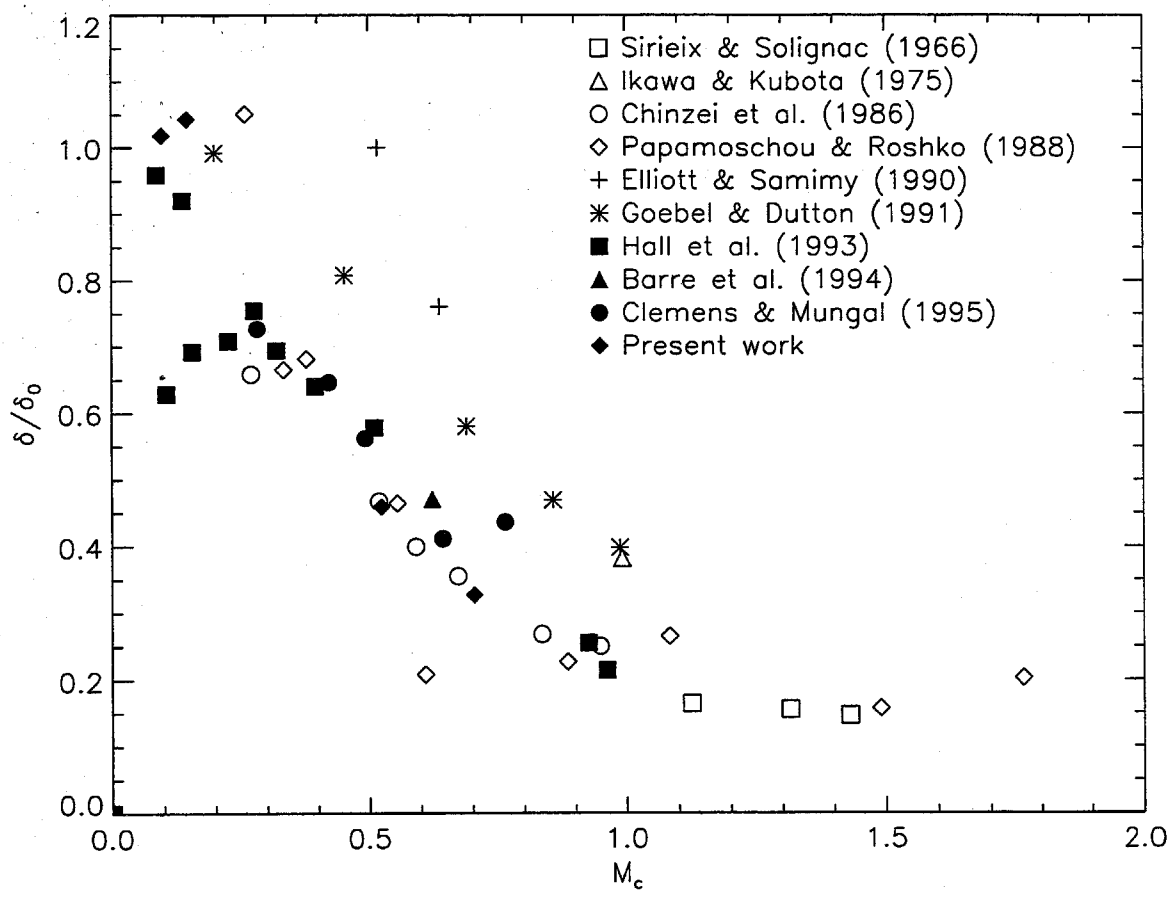

FIG. 6.1a Normalized compressible shear-layer growth rates as parameterized by the total convective Mach number, M_c (Eq. 1.5). Normalization by Eq. 1.2, with C_δ's as suggested (when documented) by the various investigators.

to experimental error. This systematic departure is indicative of a shortcoming on one of two counts:

1. An inaccurate representation of the (normalizing) incompressible shear-layer growth rate, δ_0/x (Eq. 1.2),

or,

2. An inaccurate representation of flow compressibility, as provided by the total convective Mach number, M_c (Eq. 1.5).

These two possibilities will be explored below.

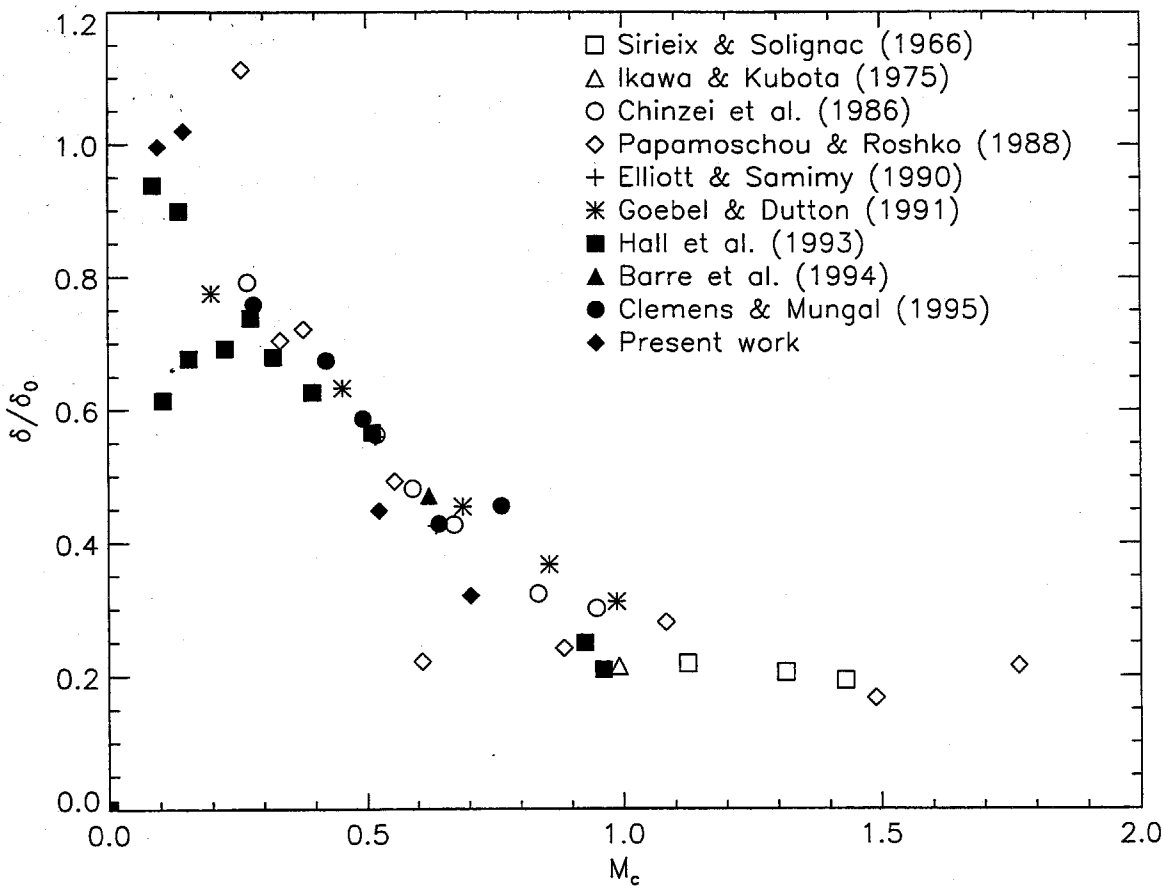

FIG. 6.1b Normalized compressible shear-layer growth rates as parameterized by the total convective Mach number, M_c (Eq. 1.5). Normalization provided by Eq. 1.2, with C_δ's determined as described in text.

6.2 The incompressible-flow growth rate

Lu & Lele (1994) recently reported an improved collapse of the data with the use of a modified incompressible growth-rate estimate, *i.e.*, Option 1. Their model relied on an incompressible-flow linear-stability analysis, employing the most unstable eigenvalue, $-(\alpha_i)_0$, to estimate incompressible-flow growth rates.

Compressible shear-layer growth rates appear to be well-described by such a correlation. For example, Fig. 5 of Lu & Lele (1994) illustrates that,

$$-\alpha_i \sim \frac{\delta}{x} , \tag{6.1}$$

for compressible-flow conditions. The success of such a correlation is likely due

to the relatively-small spatial-growth rates and reduced turbulent-fluctuation levels characteristic of compressible turbulent shear layers, features which enhance the formal validity of assumptions inherent to linear-stability analysis. Interestingly, as noted by Lu & Lele, their Fig. 5 also suggests a rather poor correlation for incompressible flows (*e.g.*, Cases 10 and 11 of Hall *et al.* 1993).

An additional finding of such analyses, *e.g.*, Zhuang (1990), was that the ratio of the compressible-flow to incompressible-flow most-unstable eigenvalue was found to be nearly a function of M_c, for a wide range of parameters, *i.e.*,

$$\frac{-\alpha_i}{-(\alpha_i)_0} \simeq \text{fn}(M_c) \ , \tag{6.2}$$

which, when combined with Eq. 6.2 yields,

$$\frac{\delta/x}{-(\alpha_i)_0} \simeq \text{fn}(M_c) \ . \tag{6.3}$$

The near-functional dependence observed by Lu & Lele (1994) is clear from Eq. 6.3. An issue remains, however, as to whether the incompressible-flow growth rate, δ_0/x, is correlated with the most-unstable eigenvalue from an incompressible-flow linear-stability analysis, $-(\alpha_i)_0$. This issue is especially important at extreme values of the freestream-density ratio, s, a regime in which linear-stability analysis has not been widely tested, as will be discussed below. Unfortunately, a comparison of their model with existing experimental data, *e.g.*, Brown & Roshko (1974), was not provided by Lu & Lele.

Estimates of the large-scale-structure based models of Brown (1974) and Dimotakis (1986) are tested with data from Brown & Roshko (1974) in Figs. 6.2. These data constitute a fairly complete survey of isolated density-ratio effects, *cf.* Eq. 1.3 and Ch. 3 above, with reported values for δ_0/x at density ratios of $s = 1/7, 1, \& 7$ and velocity ratios of $r = 0, 1/7, \& \sqrt{1/7}$.** Over this range of conditions, no systematic deviations of the model estimates from the data are discernible, indicating that Eq. 1.2, and its temporal-growth counterpart, provide an adequate estimate of incompressible shear-layer growth rates.

** Data was not reported for the $r = 0$, $s = 7$ flow condition.

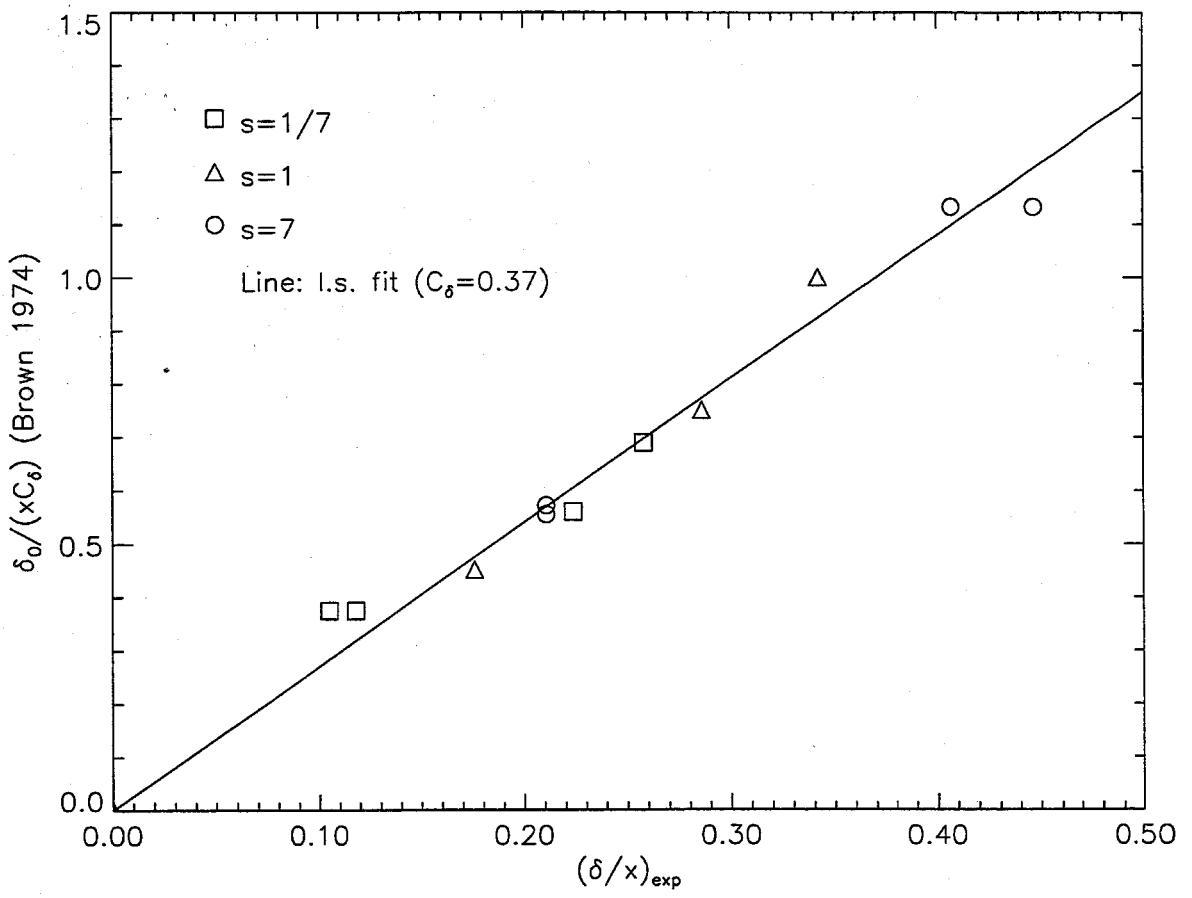

FIG. 6.2a Test of Brown (1974) model predictions for (temporally-evolving) incompressible shear-layer growth with the data of Brown & Roshko (1974).

The linear-stability estimates of Lu & Lele (1994) are provided for a velocity ratio of $r = 1/2$, which does not correspond to any existing set of experimental data. As a result, a test of their proposal that is analogous to that of Figs. 6.2 is not possible. In the interest of evaluating their proposal, however, a comparison of the three estimates, at $r = 1/2$, is presented in Fig. 6.3. Not surprisingly, at low density ratios, linear-stability-model estimates are significantly lower than those of either structure-based model, as required for the collapse observed by Lu & Lele. This reduction is extremely sensitive to the mean-profile shape imposed upon the linear equations, however, as a hyperbolic-tangent profile† yields estimates at

† Lu & Lele employed a set of profiles based on a solution to the laminar thin shear-layer equations, with the two freestreams assumed to have the same composition, *cf.* Hall *et al.* (1993) Case 9 He/Ar flow.

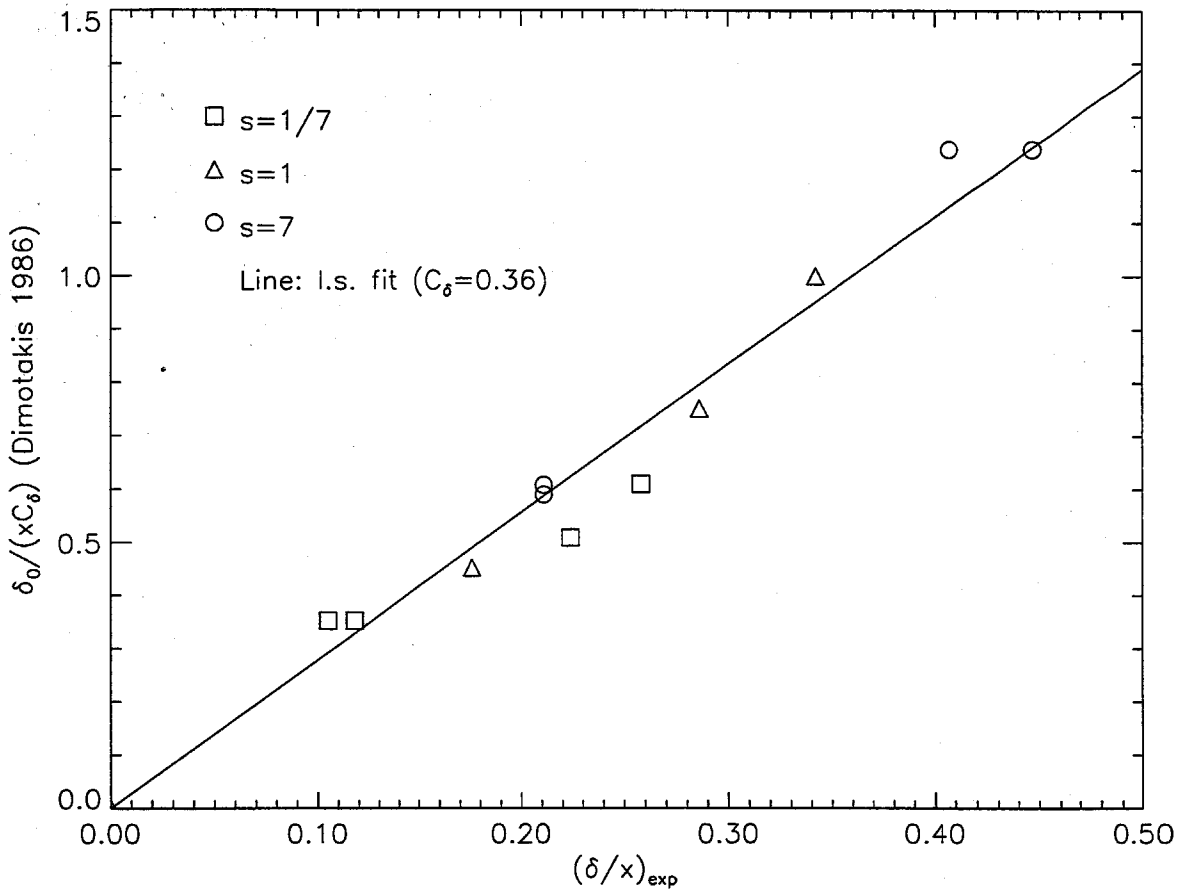

FIG. 6.2b Test of Dimotakis (1986) model predictions for (spatially-evolving) incompressible shear-layer growth with the data of Brown & Roshko (1974).

small s which *exceed* that of both structure-based models (Zhuang 1995, private communication). In addition, a non-monotonic behavior of growth rate with density ratio is indicated for the linear-stability estimates, in contrast to the structure-based-model estimates.

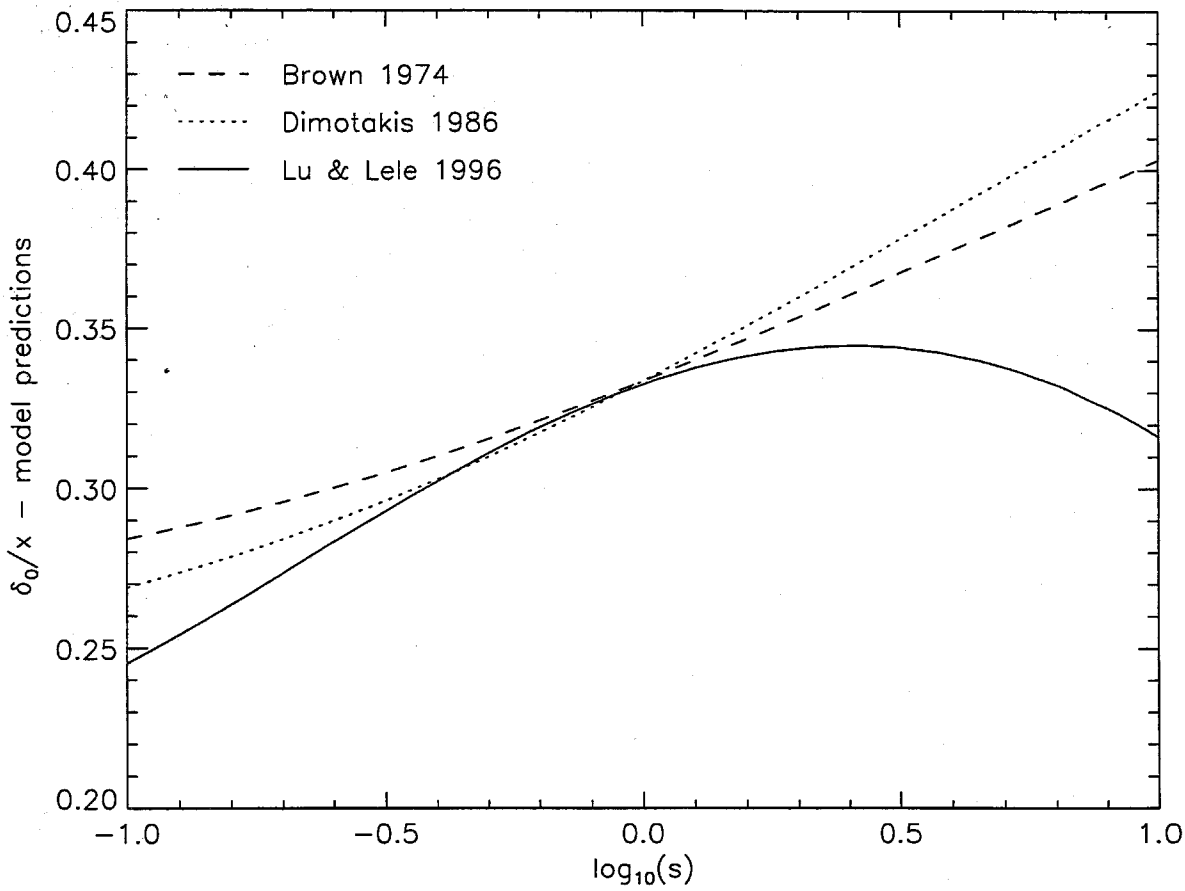

FIG. 6.3 Comparison of Brown (1974), Dimotakis (1986), and Lu & Lele (1994) model estimates for incompressible shear-layer growth rates at $r = 1/2$. Model predictions normalized to coincide at $s = 1$.

6.3 An alternate flow-compressibility measure

Turbulent velocity fluctuations are intimately linked to shear-layer growth. Experimental support for such an association includes observation of decreased (rms) velocity fluctuations with reduced shear-layer growth rates by Goebel & Dutton (1991), in addition to measurements of diminished values of $\overline{u'v'}$ at compressible-flow conditions by Samimy & Elliott (1990). More recently, this relationship has been formally shown in terms of turbulent kinetic energy by Sarkar (1995), and in terms of Reynolds-stress production by Vreman *et al.* (1996) and Freund *et al.* (1997).

There also exists considerable evidence to suggest that growth-rate suppression is due to inviscid energy-exchange mechanisms, and not due to increased viscous (dilatational) dissipation, as was suggested in the past (*e.g.*, Zeman 1990). The data indicate no dependence of growth rate on Reynolds number, as would be expected if a viscous mechanism were dominant. In particular, a fortuitous balance would be required for self-similar (conical) layer growth, as the Reynolds number, Re_δ, is increasing as the flow evolves downstream (Dimotakis 1991a). The success of inviscid linear-stability analyses in predicting the *relative* reduction in growth rate, *e.g.*, Eq. 6.2, lends further support to the notion that the dominant growth-suppression mechanisms are inviscid.

In the most general terms, flow compressibility acts to couple kinetic and thermal energy, for example, in the steady-flow kinetic-to-thermal energy (enthalpy) ratio,

$$\frac{U^2}{2h} = \frac{h_0 - h}{h} = \frac{\gamma - 1}{2} M^2 \ , \tag{6.4}$$

where U is the velocity, and M the Mach number. This scaling is ubiquitous in all forms of the dimensionless energy equation (*e.g.*, Lagerstrom 1964), even in the full unsteady form. Such a balance must be observed by the conversion of kinetic energy into thermal energy by the variety of mechanisms available to compressible turbulence. Such mechanisms, *e.g.*, dilatation, are unavailable to incompressible flow and must observe Eq. 6.4, *independently* of the specific details of their dynamics and character. Consequently, as flow compressibility increases, velocity-field fluctuations can no longer take place autonomously, but instead result in corresponding thermal-energy (enthalpy) fluctuations.

In a shear-layer, the freestream-density ratio, s, is related to the speed-of-sound ratio, *i.e.*,

$$\frac{a_2}{a_1} = \sqrt{\frac{\gamma_2}{s\gamma_1}} \ . \tag{6.5}$$

If we consider a shear layer with, for example, a small density ratio (*e.g.*, Case 9 of Hall *et al.* 1993), a correspondingly large speed-of-sound ratio is indicated by Eq. 6.5. In such a low-s (or conversely, high-s) flow, however, the estimate of flow compressibility given by M_c (Eq. 1.5) will be dominated by the large speed-of-sound value. Given the propensity of these flows to dynamically attain asymmetric con-

vective speeds, resulting in correspondingly-large convective-frame Mach numbers (*e.g.*, Ch. 4), such an estimate is likely to underestimate the flow compressibility. Forming the group suggested by Eq. 6.4, using the (Galilean-invariant) freestream velocity difference, ΔU and the minimum speed of sound, yields such a maximum compressiblity scale,

$$\Pi_c = \max_i \left[\frac{\sqrt{\gamma_i - 1}}{a_i} \right] \times \Delta U \,, \tag{6.6a}$$

or explicitly in terms of the freestream values,

$$\Pi_c = \max_i \left[\sqrt{\gamma_1 - 1} \left(M_1 - \frac{a_2}{a_1} M_2 \right), \sqrt{\gamma_2 - 1} \left(\frac{a_1}{a_2} M_1 - M_2 \right) \right] . \tag{6.6b}$$

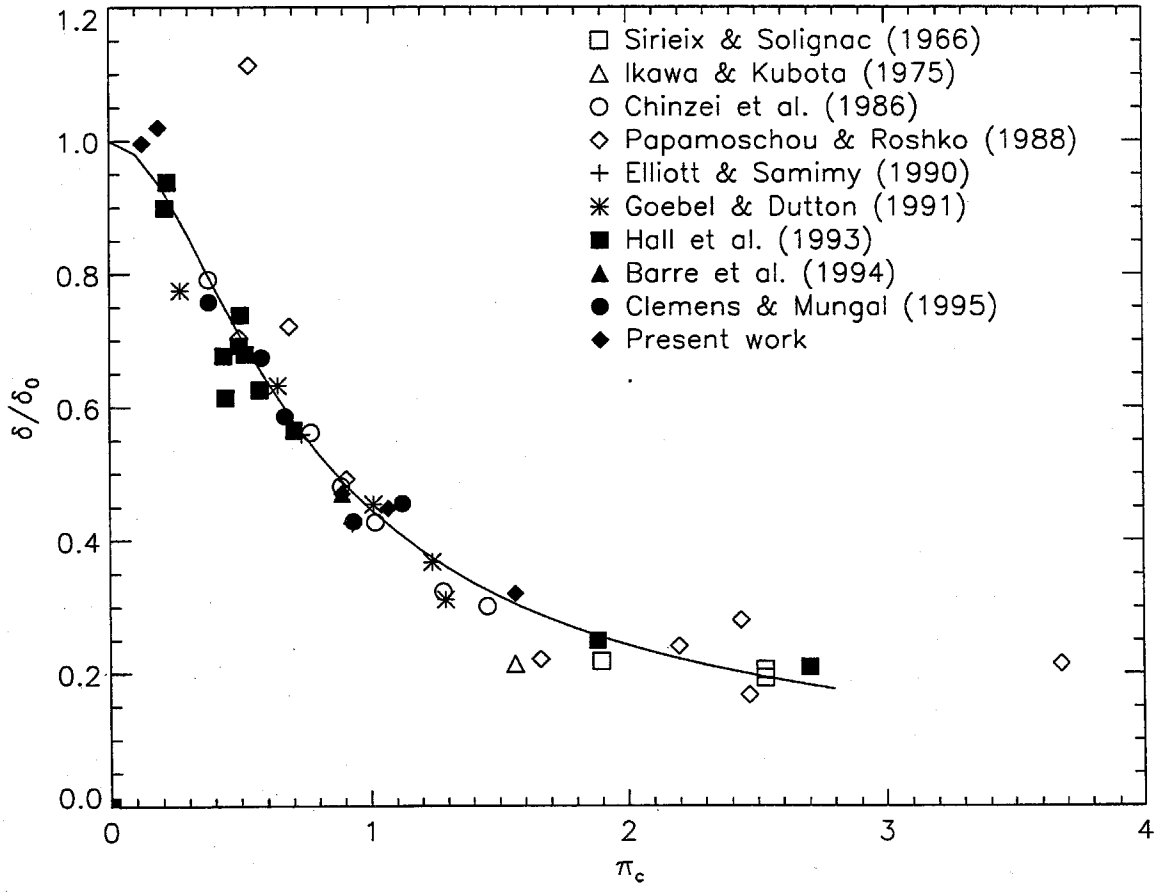

FIG. 6.4 Normalized (as in Fig. 6.1b) compressible shear-layer growth rates parameterized by the proposed compressibility parameter Π_c (Eqs. 6.6). Solid curve is Eq. 6.7.

To provide an estimate of the relative magnitude of heat release in a chemically-reacting flow, with respect to these measures, it is useful to compare the change in (bulk) fluid enthalpy from chemical reaction, $\Delta h_{\rm rxn}$, to the normalizing quantity employed in Eqs. 6.6. An estimate for this enthalpy change is provided by the bulk-dilatation correlation of Dimotakis (1991a). As an example, for Case 5.3b flow conditions, the highest heat-release condition in this work,

$$\sqrt{\Delta h_{\rm rxn}} \times \max_i \left[\frac{\sqrt{\gamma_i - 1}}{a_i} \right] \simeq 0.1 \ ,$$

corroborating the validity of the assumptions of low heat release here. At very high levels of heat release, however, interesting couplings may be operative.

The experimentally-measured growth rates, normalized as in Fig. 6.1b, are plotted against $\Pi_{\rm c}$ in Fig. 6.4. These data observe a near-functional dependence on this parameter, to a better extent than on $M_{\rm c}$. The solid curve through the data,

$$\frac{\delta}{\delta_0} \simeq \left(1 + \alpha \Pi_{\rm c}^2\right)^{-\beta} \ , \quad \alpha \simeq 4, \ \beta \simeq 0.5 \ , \tag{6.7}$$

is a form inspired by the static-to-stagnation enthalpy ratio, Eq. 6.4 above. At high-compressibility conditions, this functional form is in agreement with the high-Mach-number behavior, *i.e.*, $1/M$, suggested by Brown & Roshko (1974). The solid curve in Fig. 6.4 is not extended to high-compressibility conditions, as additional energy-transfer mechanisms *e.g.*, wave/bounding-wall radiative resonances (Zhuang *et al.* 1990), may well play a role in this regime.

The systematic deviations observed in flows with extreme density/speed-of-sound ratios are absent when scaled in this fashion. Considering that many flows reported in the literature were generated with thermodynamically-similar freestream fluids, *e.g.*, the air/air experiments of Chinzei *et al.* (1986), resulting in near-unity values of a_2/a_1 and uniform values of γ, it is not surprising that the previous collapse of normalized growth-rate data was viewed as adequate by many investigators. For such conditions,

$$a_2 = a_1 \quad \text{and} \quad \gamma_2 = \gamma_1 = \gamma \quad \Rightarrow \quad \Pi_{\rm c} = 2\sqrt{\gamma - 1} \times M_{\rm c} \ , \tag{6.8}$$

we would expect the limited ($M_{\rm c}$) collapse to be preserved by the parameterization in terms of $\Pi_{\rm c}$, as is borne out by Fig. 6.4.

6.4 Conclusions

An alternate shear-layer flow compressibility parameter was motivated on the basis of shear-layer growth-rate data and a view of compressibility as an energy-transformation mechanism. This parameter,

$$\Pi_c = \max_i \left[\frac{\sqrt{\gamma_i - 1}}{a_i} \right] \times \Delta U \, ,$$

which differs from the commonly-utilized total convective Mach number, M_c, at extreme freestream-density ratios, provides a good collapse of experimentally-observed growth rates. In addition, a functional form based on the static-to-stagnation enthalpy ratio,

$$\frac{\delta}{\delta_0} \simeq \left(1 + \alpha \Pi_c^2\right)^{-\beta} \, , \quad \alpha \simeq 4, \; \beta \simeq 0.5 \, ,$$

provides a good representation of the experimental data, for $\Pi_c \lesssim 3$.

With regard to some envisioned supersonic-combustion scenarios, *e.g.*, H_2-air propulsion, in which extreme density ratios and associated speed-of-sound ratios will doubtlessly be encountered, this parameterization may prove useful.

CHAPTER 7

Conclusions

Experimental investigations of several aspects of high-Reynolds-number, turbulent, shear-layer flows were undertaken in the GALCIT Supersonic Shear Layer Facility. These consisted of both non-reacting and chemically-reacting flows and yielded quantitative measurements of large-scale dynamics as well as small-scale (molecular) mixing, with chemically-reacting flows employing the $(H_2 + NO)/F_2$ chemical system in the fast-kinetic regime. The properties of this canonical turbulent flow are known to depend on a host of parameters. This work focused on effects of inflow/initial conditions, effects of freestream boundary conditions (supersonic/subsonic flow), and effects of compressibility.

Individual conclusions summarizing the findings of each part of the study are found following each Chapter. A summary is offered below.

Inflow conditions — Effects of perturbed inflow conditions, *i.e.*, tripping the boundary layer flows on the splitter plate upstream of shear-layer formation, were observed to persist for distances that must be considered far downstream, in a high-Re ($Re_\delta \simeq 2 \times 10^5$), incompressible flow. Growth rates and mixed-fluid properties were significantly altered by tripping the high-speed splitter-plate boundary layer. The mixed-fluid (scalar) field, at a downstream distance $x/\theta_1 \simeq 3300$ and a "pairing parameter" of 47, changed from a non-marching probability-density function (pdf), to a marching pdf, when the boundary layer was tripped. Several other perturbation configurations were explored, *e.g.*, a low-speed-side trip, with little observed effect on either growth or mixing. These observations are indicative of shear-layer behavior that depends on not only local-flow properties, but also on upstream conditions, reminiscent of results from low-dimensionality, non-linear (chaotic) systems.

Freestream conditions — The presence, or absence, of subsonic (laboratory-frame) regions on the flow was explored in a set of experiments where the freestreams were bi-subsonic, bi-supersonic, and (hybrid-flow) supersonic/subsonic. Fast-mode turbulent-structure convection speeds were observed in both bi-subsonic and bi-supersonic flows, at variance with an existing empirical rule for mode selection. This rule had suggested that the presence of (one) subsonic freestream was responsible for fast-mode dominance, *i.e.*, $M_{c1} \ll M_{c2}$. Growth rates were suppressed with increasing flow compressibility (M_c), in accord with previous data. This further indicates that turbulent shear layers are relatively insensitive, at least for the flows investigated, to laboratory-frame subsonic regions. In the transonic-flow regime, however, global flowfields, *i.e.*, the two freestreams coupled by the shear layer, were found to be sensitive to imposed boundary conditions.

Compressibility and mixing — Effects of compressibility on molecular mixing were investigated with chemically-reacting flip experiments, at two different freestream flow conditions. These conditions were characterized by nominally-fixed freestream-velocity and -density ratios, local-flow Reynolds numbers, and reactant compositions, but, a changing convective Mach number, from $M_c \simeq 0.25$ to $M_c \simeq 0.47$. This feature allows differences in the measurements to be attributed to the change in compressibility alone. Large-scale growth rates were reduced with increasing compressibility, in accord with previous findings. Mixed-fluid properties exhibit several changes associated with increasing compressibility. In particular, compressibility has little effect on the H_2-rich part of the "flip", but increases the peak temperature rise of the F_2-rich part by approximately 25%, yielding a commensurate change in mixed-fluid composition ratio. Only a small change in the mixed-fluid fraction was found to be associated with the increase in compressibility.

Compressibility and dynamics — An alternative shear-layer flow compressibility parameter, derived from consideration of compressibility as an energy-transformation mechanism, was proposed. A test of incompressible growth-rate models was conducted, indicating that large-scale-structure models provide an accurate representation of incompressible-flow data and are adequate for normalization of compressible-flow data. Normalized shear-layer growth-rate data are well represented by the proposed parameter.

APPENDIX A

Color-schlieren imaging

A.1 Introduction

The turbulent shear layer provides an ideal subject for flow visualization by refractive-index sampling techniques, *e.g.*, schlieren photography, because of the substantial gradients generated by vigorous mixing processes, as well as those produced by dilatation in compressible flows. Such visualizations, employing conventional black-and-white schlieren and shadowgraph techniques, have provided significant information regarding structure and large-scale dynamics in these flows, from the identification of spanwise-coherent large-scale structures (Brown & Roshko 1974), to the apparent absence of such features in compressible flows (*e.g.*, Goebel & Dutton 1991, Hall *et al.* 1993, and Clemens & Mungal 1995).

The information content of such black-and-white visualizations, however, can only record a scalar contraction of the two-dimensional (spanwise-integrated) index-of-refraction gradient field. A black-and-white schlieren system typically represents a single component of the field, corresponding to the direction perpendicular to the knife edge. These one-dimensional data can often lead to difficulties in interpreting flow structure, as seen in the black-and-white schlieren data (Figs. 6.7 and 6.8) of Hall (1991), in which a combination of (non-simultaneous) vertical and horizontal knife-edge realizations was required to observe the details of the unsteady pressure-wave system in a confined, supersonic, shear-layer flow. As discussed by many authors, most recently in reviews by Settles (1985) and Kleine & Grönig (1991), the additional information in a color realization allows simultaneous resolution of both components of the spanwise-integrated, refractive-index-gradient field. In interpreting complex, multi-dimensional fields characteristic of high-speed mixing environments, the additional data provided by color can be of significant benefit.

Color schlieren techniques are broadly classified into two categories: the color-dissection technique of Cords (1968) and the filtered-cutoff technique of Rheinberg (1896). The former system employs a filter mask at the optical source plane to "dissect" the light into different color components, which are then "recombined" at the observation plane. Application of this technique has found (relatively) recent use in high-speed flows, *e.g.*, Kleine & Grönig (1991). Although it alleviates the diffraction-induced resolution degradation of a slit-like cutoff-filter arrangement, *e.g.*, Rheinberg (1896), a serious drawback of the dissection technique is the relatively severe illumination requirement, since a large fraction of the light incident on the source mask is blocked. The configuration discussed by Kleine & Grönig, for example, required a custom-built spark source significantly more energetic than was required by their equivalent (same optical components) black-and-white system.‡

The latter system, a variant of which is employed here, is a direct extension of classical monochrome schlieren techniques, and as such, *potentially* shares similar sensitivity, dynamic range, and illumination demands. The only modification to the black-and-white system is the introduction of a color-filter array, in place of the usual knife edge, at the stop plane. It is often stated, *e.g.*, Settles (1985), that such a system suffers from a degradation in spatial resolution, because of diffraction at the stop plane. In the case of "colored-slit" or "lattice-filter" stop-plane arrays, diffraction resulting from the arrangement of (effective) slits can certainly be significant, especially in a system of reasonable physical dimensions. If, however, an array which codes color in the same manner as a knife edge codes intensity is employed (see Fig. A.1), then the deleterious diffractive effects are eliminated. In such a system, the introduction of the additional dimension provided by color is accompanied by the spatial resolution of the black-and-white system, at a comparable illumination level. This will be demonstrated below.

---

‡ This increase in illumination energy was partially achieved by extending the spark duration, resulting in a reduction in the temporal resolution.

A.2 Visualization of a high-speed turbulent shear-layer flow

A schematic of the optical system employed here is found in Fig. A.1. This "folded" layout is based on a design due to Liepmann (1947) (see discussion by Hermanson 1985 and Hall 1991), which, because of the symmetrical layout, is free of coma. The astigmatism in the system is minimized *via* the use of large focal-length schlieren heads ($f \simeq 2\,\mathrm{m}$ first-surface mirrors). Black-and-white visualizations of shear-layer flows, recorded with this apparatus, possess adequate contrast and dynamic range, *e.g.*, Hall *et al.* (1993), and as a consequence, extension to a filtered-cutoff system would be expected to yield good results. This performance is primarily the result of an optically-long integration path ($b = 15.3\,\mathrm{cm}$ test-section span, maintained at atmospheric static pressure) which enhances the magnitude of recorded gradients.

The color cutoff mask was fabricated from 120°-wedge segments of red, green, and blue (Lee #'s 019, 124, and 183, respectively) filters.[♯] As indicated above, this extension to a cutoff-mask color configuration, in contrast to a dissection technique, does not require a modification of the illumination source. In particular, we are still able to employ a commercially-available Nanospark N-789B spark source driven by a N-487B high-voltage source (20 ns FWHM illumination duration), fast enough to temporally resolve high-speed flows. If an equivalent-sensitivity dissection technique had been employed, the development of a longer-duration, higher-output source would have been required, with a probable loss of temporal resolution.

An image of a $f = 10\,\mathrm{m}$ lens, as viewed through the optical system, is reproduced in the schematic (Fig. A.1). This lens produces a known (light-beam) deflection, analogous to deflections produced by flow-induced index-of-refraction gradients, providing a calibration reference. The maximum light-ray deflection, observed at the edge of the lens, is estimated to be approximately 1 milliradian.

A composite image of a subsonic, but moderate-to-high speed, shear-layer flow (Case 5.2a conditions), recorded with the system described above, is shown

---

[♯] Other masks were fabricated from Kodak Wratten #'s 25 (red), 58 (green), 47 (blue), and 8 (yellow).

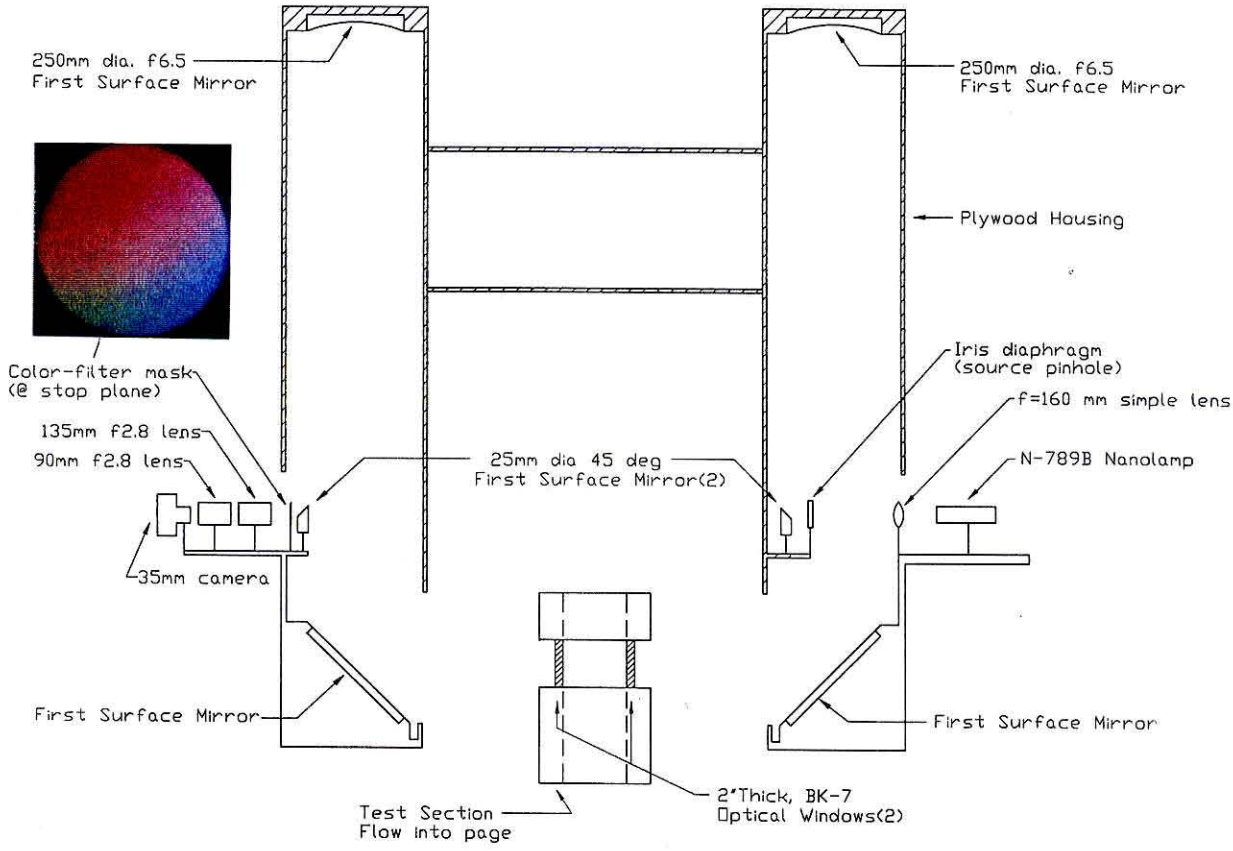

FIG. A.1 Schematic of schlieren photography system. Circular pattern at upper left is an $f = 10\,\mathrm{m}$ lens, as imaged through the schlieren optics, to illustrate the performance of the system.

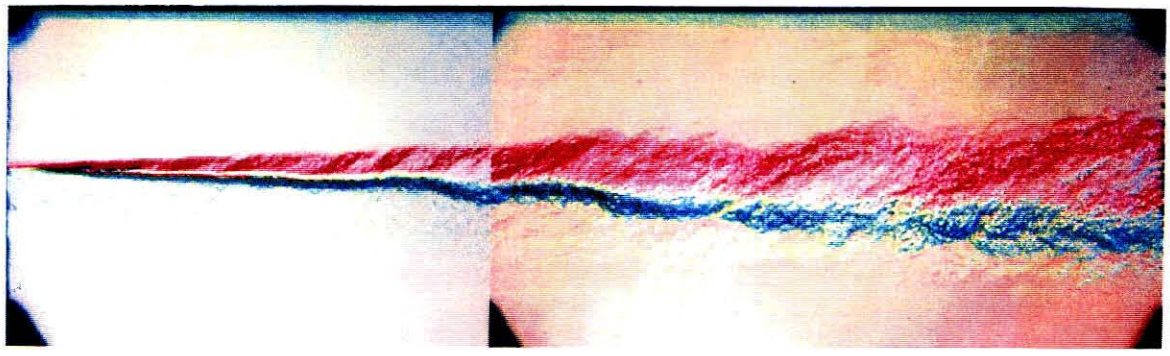

FIG. A.2 Composite color schlieren photograph Case 5.2a flow.

in Fig. A.2. As with all of the images presented in this work, the image consists of two uncorrelated photographs, taken during different runs, to visualize both the up-

stream and downstream regions of the flow. In this flow, the freestream gas mixtures have been tailored so that freestream densities are nearly uniform ($s \simeq 1$), with the *schliere* largely produced by the temperature rise from the chemical reaction.

In the flow image, the large-scale, spanwise-coherent, vortical structures, typical of these flows, are clearly visible. Compared to black-and-white visualizations of such flows, *e.g.*, Brown & Roshko (1974), we can glean additional information from this realization, because of the additional dimension of index-of-refraction gradient data recorded in the color visualization. For example, the local (instantaneous) structure of the temperature-rise field, in this chemically-reacting flow, is seen to be nearly symmetric with respect to the large-scale structures, an observation that cannot be made on the basis of monochrome schlieren data without assumptions as to local-gradient directions. Also visible in this image is the top-guidewall boundary layer, which supports a temperature gradient between the cooler, high-speed flow ($T_{\text{flow}} \simeq 265\,\text{K}$) and the warmer, room-temperature ($T_{\text{wall}} \simeq 295\,\text{K}$) guidewall.

Several general inferences, with regard to performance of this color-schlieren system, are also obtained from this image. First and foremost, it is clear from the small-scale detail present, *e.g.*, the upper-guidewall boundary-layer structure, that the spatial resolution is relatively high and has not been significantly degraded by diffractive effects. Of course, this is not surprising, since with regard to diffractive effects, the filter arrangement employed is equivalent to the classical knife-edge. Second, the high spatial resolution has been achieved with efficient use of the illumination source, relative to a dissection-based system. Consequently, the high temporal resolution associated with short-duration (20 ns) spark-source illumination is retained. It is also evident from the range of colors generated by the calibration lens that the sensitivity and dynamic range of this system are qualitatively comparable, if slightly reduced, to that of a similar dissection-based system (*cf.*, Kleine & Grönig 1991), at a much-reduced illumination level.

APPENDIX B

Compressible shear-layer growth-rate normalization

As discussed in Ch. 6, values employed for C_δ (Eq. 1.2) in the normalization of compressible shear-layer growth-rate data are usually not measured, but instead chosen to match incompressible-flow data, *e.g.*, of Brown & Roshko (1974). Given the variance exhibited in Eq. 1.3, a range which is likely also exhibited in compressible-flow data, an attempt was made to reconcile the entire data set from various facilities/experiments by recomputing the C_δ's as follows.

Since most individual data sets contain measurements near $M_c = 0.5$, the empirical correlation suggested by Dimotakis (1991a),

$$\frac{\delta}{\delta_0} \simeq f(M_c) \equiv 0.8e^{-3M_c^2} + 0.2 \ , \tag{B.1}$$

was employed to as a local interpolator of the normalized growth rate, δ/δ_0, for a particular data point at $M_{c,\mathrm{ref}}$, close to $M_c = 0.5$. This correlation was based on the data available at the time, and uses a functional form similar to that employed by Zhuang (1990) in an investigation of compressible-flow linear-stability analysis. It has a different functional form (exponential *vs.* power law) than the correlation offered in Ch. 6, which uses a different compressibility parameterization.

This estimate was then used to calculate C_δ, *i.e.*,

$$C_\delta \simeq \left(\frac{1}{C_\delta} \frac{\delta_0}{x} f(M_{c,\mathrm{ref}}) \right)^{-1} \frac{\delta}{x}(M_{c,\mathrm{ref}}) \ , \tag{B.2}$$

where $\delta_0/(xC_\delta)$ is computed using Eq. 1.2, $\frac{\delta}{x}(M_{c,\mathrm{ref}})$ is the growth rate measured at $M_c = M_{c,\mathrm{ref}}$, and $f(M_{c,\mathrm{ref}})$ is computed using Eq. B.1. Several comments are warranted:

1. The data of Sirieix & Solignac (1966) are normalized at $M_{c,\mathrm{ref}} = 1.125$, the lowest-compressibility flow reported.

2. The (single-point) data of Ikawa & Kubota (1975) employs the same C_δ as that of Samimy & Elliott (1990).

3. No correction is made for the (single-point) data of Barre *et al.* (1994).

This procedure results in the following values for C_δ, where $C_{\delta,\mathrm{o}}$ are values suggested (or deduced from) in the original publications.

	$M_{\mathrm{c,ref}}$	$f(M_{\mathrm{c,ref}})$	$\frac{1}{C_\delta}\frac{\delta_0}{x}$	$\frac{\delta}{x}(M_{\mathrm{c,ref}})$	C_δ	$C_{\delta,\mathrm{o}}$
Sirieix & Solignac[1]:	1.13	0.218	1.50	0.0345	0.106	0.140
Ikawa & Kubota[2]:	0.991	0.242	1.59	0.064	0.189	0.105
Chinzei *et al.*:	0.591	0.481	0.805	0.045	0.116	0.140
Papamoschou & Roshko:	0.555	0.517	0.400	0.026	0.132	0.140
Samimy & Elliott:	0.517	0.559	0.881	0.093	0.189	0.105
Goebel & Dutton:	0.453	0.632	0.570	0.038	0.105	0.0825
Hall *et al.*:	0.511	0.565	1.16	0.114	0.174	0.170
Barre *et al.*[3]:	0.623	0.450	1.19	0.0338	0.0606	0.0606
Clemens & Mungal:	0.493	0.586	1.05	0.100	0.163	0.17

Table C.1: Details of C_δ determination. Superscripts refer to entries in list above.

The present work employs the same values as Hall *et al.* (1993), as these experiments were in the same facility, and employ the same (visual) growth-rate measure.

References

ABRAMOVICH, G. N. 1963 *The theory of turbulent jets* (MIT Press, Cambridge, MA).

BARRE, S., QUINE, C. & DUSSAUGE, J. P. 1994 "Compressibility effects on the structure of mixing layers: Experimental results," *J. Fluid Mech.* **259**, 47–78.

BATCHELOR, G. K. 1953 *The Theory of Homogeneous Turbulence* (Cambridge U.P., London).

BATT, R. G. 1975 "Some Measurements on the Effect of Tripping the Two-Dimensional Shear Layer," *AIAA J.* **13**(2), 245–247.

BELL, J. H. & MEHTA, R. D. 1990 "Development of a two-stream mixing layer from tripped and untripped boundary layers," *AIAA J.* **28**(12), 2034–2042.

BERNAL, L. P., BREIDENTHAL, R. E., BROWN, G. L., KONRAD, J. H. & ROSHKO, A. 1979 "On the Development of Three-Dimensional Small Scales in Turbulent Mixing Layers," 2^{nd} *Int. Symposium on Turb. Shear Flows* (Springer-Verlag, New York, 1980), 305–313.

BOGDANOFF, D. W. 1983 "Compressibility Effects in Turbulent Shear Layers," *AIAA J.* **21**, 926–927.

BOND, C. L. 1998 *Reynolds Number Effects on Mixing in the Turbulent Shear Layer*, Ph.D. thesis, California Institute of Technology.

BOND, C. L. & DIMOTAKIS, P. E. 1996 "Molecular mixing in high Reynolds number, subsonic, free shear layers," Fall Technical Meeting, Western States Section (Combustion Institute), 28–29 October 1996 (U. So. California), Paper 96F–099.

BRADSHAW, P. 1966 "The effect of initial conditions on the development of a free shear layer," *J. Fluid Mech.* **26**(2), 225–236.

BRADSHAW, P. 1977 "Compressible Turbulent Shear Layers," *Ann. Rev. Fluid Mech.* **9**, 33–54.

BREIDENTHAL, R. E. 1978 *A Chemically Reacting Turbulent Shear Layer*, Ph.D. thesis, California Institute of Technology.

BREIDENTHAL, R. E. 1981 "Structure in Turbulent Mixing Layers and Wakes Using a Chemical Reaction," *J. Fluid Mech.* **109**, 1–24.

BRIO, M. & HUNTER, J. K. 1992 "Mach reflection for the two-dimensional Burgers equation," *Physica D* **60**, 194–207.

BROADWELL, J. E. & BREIDENTHAL, R. E. 1982 "A simple model of mixing and chemical reaction in a turbulent shear layer," *J. Fluid Mech.* **125**, 397–410.

BROADWELL, J. E. & MUNGAL, M. G. 1991 "Large-scale structures and molecular mixing," *Phys. Fluids* A **3**(5), Pt. 2, 1193–1206.

BROWAND, F. K. & LATIGO, B. O. 1979 "Growth of the two-dimensional mixing layer from a turbulent and non-turbulent boundary layer," *Phys. Fluids* **22**(6), 1011–1019.

BROWN, G. L. 1974 "The Entrainment and Large Structure in Turbulent Mixing Layers," 5th *Australasian Conf. on Hydraulics and Fluid Mechanics*, 352–359.

BROWN, G. L. & ROSHKO, A. 1974 "On Density Effects and Large Structure in Turbulent Mixing Layers," *J. Fluid Mech.* **64**, 775–816.

CHINZEI, N., MASUA, G., KOMURO, T., MURAKAMI, A. & KUDOU, K. 1986 "Spreading of two-stream supersonic turbulent mixing layers," *Phys. Fluids* **29**, 1345–1347.

CLEMENS, N. T. & MUNGAL, M. G. 1992a "Two- and Three-Dimensional Effects in the Supersonic Mixing Layer," *AIAA J.* **30**(4), 973–981.

CLEMENS, N. T. & MUNGAL, M. G. 1992b "Effects of Sidewall Disturbances on the Supersonic Mixing Layer," *J. Prop. Power* **8**(1), 249–251.

CLEMENS, N.T. & MUNGAL, M.G. 1995 "Large-scale structure and entrainment in the supersonic mixing layer," *J. Fluid Mech.* **284**, 171–216.

CLEMENS, N. T. & PAUL, P. H. 1995 "Scalar measurements in compressible axisymmetric mixing layers," *Phys. Fluids* , **7**(5) 1071–1081.

COATS, C. M. 1996 "Coherent Structures in Combustion," *Prog. Energy Combust. Sci.* **22**, 427–509.

COLELLA, P. & HENDERSON, L. F. 1990 "The von Neumann paradox for the diffraction of weak shock waves," *J. Fluid Mech.* **213**, 71–94.

COLES, D. 1965 "Transition in circular Couette flow," *J. Fluid Mech.* **21**, 385–425.

CORDS, P. H. 1968 "A high-resolution, high-sensitivity color schlieren method," *SPIE Journal*, **6** (3), 85–88.

DANCKWERTS, P. V. 1958 "The effect of incomplete mixing on homogeneous reactions," *Chem. Eng. Sci.* **8**, 93–102.

DIMOTAKIS, P. E. 1986 "Two-Dimensional Shear-Layer Entrainment," *AIAA J.* **24**, 1791–1796.

DIMOTAKIS, P. E. 1987 "Turbulent shear layer mixing with fast chemical reactions," *Turbulent Reactive Flows.* In, *Lecture Notes in Engineering* **40** (Ed. R. Borghi and S. N. B. Murthy, Springer-Verlag, New York, 1989), 417–485.

DIMOTAKIS, P. E. 1991a "Turbulent Free Shear Layer Mixing and Combustion," *High Speed Flight Propulsion Systems*, in *Progress in Astronautics and Aeronautics* **137**, Ch. 5, 265–340.

DIMOTAKIS, P. E. 1991b "On the convection velocity of turbulent structures in supersonic shear layers," *AIAA* 22nd *Fluid Dynamics, Plasma Dynamics and Lasers Conference*, Paper 91–1724.

DIMOTAKIS, P. E. 1993 "Some issues on turbulent mixing and turbulence," GALCIT Report FM93–1a.

DIMOTAKIS, P. E. & BROWN, G. L. 1976 "The mixing layer at high Reynolds number: Large-structure dynamics and entrainment," *J. Fluid Mech.* **78**, 535–560 + 2 plates.

DIMOTAKIS, P. E., DEBUSSY, F. D. & KOOCHESFAHANI, M. M. 1981 "Particle Streak Velocity Field Measurements in a Two-Dimensional Mixing Layer," *Phys. Fluids* **24**(6), 995–999.

DIMOTAKIS, P. E. & HALL, J. L. 1987 "A simple model for finite chemical kinetics analysis of supersonic turbulent shear layer combustion," *AIAA/SAE/ASME/-ASEE* 23rd *Joint Propulsion Meeting*, Paper 87–1879.

DIMOTAKIS, P. E. & LEONARD, A. 1991 "Chemical Reactions in Turbulent Mixing Flows," AFOSR F49620–89–J–0290 Technical Report.

DZIOMBA, B. & FIEDLER, H. E. 1985 "Effect of initial conditions on two-dimensional free shear layers," *J. Fluid Mech.* **152**, 419–442.

FREUND, J. B., MOIN, P. & LELE, S. K. 1997 "Compressibility effects in a turbulent annular mixing layer," Report No. TF–72, Department of Mechanical Engineering, Stanford University.

FRIELER, C. E. & DIMOTAKIS, P. E. 1988 "Mixing and Reaction at Low Heat Release in the Non-Homogeneous Shear Layer," *First National Fluid Dynamics Congress*, Paper 88–3626.

GOEBEL, S. G. & DUTTON, J. C. 1991 "Experimental Study of Compressible Turbulent Mixing Layers," *AIAA J.* **29**(4), 538–546.

GROPENGIESSER, H. 1970 "Study of the Stability of Boundary Layers in Compressible Fluids," NASA–TT–F–12786.

GUDERELY, K. G. 1946 "Considerations on the Structure of Mixed Subsonic-Supersonic Flow Patterns," Wright Field Technical Report, F-TR-2168-ND.

HALL, J. L. 1991 *An Experimental Investigation of Structure, Mixing and Combustion in Compressible Turbulent Shear Layers*, Ph.D. thesis, California Institute of Technology.

HALL, J. & DIMOTAKIS, P. E. 1989 "Design Overview of the Supersonic Hydrogen-Fluorine Facility (V4.0)," GALCIT Internal Report, 30 August 1989.

HALL, J. L., DIMOTAKIS, P. E. & ROSEMANN, H. 1991 "Some measurements of molecular mixing in compressible turbulent mixing layers," *AIAA* 22nd *Fluid Dynamics, Plasma Dynamics and Lasers Conference*, Paper 91–1719.

HALL, J. L., DIMOTAKIS, P. E. & ROSEMANN, H. 1993 "Experiments in non-reacting compressible shear layers," *AIAA J.* **31**(12), 2247–2254.

HERMANSON, J. C. 1985 *Heat Release Effects in a Turbulent, Reacting Shear Layer*, Ph.D. thesis, California Institute of Technology.

HERMANSON, J. C. & DIMOTAKIS, P. E. 1989 "Effects of heat release in a turbulent reacting shear layer," *J. Fluid Mech.* **199**, 333–375.

HO, C.-M. & HUANG 1982 *J. Fluid Mech.* **119**, 443–73.

HO, C.-M. & HUERRE, P. 1984 "Perturbed Free Shear Layers," *Ann. Rev. Fluid Mech.* **16**, 365–424.

HORNUNG, H. 1986 "Regular and Mach Reflection of Shock Waves," *Ann. Rev. Fluid Mech.* **18**, 33–58.

HORNUNG, H. G., OERTEL, H. & SANDEMAN, R. J. 1979 "Transition to Mach reflection of shock waves in steady and pseudosteady flow with and without relaxation," *J. Fluid Mech.* **90**, 541–560.

HUANG, L.-S. & HO, C.-M. 1990 "Small-scale transition in a plane mixing layer," *J. Fluid Mech.* **210**, 475–500.

IKAWA, H. & KUBOTA, T. 1975 "Investigation of supersonic turbulent mixing layer with zero pressure gradient," *AIAA J.* **13**, 566–572.

ISLAND, T. C. 1997 "Quantitative Scalar Measurements and Mixing Enhancement in Compressible Shear Layers," Stanford HTGL Report No. TSD–104.

KARASSO, P. S. & MUNGAL, M. G. 1996 "Scalar mixing and reaction in plane liquid shear layers," *J. Fluid Mech.* **323**, 23–63.

KLEINE, H. & GRÖNIG, H. 1991 "Color schlieren methods in shock wave research," *Shock Waves* **1**, 51–63.

KOBAYASHI, S., ADACHI, T. & SUZUKI, T. 1995 "Examination of the von Neumann paradox for a weak shock wave," *Fluid Dyn. Research* **17**, 13–25.

KONRAD, J. H. 1976 *An Experimental Investigation of Mixing in Two-Dimensional Turbulent Shear Flows with Applications to Diffusion-Limited Chemical Reactions*, Ph.D. thesis, California Institute of Technology.

KOOCHESFAHANI, M. M. & DIMOTAKIS, P. E. 1986 "Mixing and chemical reactions in a turbulent liquid mixing layer," *J. Fluid Mech.* **170**, 83–112.

KOOCHESFAHANI, M. M. & FRIELER, C. E. 1989 "Instability of Nonuniform Density Free Shear Layers with a Wake Profile," *AIAA J.* **27**, 1735–1740.

KOOCHESFAHANI, M. & MACKINNON, C. 1991 "Influence of forcing on the compositions of mixed fluid in a two-stream shear layer," *Phys. Fluids A* **3**(5), 1135–1142.

LAGERSTROM, P. A. 1964 "Laminar flow theory," in *Theory of Laminar Flows*, *High Speed Aerodynamics and Jet Propulsion*, **4** (Princeton U.P., Princeton, NJ), 20–285.

LANG, D. B. 1985 *Laser Doppler Velocity and Vorticity Measurements in Turbulent Shear Layers*, Ph.D. thesis, California Institute of Technology.

LELE, S. K. 1994 "Compressibility Effects on Turbulence," *Ann. Rev. Fluid Mech.* **26**, 211–254.

LIEPMANN, H. W. 1945 "Investigation of boundary layer transition on concave walls," NACA Wartime Report W–87.

LIEPMANN, H. W. 1947 "The interaction between boundary layer and shock waves in transonic flow," *J. Aeronaut. Sci.* **13**, 623–635.

LIEPMANN, H. W. & LAUFER, J. 1947 "Investigations of Free Turbulent Mixing," NACA TN–1257.

LIEPMANN, H. W. & ROSHKO, A. 1957 *Elements of Gasdynamics* (John Wiley, New York).

LOWSON, M. V. & OLLERHEAD, J. B. 1968 "Visualization of noise from cold supersonic jets," *J. Acoust. Soc. Am.* **44**, 624.

LU, G. & LELE, S. K. 1994 "On the density ratio effect on the growth rate of a compressible mixing layer," *Phys. Fluids* **6**, 1073–1075.

MACK, L. M. 1969 "Boundary Layer Stability Theory," Jet Propulsion Laboratory, Doc. No. 900–277 (Rev. A).

MACK, L. M. 1975 "Linear Stability and the Problem of Supersonic Boundary-layer Transition," *AIAA J.* **13**, 278–289.

MACK, L. M. 1984 "Boundary-Layer Linear Stability Theory," AGARD Report 709.

MARTENS, S., KINZIE, K. W. & MCLAUGHLIN, D. K. 1994 "Measurements of Kelvin-Helmholtz instabilities in a supersonic shear layer," *AIAA J.* **32**(8), 1633–1639.

MILLER, P. L. 1991 *Mixing in High Schmidt Number Turbulent Jets*, Ph.D. thesis, California Institute of Technology.

MUNGAL, M. G., HERMANSON, J. C. & DIMOTAKIS, P. E. 1985 "Reynolds Number Effects on Mixing and Combustion in a Reacting Shear Layer," *AIAA J.* **23**, 1418–1423.

OERTEL, H. 1979 "Mach wave radiation of hot supersonic jets investigated by means of the shock tube and new optical techniques," 12th *Int. Symp. on Shock Tubes and Waves*, 266–275.

OSTER, D. & WYGNANSKI, I. 1982 "The forced mixing layer between parallel streams," *J. Fluid Mech.* **123**, 91–130.

OSTER, D., WYGNANSKI, I. & FIEDLER, H. 1976 "Some preliminary observations on the effect of initial conditions on the structure of the two-dimensional turbulent mixing layer," *Turbulence in Internal Flows*, Project SQUID Workshop (Ed. S. N. B. Murthy. Hemisphere, Washington), 67–87.

PAPAMOSCHOU, D. 1986 *Experimental Investigation of Heterogeneous Compressible Shear Layers*, Ph.D. thesis, California Institute of Technology.

PAPAMOSCHOU, D. 1989 "Diffuser Performance of Two-Stream Supersonic Wind Tunnels," *AIAA J.* **27**(8), 1124–1127.

PAPAMOSCHOU, D. 1989 "Structure of the compressible turbulent shear layer," *AIAA* 27th *Aerospace Sciences Meeting*, Paper 89–0126.

PAPAMOSCHOU, D. 1991 "Structure of the compressible turbulent shear layer," *AIAA J.* **29**, 680–681.

PAPAMOSCHOU, D. & BUNYAJITRADULYA, A. 1996 "Evolution of large eddies in compressible shear layers," *Phys. Fluids A* **9** (3), 756–765.

PAPAMOSCHOU, D. & ROSHKO, A. 1988 "The Compressible Turbulent Shear Layer: An Experimental Study," *J. Fluid Mech.* **197**, 453–477.

PEPIN, F. E. & DIMOTAKIS, P. E. 1989 "The DUCT Solver," Internal CADRE Documentation, California Institute of Technology.

RAGAB, S. A. & WU, J. L. 1988 "Linear instabilities in two-dimensional compressible mixing layers," *Phys. Fluids* A **1**(6), 957–966.

RHEINBERG, J. 1896 "On an addition to the methods of microscopical research, by a new way of optically-producing color contrast between an object and its background or between definite parts of the object itself," *J. Royal Microscop. Soc.*, Aug. 1896, 373–388.

ROBERTS, F. A. 1985 *Effects of a Periodic Disturbance on Structure and Mixing in Turbulent Shear Layers and Wakes*, Ph.D. thesis, California Institute of Technology.

ROBERTS, F. A. & ROSHKO, A. 1985 "Effects of Periodic Forcing on Mixing in Turbulent Shear Layers and Wakes," *AIAA Shear Flow Control Conference*, Paper 85–0570.

ROGERS, M. M. & MOSER, R. D. 1992 "The three-dimensional evolution of a plane mixing layer: the Kelvin-Helmholtz rollup," *J. Fluid Mech.* **243**, 183–226.

ROGERS, M. M. & MOSER, R. D. 1994 "Direct simulation of a self-similar turbulent mixing layer," *Phys. Fluids* **6**(2), 903–923.

ROSHKO, A. 1976 "Structure of Turbulent Shear Flows: A New Look," *AIAA J.* **14**, 1349–1357, and **15**, 768.

SABIN, C. M. 1965 "An analytical and experimental investigation of the plane, incompressible, turbulent free-shear layer with arbitrary velocity ratio and pressure gradient," *Trans. of the ASME* D **87**, 421–428.

SAMIMY, M. & ELLIOTT, G. S. 1990 "Effects of Compressibility on the Characteristics of Free Shear Layers," *AIAA J.* **28**(3), 439–445.

SANDEMANN, R. J. 1997 "Conditions at the triple point in weak Mach reflection," Paper 8999, 21st International Symposium on Shock Waves, Great Keppel Island, Australia.

SANDHAM, N. D. & REYNOLDS, W. C. 1989 "A Numerical Investigation of the Compressible Mixing Layer," Stanford Report TF–45.

SANDHAM, N. D. & REYNOLDS, W. C. 1990 "Compressible Mixing Layer: Linear Theory and Direct Simulation," *AIAA J.* **28**(4), 618–624.

SARKAR, S. 1995 "The stabilizing effect of compressibility in turbulent shear flow," *J. Fluid Mech.* **282**, 163–186.

SCHLICHTING, H. 1968 *Boundary-Layer Theory* (6th ed., McGraw-Hill, New York).

SETTLES, G. S. 1985 "Colour-coding schlieren techniques for the optical study of heat and fluid flow," *Int. J. Heat and Fluid Flow*, **6** (1), 3–15.

SHAU, Y. R., DOLLING, D. S. & CHOI, K. Y. 1993 "Organized structure in a compressible turbulent shear layer," *AIAA J.* **31**(8), 1398–1405.

SIRIEIX, M. & SOLIGNAC, J. L. 1966 "Contribution a l'etude experimentale de la couche de melange turbulent isobare d'un ecoulment supersonique," AGARD Conference Proceedings No. 4, Separated Flows.

SIVELLS, J. C. 1978 "A computer program for the aerodynamic design of axisymmetric and planar nozzles for supersonic and hypersonic wind tunnels," AEDC–TR–78–63.

SMITS, A. J. & DUSSAUGE, J. P. 1996 "Turbulent shear layers in supersonic flow," AIP Press, NY.

TAM, C. K. W. 1971 "Directional acoustic radiation from a supersonic jet," *J. Fluid Mech.* **46**, 757–768.

TAM, C. K. W. & HU, F. Q. 1989 "The instability and acoustic wave modes of supersonic mixing layers inside a rectangular channel," *J. Fluid Mech.* **203**, 51–76.

UMEMURA, A., MIURA, K. & TAKADA, K. 1996 "Supression of embedded shocks in supersonic free-shear-layer structures," *Shock Waves* **6**, 167–175.

VAN DYKE, M. 1982 *An Album of Fluid Motion* (Parabolic Press, Stanford, CA).

VREMAN, A. W., SANDHAM, N. D. & LUO, K. H. 1996 "Compressible mixing layer growth rate and turbulence characteristics," *J. Fluid Mech.* **320**, 235–258.

WEISBROT, I., EINAV, S. & WYGNANSKI, I. 1982 "The non unique rate of spread of the two-dimensional mixing layer," *Phys. Fluids* **25**(10), 1691–1693.

WHITE, F. M. 1974 *Viscous Fluid Flow* (McGraw-Hill, New York).

WIGGINS, S. 1990 *Introduction to Applied Nonlinear Dynamical Systems and Chaos* (Springer-Verlag, New York).

WILKE, C. R. 1950 "A Viscosity Equation for Gas Mixtures," *J. Chem. Phys.* **18**, 517.

WYGNANSKI, I., CHAMPAGNE, F. & MARASLI, B. 1986 "On the large-scale structures in two-dimensional, small-deficit turbulent wakes," *J. Fluid Mech.* **38**, 577–612.

WYGNANSKI, I. & FIEDLER, H. E. 1970 *J. Fluid Mech.* **41**(2), 327-361.

WYGNANSKI, I., OSTER, D. & FIEDLER, H. 1979 "A Forced, Plane, Turbulent Mixing-Layer: A Challenge for the Predictor," 2^{nd} *Int. Symposium on Turb. Shear Flows* (Springer-Verlag, New York, 1980), 314–326.

YAO, L.S. & GHOSH MOULIC, S. 1995 "Nonlinear instability of traveling waves with a continuous spectrum," *Int. J. Heat Mass Transfer* **38**, 1751–1772.

ZEMAN, O. 1990 "Dilatation dissipation: The concept and application in modeling compressible mixing layers," *Phys. Fluids A* bf 2(2), 178–187.

ZHUANG, M. 1990 *An Investigation of the Inviscid Spatial Instability of Compressible Mixing Layers*, Ph.D. thesis, California Institute of Technology.

ZHUANG, M. & DIMOTAKIS, P. E. 1995 "Instability of wake-dominated compressible mixing layers," *Phys. Fluids* **7**(10), 2489–2495.

ZHUANG, M., DIMOTAKIS, P. E. & KUBOTA, T. 1990 "The Effect of Walls on a Spatially Growing Supersonic Shear Layer," *Phys. Fluids* A **2**, 599–604.

ZHUANG, M., KUBOTA, T. & DIMOTAKIS, P. E. 1990 "Instability of Inviscid, Compressible Free Shear Layers," *AIAA J.* **28**, 1728–1733.